



# **NATIONAL POLAR-ORBITING OPERATIONAL ENVIRONMENTAL SATELLITE SYSTEM (NPOESS)**

## **VIIRS IMAGERY PRODUCTS ALGORITHM THEORETICAL BASIS DOCUMENT (ATBD) (REF Y2466) (D43767 Rev B)**

**CDRL No. A032**

**Northrop Grumman Space & Mission Systems Corporation  
One Space Park  
Redondo Beach, California 90278**

**Copyright © 2004-2010  
Northrop Grumman Corporation and Raytheon Company  
Unpublished Work  
ALL RIGHTS RESERVED**

Portions of this work are the copyrighted work of Northrop Grumman and Raytheon. However, other entities may own copyrights in this work.

This documentation/technical data was developed pursuant to Contract Number F04701-02-C-0502 with the US Government. The US Government's rights in and to this copyrighted data are as specified in DFAR 252.227-7013, which was made part of the above contract.

This document has been identified per the NPOESS Common Data Format Control Book – External Volume 5 Metadata, D34862-05, Appendix B as a document to be provided to the NOAA Comprehensive Large Array-data Stewardship System (CLASS) via the delivery of NPOESS Document Release Packages to CLASS.

The information provided herein does not contain technical data as defined in the International Traffic in Arms Regulations (ITAR) 22 CFR 120.10.

This document has been approved by the United States Government for public release in accordance with NOAA NPOESS Integrated Program Office.

**Distribution: Statement A:** Approved for public release; distribution is unlimited.



# **NATIONAL POLAR-ORBITING OPERATIONAL ENVIRONMENTAL SATELLITE SYSTEM (NPOESS)**

## **VIIRS IMAGERY PRODUCTS ALGORITHM THEORETICAL BASIS DOCUMENT (ATBD) (REF Y2466) (D43767 Rev B)**


### **ELECTRONIC APPROVAL SIGNATURES:**

_____ Roy Tsugawa Algorithm & Data Processing IPT Lead & Algorithm Change Control Board Chairperson	_____ Date
--	---------------

_____ Gerald J. Mulvey Senior Systems Engineer	_____ Date
--	---------------

The following individuals are recognized for their contributions to the current or previous versions of this document.

Duane Apling  
Igor Appel  
Randy Arbeiter  
Keith Hutchison  
Kenneth A. Jensen  
Richard Julian  
North Larsen  
Robert Mahoney  
Stephen Mills  
Tohru Ohnuki  
Wenli Yang

			
<b>Revision/Change Record</b>			<b>Document Number</b> D43767
<b>Revision</b>	<b>Document Date</b>	<b>Revision/Change Description</b>	<b>Pages Affected</b>
---	1/26/2007	Initial PCIM Release to bring document into Matrix Accountability. Reference original document number: Y2466 v5.1 rev 2 delivered in 2003	All
A	01/08/2008	Update to title of document to remove reference to “Clouds”	All
B	02/04/2009	Incorporates ECR A-192. Approval for Public Release per Contracts Letter 100323-01.	All

**Revision/Change Record      For Document No. Y2466**

<b>Symbol</b>	<b>Document Date</b>	<b>Authorization Date</b>	<b>Revision/Change Description</b>	<b>Pages Affected</b>
	2/27/2003	Stephen Mills	SPCR ALG00000027 & ALG00000028 NP-EMD.03.591.009 (assigned) NP-EMD.03.591.009 (closed)	p. i-xi, 1,2, 3, 5, 9, 10, 35, 46, 48. 50, 52- 55
B	2/04/09	Keith Hutchison	Changes required per CDA RFAs	All

# TABLE OF CONTENTS

	<u>Page</u>
LIST OF FIGURES.....	v
LIST OF TABLES .....	vii
GLOSSARY OF ACRONYMS .....	viii
ABSTRACT .....	xii
1.0 INTRODUCTION.....	1
1.1 PURPOSE .....	1
1.2 SCOPE .....	1
1.3 VIIRS DOCUMENTS .....	3
1.4 REVISIONS .....	4
2.0 EXPERIMENT OVERVIEW .....	7
2.1 EDR DEFINITION .....	7
2.2 EXPLICIT IMAGERY REQUIREMENTS .....	7
2.3 NEAR CONSTANT CONTRAST (NCC) VISIBLE IMAGERY .....	10
2.4 GROUND-TRACK MERCATOR IMAGERY .....	11
2.5 APPLICATION-RELATED REQUIREMENTS .....	11
2.5.1 Requirements for Cloud Cover .....	11
2.5.2 Requirements for Cloud Type:.....	12
2.5.3 Requirements for Ice Edge Location .....	13
2.5.4 Requirements for Ice Concentration .....	14
2.6 INSTRUMENT CHARACTERISTICS.....	14
2.6.1 Daytime/Nighttime Visible Band (DNB) .....	16
2.6.2 VIIRS Imagery Band Selection Process .....	17
2.6.3 Daytime Visible Band (DV) .....	18
2.6.4 Long-Wave Infrared Band (LWIR) .....	19
2.6.5 Mid-Wave Infrared Band (MWIR) .....	20
2.6.6 Additional Imagery Bands .....	22
2.6.7 Imagery Assist Bands.....	23
2.7 RETRIEVAL STRATEGY .....	23
2.7.1 Explicit Imagery .....	23

2.7.2	Top-of-Atmosphere Radiance .....	23
2.7.3	Top-of-Atmosphere Reflectance .....	24
2.7.4	Equivalent Blackbody Temperature .....	24
2.7.5	Near Constant Contrast (NCC) Visible Imagery .....	24
2.7.6	Manually-Generated Cloud Data.....	24
2.7.7	Sea Ice Data .....	24
3.0	ALGORITHM DESCRIPTION .....	25
3.1	OVERVIEW .....	25
3.2	EXPLICIT IMAGERY PRODUCTION .....	25
3.2.1	Processing Outline .....	25
3.2.2	Algorithm Input .....	25
3.2.2.1	VIIRS Data .....	25
3.2.2.2	Non-VIIRS Data .....	25
3.2.3	Theoretical Description .....	26
3.2.4	Archived Algorithm Output.....	26
3.2.5	Performance of Explicit Imagery.....	26
3.2.5.1	Daytime/Nighttime Visible Band .....	29
3.2.5.2	Other Imagery Bands .....	31
3.3	NCC VISIBLE IMAGERY PRODUCTION .....	32
3.3.1	Processing Outline .....	32
3.3.1.1	Baseline Approach – Gain Management Algorithm .....	32
3.3.1.2	Enhanced Algorithm Approach - Atmospheric Correction .....	34
3.3.2	Algorithm Input .....	35
3.3.3	Theoretical Description .....	35
3.3.3.1	Physics of the Problem .....	35
3.3.3.2	Mathematical Description of the Algorithm.....	37
3.3.4	Archived Algorithm Output.....	38
3.3.5	Performance of NCC Visible Imagery .....	38
3.3.5.1	Baseline Algorithm .....	38
3.3.5.2	Atmospheric Correction Enhancement.....	39
3.3.6	Initialization and Validation .....	42
3.3.6.1	Initialization .....	42
3.3.6.2	Pre-Launch Characterization .....	42
3.3.6.3	Validation .....	42
3.3.7	Practical Considerations .....	42
3.3.7.1	Numerical Computation Considerations.....	42
3.3.7.2	Programming and Procedural Considerations .....	43
3.3.7.3	Configuration of Retrievals .....	43
3.3.7.4	Quality Assessment and Diagnostics.....	43

3.3.8	Algorithm Watch List .....	43
3.4	GROUND-TRACK MERCATOR IMAGERY PRODUCT DESCRIPTION .....	43
3.4.1	Processing Outline .....	46
3.4.2	Algorithm Input.....	46
3.4.3	Theoretical Description.....	47
3.4.4	Archived Algorithm Output .....	48
3.4.5	Practical Considerations.....	50
3.4.5.1	Graceful Degradation .....	50
3.4.5.2	Exception Handling.....	50
3.5	MANUAL CLOUD ANALYSIS ARP DESCRIPTION .....	51
3.5.1	Processing Outline .....	51
3.5.2	Algorithm Input.....	51
3.5.2.1	VIIRS Data.....	52
3.5.2.2	Non-VIIRS Data .....	52
3.5.3	Theoretical Description.....	53
3.5.3.1	Physics of the Problem.....	53
3.5.3.2	Image Processing to Enhance Cloud Detection in Multispectral Imagery .....	55
3.5.3.3	Mathematical Description of the Algorithm .....	60
3.5.3.4	VIIRS Imagery and Imagery Assist Color Composites .....	61
3.5.3.5	VIIRS Cloud Mask for Imagery.....	71
3.5.4	Performance of Manually-Generated Cloud Data .....	71
3.5.4.1	Cloud Cover .....	73
3.5.4.2	Cloud Type.....	75
3.5.5	Initialization and Validation .....	77
3.6	MANUAL SEA ICE ANALYSIS ARP DESCRIPTION.....	78
3.6.1	Processing Outline .....	78
3.6.2	Algorithm Input.....	78
3.6.2.1	VIIRS Data.....	80
3.6.2.2	Non-VIIRS Data .....	80
3.6.3	Theoretical Description of the Retrieval.....	80
3.6.3.1	Physics of the Problem.....	80
3.6.3.2	Mathematical Description of the Sea Ice Algorithms.....	83
3.6.3.2.4	Supplemental Microwave Sensor Image Analysis.....	89
3.6.4	Performance of Sea Ice Data.....	89
3.7	PRACTICAL CONSIDERATIONS .....	90
3.7.1	Numerical Computation Considerations .....	90
3.7.2	Programming and Procedural Considerations.....	91
3.7.3	Configuration of Retrievals.....	92
3.7.4	Quality Assessment and Diagnostics .....	92
3.7.5	Exception Handling.....	92

3.8 ALGORITHM VALIDATION.....92

4.0 ASSUMPTIONS AND LIMITATIONS .....94

4.1 ASSUMPTIONS.....94

4.2 LIMITATIONS.....94

5.0 REFERENCES .....95

## LIST OF FIGURES

	<u>Page</u>
Figure 1. Comparison of the VIIRS band set for Imagery with OLS and AVHRR-3. ....	10
Figure 2. Reflectivity, absorptivity, and transmissivity of atmosphere, surface, and clouds in the Short-Wave Infrared (SWIR). ....	17
Figure 3. Phenomenology of the VIIRS Daytime Visible (DV) Imagery band, centered at 640 nm. ....	18
Figure 4. Phenomenology of the VIIRS Long-Wave Infrared (LWIR) Imagery band, centered at 11.45 microns. ....	20
Figure 5. Phenomenology of the VIIRS Mid-Wave Infrared (MWIR) Imagery band, centered at 3.74 microns. ....	21
Figure 8. Horizontal Sampling Interval (HSI) for imagery bands (aggregation in scan direction).....	28
Figure 10. Signal-to-noise performance of the Daytime/Nighttime Visible Imagery Band at nadir, for each of the three CCD gain stages. SNR performance over the specified measurement range ( $4.E-9 - 3.E-2$ W/cm <sup>2</sup> /sr) is 30 to 1000. SNR greater than 3 is achieved at a radiance as low as $3.2E-10$ W/cm <sup>2</sup> /sr. ....	29
Figure 12. Spectral Response of the Daytime/Nighttime Visible Imagery band, compared with the lunar signal. ....	30
Figure 13. SNR Performance of the Daytime/Nighttime Visible Imagery under quarter- moon illumination conditions, as a function of scan angle. ....	31
Figure 17. Input radiance image to the NCC algorithm.....	41
Figure 18. NCC Algorithm Output .....	41
Figure 19. GTM Map Attributes .....	45
Figure 20. Fine Map Pixels with Emphasized Coarse Pixels .....	45
Figure 21. NOAA-12 AVHRR Channel 1 and Channel 2 imagery collected over western U.S. at 1505 GMT on March 19, 1996. ....	57
Figure 22. NOAA-12 AVHRR Channel 3 and Channel 5 imagery collected over western U.S. at 1505 GMT on March 19, 1996. ....	58
Figure 23. NOAA-12 AVHRR Channel 1 and the derived 3.7- $\mu$ m (albedo) data for the scene collected 1505 GMT on March 19, 1996. ....	59



Figure 24. Color composite of NOAA-12 AVHRR imagery created by assigning Channels 1, 3, and 5 to the red, green and blue guns of a CRT.....	59
Figure 26. RGB Composites of bands (0.64, 1.61, 10.8./11.45) .....	63
Figure 27. RGB Composites of bands RGB (1.38[1.88], 1.61,11.45).....	64
Figure 28. RGB Composites of bands RGB (1.61, Invert BT8.6, 0.64).....	65
Figure 29. Day/Night Composite #4 – RGB (BT11.45, BT8.6, BT3.75) .....	66
Figure 30. Color composite of MAS data collected over Denver, CO [RGB= (0.64 $\mu$ m, 0.858 $\mu$ m, 0.64 $\mu$ m)]. .....	67
Figure 31. Color composite of NOAA-15 AVHRR imagery created by assigning the 0.64 $\mu$ m, 1.61 $\mu$ m, 10.8 $\mu$ m channels to the red, green and blue guns of a CRT.....	68
Figure 32 (a.) Color Composite of MAS imagery over Denver, CO [RGB (0.64, 1.61, 3.75 albedo] (b.) [RGB (3.75, 10.8,11.45)].....	70
Figure 34. VIIRS sensing requirements were based upon a variety of surface classifications. ....	72
Figure 36. Enhanced VIIRS Imagery SDR RGB (1.6, 0.865, 0.64 $\mu$ m) image of Bering Strait. ....	84
Figure 37. Zoomed region of VIIRS Imagery SDR RGB (1.6, 0.865, 0.64 $\mu$ m) imagery. ....	84
Figure 38. Progressive zooms of VIIRS Imagery SDR RGB (1.6, 0.865, 0.64 $\mu$ m) showing St. Lawrence Island region. ....	85
Figure 39. VIIRS Surface Temperature IP Bering Strait night scene for March 27, 2001 09:15 UTC.....	86
Figure 40. VIIRS Sea Ice Concentration IP zoom of boxed region in figure 39.....	86
Figure 41. Antarctica scene March 25, 2003 09:10 UTC, MODIS Proxy VIIRS Imagery SDR RGB (1.6, 0.865, 0.64 $\mu$ m) with zoom window showing Sea Ice Concentration IP.....	87
Figure 42. Comparison of VIIRS Ice Concentration IP with MODIS MOD29 derived ice concentrations. ....	89
Figure 43. Comparison of sea ice edge location with enhanced VIIRS Imagery SDR enhanced reflectance imagery. ....	90

## LIST OF TABLES

	<u>Page</u>
Table 1. Imagery EDR Products .....	2
Table 2. Explicit Requirements for the VIIRS Imagery EDR .....	8
Table 3. Specifications for the VIIRS Cloud Cover Imagery ARP .....	12
Table 4. Specifications for the VIIRS Cloud Type Imagery ARP .....	13
Table 5. Specifications for the VIIRS Ice Edge Location Imagery ARP .....	13
Table 6. Specifications for the VIIRS Ice Concentration Imagery ARP .....	14
Table 7. Imagery EDR – Input Data Summary (Spatial) .....	15
Table 8. Imagery EDR – Input Data Summary (Radiometric) .....	15
Table 9. VIIRS I-Channel Imagery EDR Inputs .....	46
Table 10. VIIRS I-Channel Imagery EDR Outputs .....	48
Table 11. VIIRS I-Channel Imagery EDR Pixel Level Quality Flags .....	48
Table 12. VIIRS I-Channel Imagery GEO Outputs .....	49
Table 13. VIIRS I-Channel Imagery GEO Pixel Level Quality Flags .....	50
Table 14. VIIRS I-Channel Imagery GEO Scan Level Quality Flags .....	50
Table 15. Ancillary data to augment manual cloud analysis. ....	51
Table 16. Cloud Cover Measurement Uncertainty .....	74
Table 17. Measurement Uncertainty versus HCS from manual analysis of cirrus with visible optical depth of 0.03. ....	74
Table 18. Approach to the positive identification of cloud types by human analysts using VIIRS imagery and imagery assist bands .....	76
Table 19. Data to Augment Manual Analysis of Sea Ice Concentration and Ice Edge Location .....	78
Table 19. Sea Ice Manual ARP Analysis Input Imagery Data Summary. ....	80

## GLOSSARY OF ACRONYMS

ADVCLD	Global cloud forecast model based upon trajectory scheme
AFWA	Air Force Weather Agency
ARP	Application-Related Product
ASGC	Along Scan Gain Control
ASP	Analog Signal Processor
ATBD	Algorithm Theoretical Basis Document
AVHRR	Advanced Very High Resolution Radiometer
AVIRIS	Airborne Visible/Infrared Imaging Spectrometer
BRDF	Bidirectional Reflectance Distribution Function
BT	Brightness Temperature
BTD	Brightness Temperature Difference
CCD	Charge Coupled Device
CDFS	Cloud Depiction and Forecast System
CDR	Critical Design Review
CGTA	Cloud Ground Truth Analysis
CI	Cirrus
CLAVR	Clouds from AVHRR
cm	centimeter
MIS	Microwave Imager/Sounder
CNC	Cloud-No Cloud
CRT	Cathode Ray Tube
CU	Cumulus
DMSP	Defense Meteorological Satellite Program
DN	Digital Number
DNB	Daytime Nighttime Band
DoD	Department of Defense
DV	Daytime Visible
EBBT	Equivalent Blackbody Temperature
EDC	EROS (Earth Resources Observation System) Data Center
EDR	Environmental Data Record
EOSDIS	Earth Observing System Data and Information System
FIRE-ACE	First ISCCP Regional Experiment – Arctic Cloud Experiment
FOV	Field of View
GIFOV	Ground Instantaneous Field of View
GLI	Global Imager
GMA	Gain Management Algorithm

GMT	Greenwich Meridian Time
GOES	Geostationary Operational Environmental Satellite
GSD	Ground Sample Distance
GTOPO30	Global Topographic 30 arc second map
HCS	Horizontal Cell Size
HRCP	High-Resolution Cloud Prognosis
HRD	High Rate Data; also High Resolution Diode
HRI	Horizontal Reporting Interval
HSI	Horizontal Sampling Interval
HSR	Horizontal Spatial Resolution
IDPS	Interface Data Processor Segment
IORD	Integrated Operational Requirements Document
IP	Intermediate Product
IPO	Integrated Program Office
IPT	Integrated Product Team
IR	Infrared
ISCCP	International Satellite Cloud Climatology Project
K	Kelvin
km	kilometer
LLS	Low Level Light Sensor
LOS	Loss of Signal
LRD	Low Rate Data
LUT	Look Up Table
LUTGT	Look Up Table Generation Tool
LWIR	Long-Wave Infrared
m	meter
MAS	MODIS Airborne Simulator
MODIS	Moderate Resolution Imaging Spectroradiometer
MODTRAN	Moderate Resolution Atmospheric Radiance and Transmittance Model
MOSART	Moderate Spectral Atmospheric Radiance and Transmittance
MTF	Modulation Transfer Function
MWIR	Mid-Wave Infrared
NASA	National Aeronautics and Space Administration
NCC	Near Constant Contrast
NEdT	Noise Equivalent delta Temperature
NGDC	National Geophysical Data Center
NIC	National Ice Center

NIR	Near Infrared
NOAA	National Oceanic and Atmospheric Administration
NPOESS	National Polar-Orbiting Operational Environmental Satellite System
NPP	NPOESS Preparatory Project
OLS	Operational Linescan System
P <sup>3</sup> I	Pre-Planned Product Improvement
PDR	Preliminary Design Review
QC	Quality Control
RDR	Raw Data Record
RGB	Red-Green-Blue
RMS	Root Mean Square
RMSE	Root Mean Square Error
RSS	Root Square Sum
RT	Radiation Transfer
RTNEPH	Real Time NEPH Analysis
SBIRS	Space-Based Infrared System
SBRS	Santa Barbara Remote Sensing
SDHS	Satellite Data Handling System
SDR	Sensor Data Record
SDSM	Solar Diffuser Stability Monitor
SeaWiFS	Sea-viewing, Wide-Field-of-View Sensor
SERCAA	Support of Environmental Requirements for Cloud Analysis and Archive
SNR	Signal-to-Noise Ratio
sr	steradian
SRD	Sensor Requirements Document
ST	Stratus
SWIR	Short Wave Infrared
SZA	Solar Zenith Angle
TBD	To Be Determined
TBR	To Be Reviewed
TBS	To Be Specified
TDI	Time Delay and Integration
TERCAT	Terrain Categorization
THEMIS	Thermal Emission Imaging System
TIM	Technical Interchange Meeting
TIROS	Television Infrared Observation Satellite
TOA	Top of Atmosphere

VCM	VIIRS Cloud Mask
VDGA	Variable Digital Gain Amplifier
VIIRS	Visible/Infrared Imager/Radiometer Suite
VIS	Visible
VMCD	VIIRS Manually-Generated Cloud Data
VNIR	Visible/Near Infrared
VOAT	VIIRS Operational Algorithm Team
W	Watts
WINCE	Winter Cloud Experiment

## ABSTRACT

This Imagery Algorithm Theoretical Basis Document (ATBD) describes the background, theory, and analysis of the algorithmic process required to create Imagery Environmental Data Records (EDRs) from the sensor Raw Data Records (RDRs) of the National Polar-orbiting Operational Environmental Satellite System (NPOESS) Visible/Infrared Imager/Radiometer Suite (VIIRS).

This document covers all VIIRS imagery processing. In particular, it describes algorithms for producing Explicit Imagery, Near Constant Contrast (NCC), and imagery produced in the Ground-track Mercator (GTM) projection. In addition, it overviews processing that might be used to manually create applications related products (ARPs), i.e. cloud and ice products.

Six imagery bands are specified. The Daytime/Nighttime Visible Band (DNB), Daytime Visible Band (DV), Mid-Wave Infrared Band (MWIR), and Long-Wave Infrared Band (LWIR) were explicitly required to meet the Imagery ARP requirements. A sixth imagery band was necessary to address the sub-pixel snow cover EDR and this imagery channel further improved the manually-generated cloud ARP. For each spectral band for which imagery is provided, Explicit Imagery includes the following two data products, both generated by ground processing of VIIRS data:

- (a) a two-dimensional array of locally averaged absolute in-band radiances at the top of the atmosphere, measured in the direction of the viewing instrument, and
- (b) the corresponding array of equivalent blackbody temperatures (EBBT) if the band is primarily emissive, or the corresponding array of top-of-the-atmosphere (TOA) reflectance if the band is primarily reflective during daytime.

The VIIRS Imagery EDR benefits from true multispectral capability and compatibility with heritage from the Department of Defense (DoD) Defense Meteorological Satellite Program (DMSP) Operational Linescan System (OLS). The radiometric performance of the bands exceeds the specification for Measurement Uncertainty with margins that allow the performance of the Application-Related Products (ARPs) to meet or approach objective requirements.

The Explicit Imagery is computed from the VIIRS RDRs in the Build-SDR module, which applies geo-location, Earth gridding, and calibration to the RDRs. The functionality of the Build-SDR module will allow it to produce Sensor Data Records (SDRs) that fully meet the explicit imagery requirements. All Imagery products shall be calibrated, geolocated, and reported for a set of earth locations forming an approximately rectangular lattice. The lattice spacing will be 742 meters +/- 5% for the DNB, and approximately equivalent to the Horizontal Spatial Resolution (HSR) for the other imagery bands.

DNB data are obtained from a sensitive, very-wide-dynamic range Charge-Coupled Device (CCD) detector in the main VIIRS Sensor. To encompass the extreme radiometric dynamic range of day and night scenes, the DNB CCD includes four regions of light-sensitive photosites with three different sensitivities. The three regions are designed so that before a more sensitive

region saturates, the next less sensitive region will have received a signal sufficient to produce an acceptable signal-to-noise ratio (SNR). Analog signals from all three regions are converted into digital form and processed digitally to select the signal from the region offering the best SNR for each pixel. The CCD design allows any number of subpixel elements to be aggregated into single pixels as they are read from the CCD. In the VIIRS sensor this capability will be used to generate pixels with near-rectangular sample spacing on the ground. At nadir, SNR performance of the DNB over the specified measurement range ( $4.E-9 - 3.E-2$  Watts/cm<sup>2</sup>/sr) is 30 to 1000. SNR greater than 3 is achieved at a radiance as low as  $3.2E-10$  Watts/cm<sup>2</sup>/sr. At edge of scan, SNR performance of the DNB over the specified measurement range ( $4.E-9 - 3.E-2$  Watts/cm<sup>2</sup>/sr) is 7 to 250. SNR greater than 3 is achieved at a radiance as low as  $1.8E-9$  Watts/cm<sup>2</sup>/sr. SNR greater than 10 is achieved at the minimum radiance for almost the entire scan.

NCC Visible Imagery is derived from the broad day/night band near the terminator region. Due to the significant change in solar irradiance across the terminator, a three-stage CCD sensor is designed to record the radiance in this region. The individual detectors in the three portions of the CCD are used to record daytime, day/night crossing time, and nighttime radiance, respectively. The SDR for this band consists of a single set of data that contains all three stages in all illumination conditions. DNB calibration will provide calibrated TOA radiance over a dynamic range of  $4E-9$  to  $3E-2$  Watts/cm<sup>2</sup>/sr. The NCC algorithm converts the TOA radiance to albedo by modeling the solar and lunar source radiance for each pixel. The algorithm preserves heritage from the OLS Gain Management Algorithm (GMA) through the use of look up tables (LUTs) designed to mimic the GMA. An enhanced NCC algorithm removes atmospheric path radiance. The enhancement will require an improved radiative transfer model, as the latest version of MODTRAN is not accurate at the terminator. The enhancement will be implemented when and if superior performance is validated with NPP/VIIRS data. Therefore, the current implementation does not adjust for atmospheric effects.

Manual cloud analysis is based upon the contrast, measured in brightness temperature or reflectance, between the cloud and the surrounding cloud-free background. In infrared (IR) imagery, cloud detection is enhanced not only by temperature contrasts between the features but also by observing the features in spectral bands where their emissivity contrasts exist. In visible and near-infrared imagery, cloud detection relies on contrasts in the reflectivities of the features while at mid-infrared wavelengths, e.g. 3-5 microns, both temperature and reflected solar energy can be exploited in the manual cloud analysis process. Image enhancement techniques such as histogram equalization and thresholding enable the analyst to delineate individual features. False-colored compositing of multispectral images facilitates manual interpretation of the clouds and background features by assigning colors to those pixels with different multispectral responses. Using these tools, the analyst can systematically and quickly identify and classify the various clouds in the imagery. A User's Guide has been developed for the training of VIIRS Imagery analysts. The first version of the User's Guide is included as an appendix to this ATBD.

The VIIRS System Specification requires that the content and quality of the Imagery EDR be adequate to allow for requirements to be met on sea ice edge location and sea ice concentration. Sea ice data may be generated interactively by a trained analyst viewing unprocessed or processed imagery at a computer workstation, or automatically via an algorithm. Ice



concentration is defined as the fraction of a given area of sea water covered by ice. It is typically derived from imagery and reported on ice charts for areas

between contours generated by an analyst. But for the purpose of verifying the measurement uncertainty requirement, algorithms were developed to retrieve sea ice concentration from imagery and non-imagery VIIRS data and discussed in this document. This allowed ice concentration to be analyzed as a gridded product for areas of size limited by the Horizontal Cell Size (HCS) requirement and separation limited by the Horizontal Reporting Interval (HRI) requirement.

## 1.0 INTRODUCTION

### 1.1 PURPOSE

This Visible/Infrared Imager/Radiometer Suite (VIIRS) Imagery Algorithm Theoretical Basis Document (ATBD) describes the processing steps required to transform all VIIRS Imagery Raw Data Records (RDR) generated by the VIIRS sensor into Imagery Environmental Data Records (EDRs) and Imagery Application-Related Products (ARPs).

The NPOESS VIIRS Sensor Requirements Document (SRD), used to design the VIIRS sensor, identified three classes of imagery requirements that were used to create the original VIIRS sensor design: (a) explicit imagery which included at least one daytime visible, one nighttime visible, and one infrared imagery channel, (b) application-related imagery, which identified imagery channels needed to satisfy a minimum set of requirements for manually-generated cloud and sea ice data, and (c) derived imagery requirements, which were contractor-derived to support other EDRs requirements, e.g. snow/ice and vegetation index EDRs. Based upon this design, algorithms were then created to satisfy the following Imagery EDR processing functions:

- (1) Generation of the Explicit Imagery from the imagery resolution (EV\_375M) and Day/Night Band (EV\_DNB) Sensor Data Records (SDRs).
- (2) Creation of Near Constant Contrast (NCC) visible imagery from the daytime/nighttime visible imagery SDR (EV\_DNB).
- (3) Display VIIRS Imagery into a Ground-Track Mercator (GTM) projection.
- (4) In addition, procedures and algorithms were developed to ensure VIIRS imagery would satisfy the applications related requirements for clouds and sea ice. However, since these products, by definition are manually-generated products, these procedures/algorithms are not part of the VIIRS algorithm suite. As a result, they are only briefly highlighted in this document..

### 1.2 SCOPE

All aspects of VIIRS imagery processing are described in this ATBD. This section of the ATBD introduces the Imagery algorithms. Section 2 provides an overview of the Imagery EDR requirements, specifications, and retrieval strategy. Section 3 describes the algorithms' functions in detail, including the process flow, input data, theoretical basis, mathematical description, performance analysis, practical considerations, initialization, and validation. Section 4 states the assumption and limitations on which each algorithm is based, and Section 5 provides references for the publications cited in this document. A User's Guide for VIIRS Manually-generated Cloud ARP is included as an Appendix.

The VIIRS Imagery EDR and ARP Requirements based on Imagery are achieved with the 9 EDR products listed in Table 1.

**Table 1. Imagery EDR Products**

<b>Imagery EDR Product</b>	<b>VIIRS Band(s)</b>	<b>Wavelength (μm)</b>	<b>Horizontal Resolution Nadir / At 3000 km swath</b>
* Daytime Visible (DV), TOA Radiance, TOA Reflectance	I1	0.60 - 0.68	0.4 km / 0.8 km
*** Near Infrared (NIR), TOA Radiance, TOA Reflectance	I2	0.8455 - 0.8845	0.4 km / 0.8 km
*** Short Wave Infrared (SWIR), TOA Radiance, TOA Reflectance	I3	1.58 - 1.64	0.4 km / 0.8 km
* Daytime/Nighttime Visible (DNB), TOA Radiance, TOA Reflectance	DNB	0.5 – 0.9	0.74 km **
* NCC Visible Imagery	DNB	0.5 – 0.9	0.74 km **
* Mid Wave IR (MWIR), TOA Radiance, Equivalent Blackbody Temperature	I4	3.55 – 3.93	0.4 km / 0.8 km
* Long Wave IR (LWIR), TOA Radiance, Equivalent Blackbody Temperature	I5	10.5 – 12.4	0.4 km / 0.8 km
*** Manually Generated Cloud Cover	I1, I4, I5	N/A	1.2 km / 2.4 km
*** Manually Generated Cloud Type	I1, I4, I5	N/A	1.2 km / 2.4 km
***Land Products, Snow Cover (SYS070700)	I1, I2, I3	N/A	0.4 km / 0.8 km
***High-Resolution Vegetation Index (SYS070700)	I1, I2	N/A	0.4 km / 0.8 km
*** Sea Ice Concentration	I1, I2, I5	N/A	0.4 km / 0.8 km
*** Sea Ice Edge Location	I1, I2, I5	N/A	0.4 km / 0.8 km

\* Explicit Imagery EDR Requirement

\*\* Constant to within 5% in both directions within a swath

\*\*\* Imagery Application-Related Product

### 1.3 VIIRS DOCUMENTS

This document contains references to other Raytheon VIIRS documents, designated by a document number, which is given in italicized brackets. The VIIRS documents cited in this document are:

*[SS 154640-001]* - VIIRS System Specification  
*[PS 154640-101]* - VIIRS Sensor Specification  
*[TP 154640-001]* - VIIRS System Verification and Validation Plan Document  
*[TP 154640-118]* - VIIRS Radiometric Calibration and Validation Plan  
*[Y2400]* - VIIRS Vegetation Index ATBD  
*[D41063]* - VIIRS Sea Ice Characterization ATBD  
*[D43758]* - VIIRS Snow Cover ATBD  
*[D43761]* - VIIRS Ice Surface Temperature ATBD  
*[Y2411]* - VIIRS Surface Reflectance ATBD  
*[Y2412]* - VIIRS Cloud Mask ATBD  
*[Y2468]* - VIIRS Operations Concept document  
*[Y2469]* - VIIRS Context Level Software Architecture  
*[Y2470]* - VIIRS Interface Control Document  
*[Y2471]* - VIIRS Aerosol Module Level Software Architecture  
*[Y2472]* - VIIRS Cloud Module Level Software Architecture  
*[Y2477]* - VIIRS Snow Ice Module Level Software Architecture  
*[Y2478]* - VIIRS Build-RDR Module Level Software Architecture Document  
*[Y2479]* - VIIRS Build SDR Module Level Software Architecture  
*[Y2506]* - VIIRS Ice Edge Location Unit Level Detailed Design Document  
*[D42820]* - Operational Algorithm Description Document for the VIIRS Sea Ice Concentration Intermediate Product  
*[Y3236]* - VIIRS Software Integration and Test Plan  
*[Y3237]* - VIIRS Algorithm Verification and Validation Plan  
*[Y3258]* - VIIRS Geolocation ATBD  
*[Y3261]* - VIIRS Radiometric Calibration ATBD

[Y3270] - VIIRS System Verification and Validation Plan

[Y3273] - VIIRS Imagery Unit Level Detailed Design Document

[Y3277] - VIIRS Aerosol Module Level Interface Control Document

[Y3278] - VIIRS Cloud Module Level Interface Control Document

[Y4963] - VIIRS Imagery TIM, March 8, 2000

[Y6635] - VIIRS Algorithm Software Development Plan

[Y6661] - VIIRS Algorithm Software Maturity Assessment Document

[Y7040] - VIIRS Algorithm/Data Processing Technical Report

[Y10810] - VIIRS Look up Table Generation Tool (LUTGT) Detailed Design Document

[D42821] - Operational Algorithm Description Document for VIIRS Sea Ice Quality Intermediate Product (IP) and Surface Temperature (ST) IP

## 1.4 REVISIONS

This is Revision B to the VIIRS Imagery Products ATBD. This update was required to address actions identified by audits made in preparation for the VIIRS Critical Design Review (CDR). The major modification required in this update was a discussion of the procedures used to transform VIIRS Imagery into the Ground Track Mercator (GTM) projection. In addition, procedures and automated algorithms used to support the manually-generated cloud and sea ice ARPs were highlighted since these processes are covered in other reports, e.g. Sea Ice Characterization ATBD.

Revision A of this document was the initial PCIM release to bring it into Matrix Accountability. Prior to this, all versions were based upon naming conventions used by Raytheon ITSS, the originally developer of this ATBD. In that series of updates, Version 5.1 revision 2, made three changes to the document. First, bands I2 and I3 are now included as imagery EDR bands, per the NPOESS system specification, and references to these two additional bands were added throughout the document. Also, the mathematical description added some equations to clarify the theory and explain the relationship between the theory and the LUTs in the algorithm. Finally, in section 3.3.5.2 describing the atmospheric correction enhancement, additional text was added to indicate that changes to the algorithm would be necessary to implement aerosol scattering removal if deemed desirable. Text was added to consider the benefits of removing Rayleigh atmospheric effects without removing aerosols.

Version 5.1 of the VIIRS Imagery ATBD, was dated April 2002. It was a minor revision of version 5.0, which was released in March 2002 as part of the Raytheon NPOESS/VIIRS Critical Design Review (CDR) package. The first two versions were developed in response to VIIRS Sensor Requirements Document (SRD), revision 1, dated August 3, 1998. The first version was dated October 1998. The second version was dated June 1999. The third version, dated May 2000, was developed in response to VIIRS Sensor Requirements Document

(SRD), Version 2, Revision A, dated 04 November 1999 and was submitted as part of the Raytheon NPOESS/VIIRS Preliminary Design Review (PDR) and Proposal packages.

Changes for version 3 were largely in response to revisions in the new SRD. They included:

- Modification of the process flow
- Addition of an algorithm for producing the NCC imagery
- Performance summary for meeting manual cloud detection thresholds and objectives
- Identification of cloud type classifications that meet system level thresholds and objectives
- Plans for developing a VIIRS users guide for manual cloud identification and typing
- Development of scene-specific tie point analysis of reflectance and/or surface temperature for the automated sea ice concentration algorithm
- Development of an automated algorithm to retrieve ice edge location
- Reporting of ice edge location as an ice edge map and a set of latitude/longitude coordinates
- Additional sea ice test results, from an expanded test data set
- A revised sea ice specification, with supporting error analysis and error budget

The primary purpose of version 4 was to respond to VIIRS Algorithm Watch List items generated by the VIIRS Operational Algorithm Team (VOAT). An additional purpose is to incorporate minor revisions generated by an internal Raytheon review since the VIIRS PDR. Changes since version 3 included:

- A new baseline algorithm for NCC Imagery, adapted from the OLS on-board algorithm
- Expanded description of input data
- Revision and enhancement of the process flow description
- Responses to relevant VOAT Watch List Items

Version 5 incorporates the post-PDR developments in software architecture and detailed design that bring the algorithm to a CDR level of maturity. Changes since version 4 include:

- A change to the specification for the Daytime Visible band (I1)
- A modification of the high rate data (HRD) stream, implementing bow tie deletion
- Additional development of the algorithm for NCC Imagery, with a detailed process flow and a detailed description of the Look Up Tables (LUTs).
- Development of the User's Manual for VIIRS Cloud Imagery

- Additional development of the algorithm for the Sea Ice ARPs, with a detailed process flow and a detailed description of the LUTs.
- Detailed development of quality flags for all of the Imagery EDR automated products

## 2.0 EXPERIMENT OVERVIEW

### 2.1 EDR DEFINITION

As noted in Section 1.1, the VIIRS imagery requirements fall into three classes: (a) explicit requirements on the EDR content, quality, reporting frequency, and timeliness; (b) Requirements to be derived based on specific applications utilizing the imagery EDR, such as manual generation of cloud and sea ice data; and (c ) requirements to be derived from requirements for other EDRs supported by the imagery. This section discusses the Imagery requirements of the VIIRS sensor.

### 2.2 EXPLICIT IMAGERY REQUIREMENTS

As specification by the NPOESS System Specification, Rev N, dated 12 Sep 2008, for each spectral band for which imagery is provided, the Imagery EDR includes the following two data products, both generated by ground processing of VIIRS data:

1. A two-dimensional array of locally averaged absolute in-band radiances at the top of the atmosphere, measured in the direction of the viewing instrument.
2. The corresponding array of equivalent blackbody temperatures (EBBT) if the band is primarily emissive, or the corresponding array of top-of-the-atmosphere (TOA) reflectance if the band is primarily reflective during daytime. TOA reflectance is also provided for the day-night- band (DNB).

The local averages are reported for the points of a two-dimensional approximately rectangular lattice. The form of the weighting function that determines the local average is constrained by the horizontal spatial resolution requirement. Data collected by VIIRS imagery channels are characterized by a horizontal spatial resolution of 375 m at nadir from a nominal NPOESS altitude. The term "derived" for measurement uncertainty refers to the guaranteed VIIRS radiometric uncertainty with an allowed noise increase by x1.02 for imagery that is resampled.

The Imagery EDR must also satisfy the following additional requirements:

- 1) The Near Constant Contrast (NCC) Imagery EDRs shall be generated from the VIIRS Day Night Band (DNB) SDRs so as to minimize the apparent transition across the terminator.
- 2) The VIIRS Imagery EDRs shall be produced in a Ground Track Mercator (GTM) projection.
- 3) The VIIRS Imagery EDRs shall provide a mapping from the resultant projected VIIRS Imagery EDR geolocation to the source VIIRS SDR geolocation.

The explicit requirements and specifications are summarized in Table 2.



**Table 2. Explicit Requirements for the VIIRS Imagery EDR**

Paragraph	Subject	Specified Value	NPP Exclusion
	a. Visible and Infrared Imagery Spectral Bands		
40.2.3.1-21a	1. Visible Daytime/Nighttime Band (DNB)	0.50 - 0.90 micrometer, Nominal	
40.2.3.1-21b	2. I1 Band (Daytime Visible)	0.60 - 0.68 micrometer, Nominal	
40.2.3.1-21c	3. I2 Band (Imagery Application Enhancement)	0.8455 - 0.8845 micrometer, Nominal	
40.2.3.1-21d	4. I3 Band (Imagery Application Enhancement)	1.58 - 1.64 micrometer, Nominal	
40.2.3.1-21e	5. I4 Band (MWIR)	3.55 - 3.93 micrometer, Nominal	
40.2.3.1-21f	6. I5 Band (LWIR)	10.5 - 12.4 micrometer, Nominal	
	b. *Horizontal Spatial Resolution (HSR)		
40.2.3.1-4	1. *Nadir, Bands I1, I2, I3, I4, and I5	0.4 km	
40.2.3.1-5	2. Edge of Swath, Bands I1, I2, I3, I4 and I5	0.8 km	
40.2.3.1-6	3. DNB, Worst Case	0.8 km	
40.2.3.1-7	c. Horizontal Reporting Interval	Imagery HSR	
40.2.3.1 -8	d. Horizontal Coverage	Global	
	e. Measurement Range		
40.2.3.1-10	1. DNB (Day and Night)	3E-5 - 200 W/(m <sup>2</sup> sr)	
40.2.3.1-11a	2. I1 Band (Daytime Only)	5.0 - 718 W/(m <sup>2</sup> sr micrometer)	
40.2.3.1-11b	3. I2 Band (Daytime Only)	12.4 - 291 W/(m <sup>2</sup> sr micrometer)	
40.2.3.1-11c	4. I3 Band (Daytime Only)	1.5 - 47.2 W/(m <sup>2</sup> sr micrometer)	
40.2.3.1-11d	5. I4 Band (Day and Night)	210 K - 353 K	
40.2.3.1-11e	6. I5 Band (Day and Night)	190 K - 340 K	
40.2.3.1-12	f. Measurement Uncertainty	Derived	
	g. Mapping Uncertainty, 3 Sigma		
40.2.3.1-13	1. Nadir, Visible and IR Imaging Bands on VIIRS Native Swath	0.4 km	

Paragraph	Subject	Specified Value	NPP Exclusion
40.2.3.1-14	2. Edge of Swath, Visible and IR Imaging Bands on VIIRS Native Swath	1.5 km	
	h. *Maximum Local Average Revisit Time		
40.2.3.1-15a	1. *Visible and Infrared Imaging Bands	6.0 hrs	X
40.2.3.1-16	i. *Maximum Local Refresh, Visible and Infrared Imaging Bands	8.7 hrs	X
40.2.3.1-17	j. *Fraction of Revisit Times Less Than a Specified Value, Visible and Infrared Imaging Bands	At Any Location at Least 75% of the Revisit Times Shall be 8.7 hours or Less	X
40.2.3.1-20	k. Latency	NPP - 140 min.  NPOESS - 28 min.	
40.2.3.1-21	l. Revisit time exclusion if there is not an NPOESS spacecraft in each of the 2 nominal orbits.		

A schematic comparison of the VIIRS bands listed in Table 2 with the OLS and the National Oceanic and Atmospheric Administration (NOAA) Advanced Very High Resolution Radiometer (AVHRR) band sets is shown as Figure 1.

VIIRS bands marked “I” are required to meet the Imagery EDR threshold requirements. The legend indicates the spatial resolution of the band sets. OLS PMT channel bands (gray) are at coarse resolution. AVHRR-3 bands (blue) are at moderate resolution (green). The other band sets are at imagery resolution. The VIIRS Imagery EDR benefits from true multispectral capability and compatibility with OLS heritage.

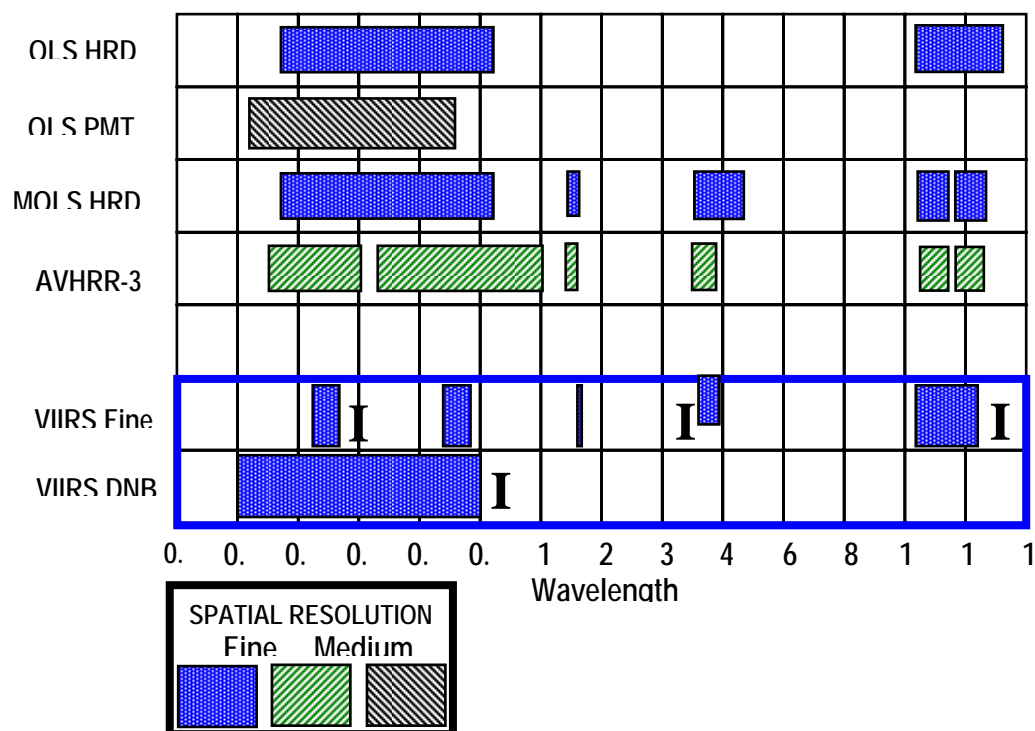


Figure 1. Comparison of the VIIRS band set for Imagery with OLS and AVHRR-3.

### 2.3 NEAR CONSTANT CONTRAST (NCC) VISIBLE IMAGERY

The Imagery EDR includes a daytime/nighttime visible imagery product that maintains apparent contrast under daytime, nighttime, and terminator region illumination conditions. This product, referred to as the Near Constant Contrast (NCC) visible imagery, is to be derived from the daytime/nighttime visible band (DNB) in addition to the calibrated DNB radiance and reflectance. Data from the daytime/nighttime band will be transmitted in the real-time High Rate Data (HRD) and Low Rate Data (LRD) streams, and the NCC visible imagery will be made available to users in near real time following the ground processing needed for its generation. In addition to derived requirements for this product, NCC visible imagery is subject to the following five explicit requirements:

- 1) The NCC visible imagery shall minimize the apparent transition across the terminator when it is viewed on a graphical display system. This means, in particular, that from the perspective of a human analyst viewing the imagery, the apparent image contrast is maintained across the imagery, and that there are no spatial or other artifacts which adversely affect the utility of the imagery.
- 2) The HSR of the NCC visible imagery shall meet the HSR requirement of the daytime/nighttime visible band.

- 3) The HRI of the NCC visible imagery shall be constant to within 5% of its nominal value in both the in-track and cross-track directions within a swath. This requirement does not apply to the horizontal sampling performed by the VIIRS instrument, and may be met by resampling the measured data.
- 4) The nominal value of the HRI of the NCC visible imagery shall provide gapless or near gapless coverage based on the minimum HSR in either the in-track or cross-track directions across the imagery swath.
- 5) The NCC visible imagery shall be geolocated by ground processing to meet the mapping uncertainty requirement.

## 2.4 GROUND-TRACK MERCATOR IMAGERY

VIIRS Imagery data will be projected onto a GTM layout. The GTM layout is a grid of pixels, where rows are at right angles to the ground track and columns are parallel to the ground track. The GTM Imagery EDR products are displayed for human viewing, i.e. the manually-generated applications-related products (ARPs).

## 2.5 APPLICATION-RELATED REQUIREMENTS

The content and quality of the imagery shall be adequate to allow certain application-related requirements to be met. The application-related requirements apply to manually generated cloud data and to sea ice data. These requirements determine the derived requirements of Horizontal Reporting Interval, Measurement Range, and Measurement Uncertainty for the VIIRS imagery bands. The content of the application-related data products (ARPs) is not part of the content of the imagery EDR, and there is no system requirement to develop algorithms to produce them. However, there was a need for requirements flowdown to explicit imagery requirements that was best met by the development of algorithms to estimate system performance for these ARPs.

- a. Manually generated cloud data are estimates of cloud cover and cloud type generated by a trained human analyst viewing the unprocessed and/or processed imagery derived from the unprocessed imagery, e.g., by data fusion, spatial rescaling, image enhancement, etc. Data products include cloud cover and cloud type.
- b. Sea ice data may be generated interactively by a trained human analyst viewing unprocessed or processed imagery at a computer workstation, or automatically via an algorithm. Data products include ice edge location and ice concentration. In addition, analysts will attempt to determine the thickness and size of leads and polynyas based on the imagery.

### 2.5.1 Requirements for Cloud Cover

Cloud cover is defined as the fraction of a given area, i.e., of a horizontal cell, on the Earth's surface for which a locally normal line segment extending between two given altitudes

intersects a detectable cloud as defined in the Glossary. For manual analyses, cloud cover is estimated for a single atmospheric layer. Specifically, the minimum and maximum altitudes of this layer are defined to be the surface of the Earth and the altitude where the pressure is 0.1-mb. Haze, smoke, dust, and rain are not to be considered clouds. For the purpose of validating this requirement, cloud cover estimates are to be generated by a trained human analyst viewing unprocessed and/or processed imagery for contiguous square areas having side length equal to the horizontal cell size specified below.

The requirements for manual analysis of cloud cover are summarized in Table 3.

**Table 3. Specifications for the VIIRS Cloud Cover Imagery ARP**

Paragraph	Subject	Specified Value
40.2.3.2.1.1-6	a. Horizontal Cell Size	3 times HSR (1.2 km at Nadir)
40.2.3.2.1.1-3	b. Horizontal Reporting Interval	Horizontal Cell Size
40.2.3.2.1.1-4	c. Measurement Range	0 – 1, 0.1 Increments
40.2.3.2.1.1-5	d. Measurement Uncertainty	0.1

## 2.5.2 Requirements for Cloud Type:

The following fourteen cloud types are to be identifiable from the imagery product: Altocumulus (AC); Altostratus (AS); Cirrocumulus (CC); Cirrocumulus (standing lenticular) (CCSL); Cirrostratus (CS); Cirrus (CI); Cumulonimbus (CB); Cumulus (CU); Towering Cumulus (TCU) ; Stratocumulus (SC); Stratocumulus (standing lenticular) (SCSL); Stratus (ST); Obscured/not cloudy; Clear.

A given area is classified as "obscured/not cloudy" if there are no detectable clouds within the atmosphere overlying the area and if the average vertical LOS extinction optical thickness of the atmosphere overlying the area is  $> 0.03$  in the  $0.640 \mu\text{m}$  region. For the purpose of addressing requirements for manually-generated cloud types with the Imagery EDR, a given area is classified as "clear" if there are no detectable clouds, as defined above, overlying the area and if the average vertical LOS extinction optical thickness of the atmosphere overlying the area is  $< 0.03$  in the  $0.640 \mu\text{m}$  region. Note that other EDRs require the type of non-cloud obscuration to be discerned and identified, e.g., smoke, dust, sand, ash, etc.

For the purpose of validating this requirement, typing is performed by a trained human analyst viewing unprocessed and/or processed imagery for contiguous square areas having side length equal to the horizontal cell size specified below. The probability of correct typing is defined as the probability that a cell reported as being of type x is in fact of type x, where x is any of the types specified above.

The requirements for manual analysis of cloud type are summarized in Table 4.

**Table 4. Specifications for the VIIRS Cloud Type Imagery ARP**

Paragraph	Subject	Specified Value
40.2.3.2.1.2-7	a. Horizontal Cell Size	3 Times HSR (1.2 km at Nadir)
40.2.3.2.1.2-3	b. Horizontal Reporting Interval	Horizontal Cell Size
40.2.3.2.1.2-4	c. Measurement Range	14 Cloud Types Listed Above
40.2.3.2.1.2-8	d. Probability of Correct Typing	85%

### 2.5.3 Requirements for Ice Edge Location

An ice edge is defined as the boundary between ice-covered sea water (ice concentration  $> 0.1$ ) and sea water not covered by ice (ice concentration  $\leq 0.1$ ). Ice concentration is defined as the fraction of a given area sea or water covered by ice. An ice edge is typically provided as a contour on a map or in digital form as a set of latitude/longitude coordinates. The ice edge location error is defined as the distance between the estimated location of an ice edge and the nearest location of a true ice edge. “Clear” for this EDR is indicated by a cloud mask indicator of “confidently clear” for the horizontal cell of interest.

The requirements for sea ice edge location are summarized in Table 5.

**Table 5. Specifications for the VIIRS Ice Edge Location Imagery ARP**

Paragraph	Subject	Specified Value
40.2.3.2.2.1-1	a. Horizontal Coverage	North of 36 deg North Latitude, South of 50 deg South Latitude for Sea Ice
40.2.3.2.2.1-2	b. Measurement Range	Any Latitude, Longitude Within Horizontal Coverage
	c. Measurement Uncertainty	
40.2.3.2.2.1-3a	1. Clear, Nadir	0.4 km
40.2.3.2.2.1-3b	2. Clear, Worst Case	1.0 km
40.2.3.2.2.1-5	d. Degraded Clear Measurement Condition, Worst Case: Thermal Contrast 1 K to 2.2 K Between Ice and Open Water	2.0 km
	d. Excluded Clear Measurement Conditions:	
40.2.3.2.2.1-6a	1. Thermal Contrast $< 1$ K Between Ice and Open Water	
40.2.3.2.2.1-6b	2. Aerosol Optical Thickness $> 1.0$	

## 2.5.4 Requirements for Ice Concentration

Ice concentration is defined as the fraction of a given area of sea water covered by ice. It is typically derived from imagery and reported on ocean geographical charts for areas between contours generated by an analyst.

The requirements for sea ice concentration are summarized in Table 6.

**Table 6. Specifications for the VIIRS Ice Concentration Imagery ARP**

Paragraph	Subject	Specified Value
40.2.3.2.2.2-1	a. Horizontal Coverage	North of 36 deg North Latitude, South of 50 deg South Latitude for Sea Ice
40.2.3.2.2.2-2	b. Measurement Range	0 – 1 HCS Area, 0.1 increments
40.2.3.2.2.2-3	c. Measurement Uncertainty	0.1

## 2.6 INSTRUMENT CHARACTERISTICS

The VIIRS instrument can be pictured as a convergence of three existing sensors. (1) The Operational Linescan System (OLS) is the operational visible/infrared scanner for the Department of Defense (DoD). Its unique strengths are controlled growth in spatial resolution through rotation of the ground instantaneous field of view (GIFOV) and the existence of a low-level light sensor (LLS) capable of detecting visible radiation at night. OLS has primarily served as a data source for manual analysis of imagery. (2) The Advanced Very High Resolution Radiometer (AVHRR) is the operational visible/infrared sensor flown on the National Oceanic and Atmospheric Administration (NOAA) Television Infrared Observation Satellite (TIROS-N) series of satellites (Planet, 1988). Its unique strengths are low operational and production cost and the presence of five spectral channels that can be used in a wide number of combinations to produce operational and research products. (3) The Moderate Resolution Imaging Spectroradiometer (MODIS) which possesses an array of thirty-two spectral bands at resolutions ranging from 250 m to 1 km at nadir.

VIIRS merges and extends the capabilities of these DoD, NOAA and NASA sensor into a single visible/infrared sensor capable of satisfying the needs of all three communities. As such, VIIRS includes key attributes of high spatial resolution with controlled growth off nadir and a large number of spectral bands to satisfy the requirements for generating accurate operational and scientific products. A description of the design concept, scanning method, and pixel formation is given in Section 3.2.5.

The VIIRS sensor specification is based on the sensor requirements of the National Polar-orbiting Operational Environmental Satellite System (NPOESS) and on EDR thresholds and objectives. These system-level requirements have been flowed down into a fundamental set of

“sensing” requirements that form the basis for the VIIRS imagery (Hutchison, 1998). The Imagery algorithm takes as input Raw Data Records (RDRs) generated from the VIIRS Imagery bands [Y2478]. The RDRs are geolocated and calibrated to produce TOA radiance Sensor Data Records (SDRs), as discussed in Sections 2.6.1 and 3.2.5. The Explicit Imagery is obtained from these SDRs and stored in the Imagery EDR. The performance characteristics of the imagery and imagery-assist bands, listed in Table 7 and Table 8, are obtained from the VIIRS Sensor Specification Document [PS 154640-101] and the VIIRS Radiometric Calibration ATBD [Y3261].

**Table 7. Imagery EDR – Input Data Summary (Spatial)**

$\lambda(\mu\text{m})$	$\Delta\lambda(\mu\text{m})$	GSD* (m) at Nadir (Track x Scan)	HSR (m) at Nadir (Track x Scan)	GSD *(m) at Edge of Scan (Track x Scan)	HSR (m) at Edge of Scan (Track x Scan)
0.7**	0.40	742 x 742	742 x 742	742 x 742	742 x 742
0.640**	0.080	371 x 131	371 x 393	800 x 800	800 x 800
0.865****	0.039	371 x 131	371 x 393	800 x 800	800 x 800
1.61****	0.06	371 x 131	371 x 393	800 x 800	800 x 800
3.74***	0.38	371 x 131	371 x 393	800 x 800	800 x 800
11.45**	1.90	371 x 131	371 x 393	800 x 800	800 x 800

\* Ground Sample Distance

\*\* Explicitly required bands

\*\*\* Additional band required to meet Imagery application-related threshold requirements

\*\*\*\* Bands used to enhancement performance of application-related products

**Table 8. Imagery EDR – Input Data Summary (Radiometric)**

$\lambda(\mu\text{m})$	$\Delta\lambda(\mu\text{m})$	Ltyp (Watts/m2-sr-um) or Ttyp	SNR / NE $\Delta$ T (Nadir)	SNR / NE $\Delta$ T (Edge of Scan)
0.7*	0.4	4.E-9 Watts/cm2/sr (night), 1.E-2 Watts/cm2/sr (day)	30 (night), 600 (day)	7 (night), 200 (day)
0.640*	0.080	23.0	275	159
0.865***	0.039	25.0	389	225
1.61***	0.06	7.3	135	78
3.74**	0.38	270 K	0.53 K	0.92 K
11.45*	1.90	210 K	0.40 K	0.69 K

\* Explicitly required bands



\*\* Additional band required to meet Imagery application-related threshold requirements

\*\*\* Bands used to enhancement performance of application-related products

The radiometric performance of the bands exceeds the specification for Measurement Uncertainty (c.f. Table 2) with margins that allow the performance of the Application-Related Products to meet or approach objective requirements (c.f. Sections 3.4.4 and 3.5.4).

### 2.6.1 Daytime/Nighttime Visible Band (DNB)

The Daytime/Nighttime Visible band (DNB) is explicitly required by the VIIRS specification.

DNB data is taken by a sensitive, very-wide-dynamic range Charge-Coupled Device (CCD) detector in the main VIIRS Sensor. The CCD is located adjacent to the Visible/Near Infrared (VNIR) detector chip on the Warm Focal Plane. It is positioned so that as the sensor scans the image of the Earth across the focal plane, a particular point on earth will be imaged first by the VNIR chip and then by the DNB CCD.

The detective elements of the DNB CCD are 15.4 micrometer by 24.2 micrometer photosites. In the VIIRS sensor each of these photosites images an angle that corresponds to approximately 17 x 11 meters on the ground at nadir. The signals from many of these photosites are combined on the CCD chip to create the analog signals corresponding to entire ground pixels.

To encompass the extreme radiometric dynamic range of day and night scenes, the DNB CCD includes four regions of light-sensitive photosites with three different sensitivities:

**Most Sensitive Regions:** The CCD includes 2 identical regions incorporating 250 subpixel detectors operated in Time Delay Integration (TDI) mode. This TDI gives a total effective integration period 250 times longer than the integration period of a single subpixel detector, and thus increases sensitivity by approximately 250 times. In normal circumstances the signals from these two identical maximum-sensitivity detector regions are added together for further improvement in SNR. However, if radiation should compromise the value of a pixel measurement made by one of the two segments, the corresponding pixel signal from the other segment would be used.

**Medium-sensitivity region:** A second detecting region on the CCD chip utilizes three subpixel detectors in TDI. This region also has a lower amplifier gain to give it a net radiometric gain that is approximately 200 times less than the gain of the most sensitive regions.

**Lowest-sensitivity region:** The CCD also incorporates a detecting region that does not incorporate multiple detectors in TDI. In addition, this region incorporates a 35:1 neutral-density filter and reduced amplifier gain, resulting in a radiometric gain approximately 1/475 of the medium-sensitivity region's gain.

The three regions are designed so that before a more sensitive region saturates, the next less sensitive region will have received a signal sufficient to produce an acceptable SNR. Analog

signals from all three regions are converted into digital form and processed digitally to select the signal from the region offering the best SNR for each pixel.

The CCD design allows a variable number of subpixel elements to be aggregated into single pixels as they are read from the CCD. In the VIIRS sensor this capability will be used to generate pixels with near-rectangular sample spacing on the ground. To accomplish this, many different aggregation modes will be used during the course of the crosstrack sensor scan. Since the subpixel aggregation is an additive process, the total number of subpixels aggregated to create each pixel appears as a factor in the radiometric gain of the pixel.

## 2.6.2 VIIRS Imagery Band Selection Process

Bands selection for the Raytheon VIIRS sensor design is based upon the strength (strong and/or weak) of three components that make up the signatures of each feature. These component are: (a) surface radiance which includes temperature and emissivity or solar reflectivity, (b) cloud absorptivity or reflectivity, and atmospheric transmissivity. Examples of these features in several VIIRS channels are shown in Figure 2.

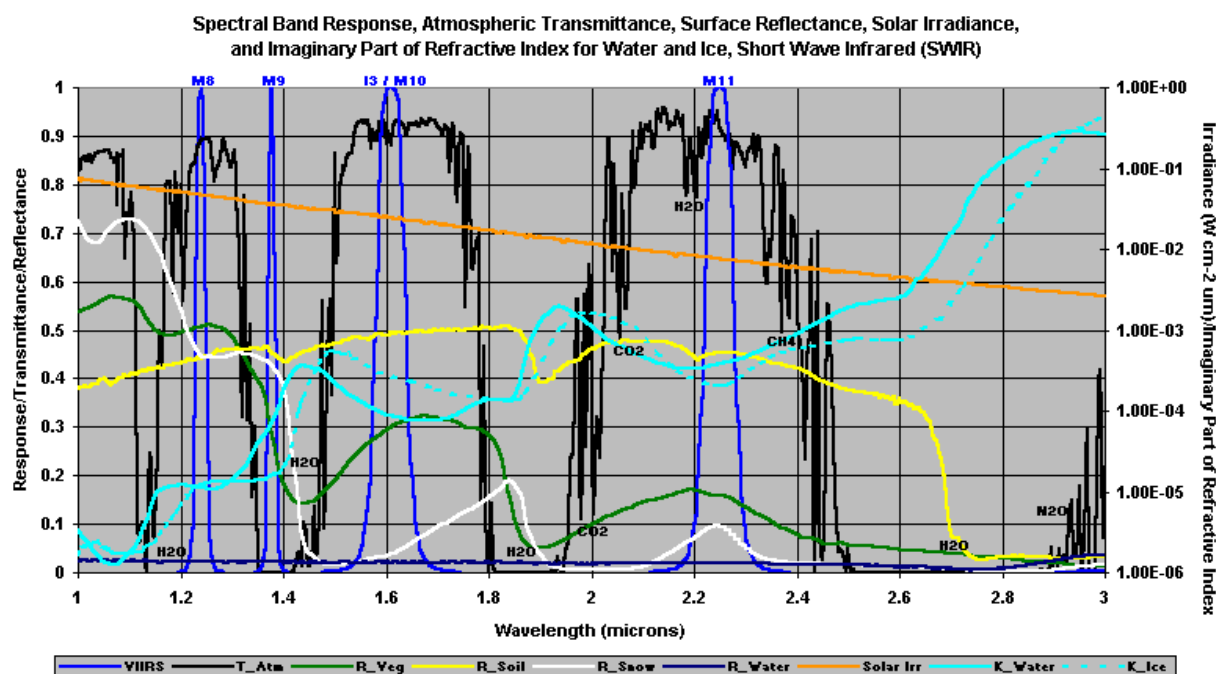


**Figure 2. Reflectivity, absorptivity, and transmissivity of atmosphere, surface, and clouds in the Short-Wave Infrared (SWIR).**

Figure 2 shows the band positions for VIIRS channels M8, M9, I3/M10, and M11 (---) along with atmospheric transmittivity (---), reflectivity of vegetated (---) and bare soil (---) ice (white) and water surfaces (---), solar irradiance (gold), and imaginary components of the index of refraction for water (---) and ice (---).

The positive identification of clouds in multispectral imagery requires that the analyst understand and exploit the properties of water droplets and ice crystals, along with the spectral characteristics of different backgrounds in VIIRS imagery and imagery-assist bands. A discussion of the phenomenology associated with the features follows along with the definition of bands selected to meet VIIRS threshold and objective requirements for the application-related products.

### 2.6.3 Daytime Visible Band (DV)

The Daytime Visible band (DV) was explicitly required by the VIIRS SRD. Unlike the DNB, the Measurement Range and Measurement Uncertainty requirements are determined by the application-related requirements on manually generated cloud data and sea ice data. Flowdown of application-related requirements to DV band requirements was performed to establish the spectral response and noise requirements for the DV band (Hutchison, 1998).

The Raytheon daytime visible imagery band (I1) is centered at 0.64 microns. The justification for this selection is shown in Figure 3.

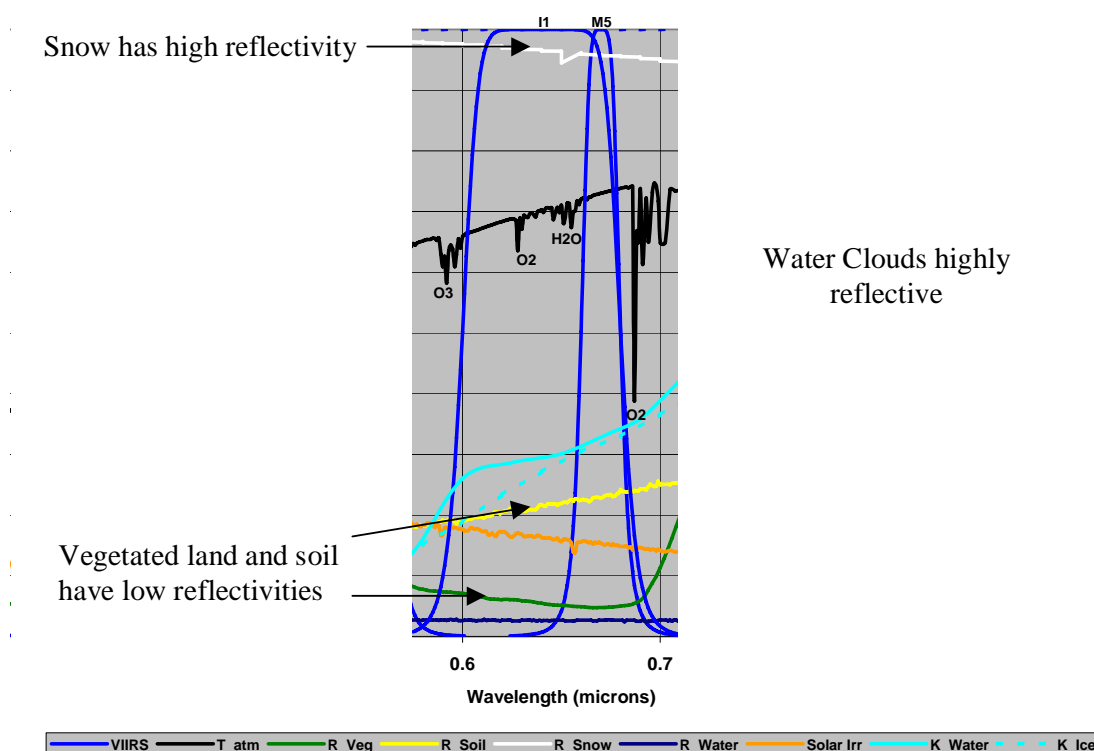


**Figure 3. Phenomenology of the VIIRS Daytime Visible (DV) Imagery band, centered at 640 nm.**

Figure 3 shows the location and spectral response function for the daytime visible band (I1), along with the characteristics of the Earth-atmosphere system. It is clear that the reflectivity of vegetated land is very small in this band but it begins to increase quite rapidly at ~ 0.7

microns. By limiting the long wave response of the band to  $< 0.7$  microns, we also avoid the water vapor absorption lines in the 0.7-0.8 micron region which could cause variations in cloud and land signatures. The reflectivity of water surfaces is even lower. On the other hand, the reflectivity of clouds is much larger which means this band is particularly valuable for discriminating between clouds and vegetated land and ocean surfaces. Additionally, the reflectivity of snow is very high. Therefore, this channel is not good for differentiating between snow and clouds nor is it particularly useful for identifying boundaries between land and ocean surfaces.

#### 2.6.4 Long-Wave Infrared Band (LWIR)

An infrared band is explicitly required by the VIIRS SRD. We have interpreted the requirement to be for a thermal infrared band, free of solar contamination, which we designate as the Long-Wave Infrared (LWIR). This interpretation is most consistent with OLS heritage. Unlike the DNB, the Measurement Range and Measurement Uncertainty requirements are determined by the application-related requirements on manually generated cloud data and sea ice data. Flowdown of application-related requirements to LWIR band requirements was performed to establish the spectral response and noise requirements for the LWIR band (Hutchison, 1998). The phenomenology of the 12 micron band used for flowdown is spectrally analogous to the 11.45 micron phenomenology. Therefore, the conclusions of our flowdown can be applied to the VIIRS LWIR imagery band at 11.45 microns.

The LWIR is explicitly required by the VIIRS SRD. Unlike the DNB, the Measurement Range and Measurement Uncertainty requirements are determined by the application-related requirements on manually generated cloud data and sea ice data. Flowdown of application-related requirements to LWIR band requirements was performed to establish the spectral response and noise requirements for the LWIR band (Hutchison, 1998).

Figure 4 shows the location and spectral response function for the VIIRS LWIR band (I5), along with the characteristics of the Earth-atmosphere system.

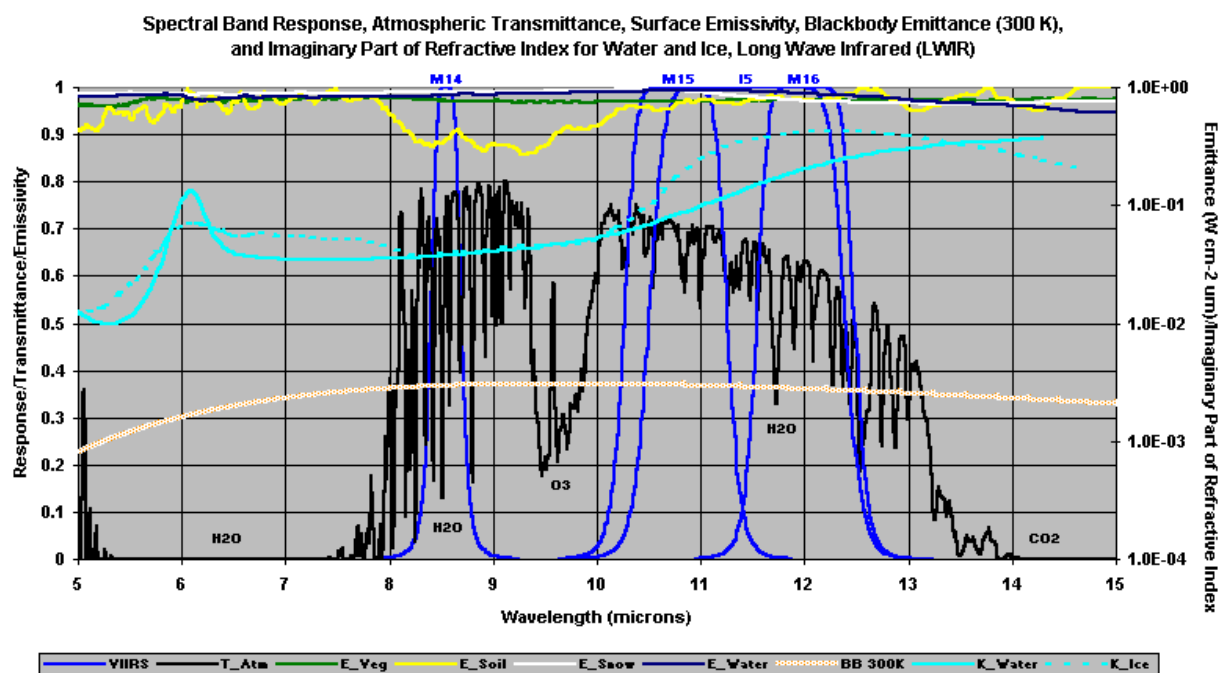


**Figure 4. Phenomenology of the VIIRS Long-Wave Infrared (LWIR) Imagery band, centered at 11.45 microns.**

Figure 4 shows the water vapor absorption across the LWIR band. The band is valuable for estimating the true radiating temperature of objects in the band after correcting for atmospheric water vapor attenuation, which makes the measured cloud top temperature slightly colder than its true radiating temperature. In addition, due to the high absorptivity of ice at these wavelengths, thin cirrus is often easily detected in nighttime conditions, when VIIRS data in the 1.378 micron band are not available.

## 2.6.5 Mid-Wave Infrared Band (MWIR)

Flowdown of application-related requirements has resulted in the specification of an additional imagery band in the Mid-Wave Infrared (MWIR), at 3.74 microns. The band, shown in Figure 5, is needed to meet the cloud typing requirement for the Cloud ARPs, i.e. distinguishing between cirrus and stratus in nighttime imagery (Hutchison, 1998).

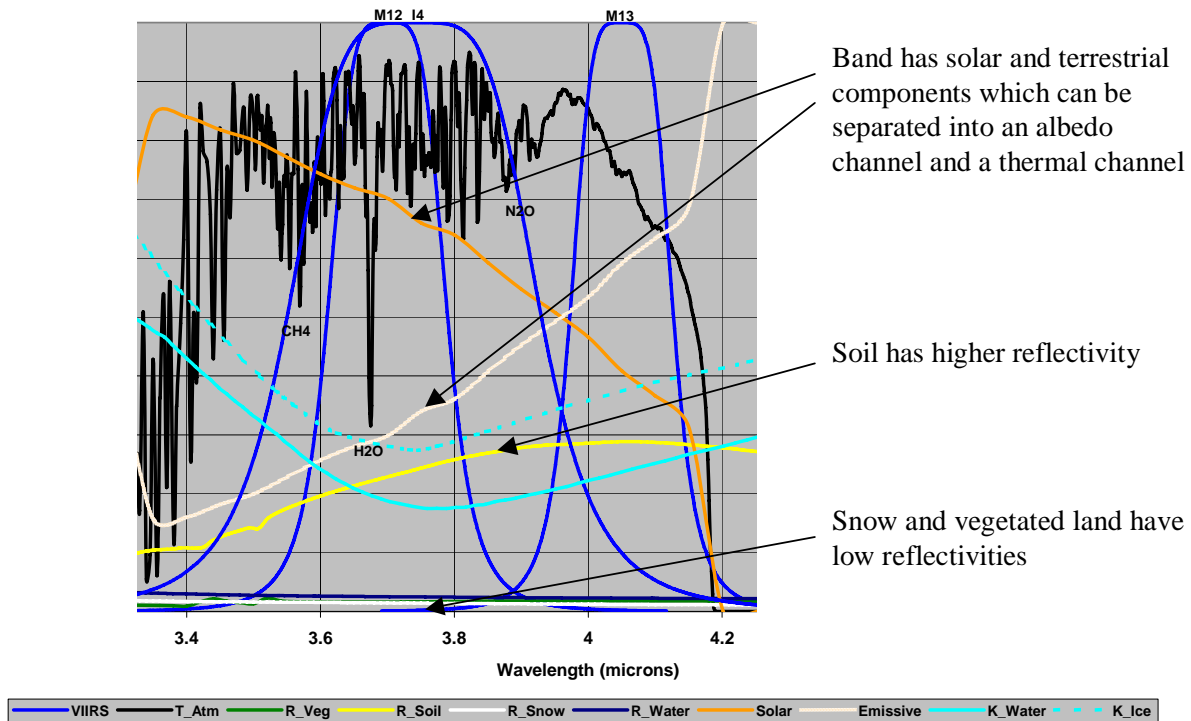


**Figure 5. Phenomenology of the VIIRS Mid-Wave Infrared (MWIR) Imagery band, centered at 3.74 microns.**

Figure 5 shows water vapor absorption lines in the VIIRS MWIR band (I4). The figure also shows that the reflectivity of snow is very low while that of clouds is much larger. It also shows that considerable solar irradiance is present while the reflectivity of bare soil is relatively large compared to snow and vegetation. Therefore, the MWIR band could be useful for differentiating between snow and clouds as well as clouds and vegetated land. However, distinction between cloud and bare soil appears difficult and the presence of terrestrial energy complicates the contrast between snow and clouds.

The VIIRS sensor requirements for the Cloud ARPs were established using a series of simulations for the following cases.

Case 1: Stratus at Night

Case 2: Daytime and Nighttime Cirrus

Case 3: Cloud Typing (Stratus versus Cirrus)

Case 4: Cumulus

Case 5: Daytime Obscurations

The simulations assumed the minimum of number of imagery bands as required by the VIIRS SRD, i.e. one for daytime visible, one nighttime visible, and one infrared imagery band. While completing the initial set of simulations, it was determined that differentiating between nighttime stratus and cirrus clouds was not possible without the MWIR band, i.e. Case 3 results did not meet specifications. Thus, the MWIR band was added to the minimum “sensing” requirement for VIIRS imagery. With the MWIR band added, Case 1 and Case 2 were re-analyzed using the brightness temperature differences (BTD) between the MWIR and LWIR imagery bands. The addition of the bi-spectral signatures of these clouds in the BTD imagery reduced the Raytheon VIIRS sensor noise model specifications necessary to meet threshold requirements. In addition, in Case 4, the daytime MWIR imagery was broken into thermal and albedo components as described in the literature (Hutchison et al., 1997) and used to differentiate between cumulus and snow fields along with stratocumulus over deserts conditions. Detection of cumulus clouds over other backgrounds is trivial. Finally, the simulations were completed for Case 5 to establish that an optical depth of aerosol greater than 1 is required for detection with the LWIR imagery band.

While the daytime MWIR imagery channel contains both solar and thermal energy, the capability has been demonstrated to separate this single channel into two channels and thus improve the discrimination between features in the spectral band. This process has been described in the literature (Hutchison et al., 1997). Use of the derived albedo channel significantly enhances the contrast between snow and water clouds. In fact the procedure also sufficiently enhances the contrast between snow and cirrus (ice) clouds so that snow can be observed through overcast cirrus cloudy conditions. Furthermore, the VIIRS flowdown process demonstrated that the thermal channel proves highly effective at differentiating between water clouds and bare soil. Finally, the nighttime MWIR band image can be widely used for detection and identification of nighttime stratus, especially when coupled with the VIIRS LWIR band.

### 2.6.6 Additional Imagery Bands

The VIIRS SRD specified that the spectral bandpasses required to meet the threshold requirements for the manually-generated Cloud ARPs must be at the “imagery” resolution.

The flowdown of these requirements determined that only three spectral bands were required to meet the threshold requirements in addition to the VIIRS DNB. These bands included the I1, I4, and I5 Imagery bands with bandpasses in the 0.65-, 3.75-, and 12-micron regions (Hutchison, 1998). However, derived requirements for other VIIRS EDRs resulted in additional imagery bands being incorporated into the VIIRS design. These bands included:

(a) I2 Band: a near infrared (NIR) imagery band (0.86-micron) is available at the resolution of the Imagery bands, because of non-Imagery EDR requirements. It is useful to improve performance of the sea ice data application-related products (c.f. Section 3.5.4) and allows NPOESS to produce high resolution vegetation index products.

(b) I3 Band: A short wave infrared (SWIR) imagery band (1.6-micron) is available at the resolution of the Imagery bands, because of non-Imagery EDR requirements. It is useful as a snow-ice/cloud discriminator and was needed to support the estimation of sub-pixel snow cover.

### 2.6.7 Imagery Assist Bands

However, the Raytheon Cloud and Imagery Integrated Product Teams (IPTs) demonstrated the use of imagery bands with imagery-assist data or radiometric (M-band) data, collected at a more coarse resolution, to advance toward meeting objective requirements, especially for the Cloud Type ARP. A number of VIIRS bands are useful for Red-Green-Blue (RGB) color composite cloud analysis (c.f. Section 3.4.3.4). These include the imagery resolution bands at 0.865  $\mu\text{m}$  and 1.61  $\mu\text{m}$ , and the moderate resolution bands at 0.41  $\mu\text{m}$ , 1.38  $\mu\text{m}$ , 4.05  $\mu\text{m}$ , 8.55  $\mu\text{m}$ , and 10.76  $\mu\text{m}$ . More details are available on the use of Imagery Assist with Imagery bands, as described in Appendix A to this ATBD, which became the basis for a book called “VIIRS – A New Operational Cloud Imagery (Hutchison and Cracknell, 2006).

## 2.7 RETRIEVAL STRATEGY

### 2.7.1 Explicit Imagery

The VIIRS EV\_375M and EV\_DNB SDRs is produced from the VIIRS RDRs by an RDR to SDR conversion. They are produced as image pixels separated by the Horizontal Reporting Interval (HRI). A process of sampling and aggregation will achieve an HRI roughly equivalent to the Horizontal Spatial Resolution (HSR).

Details of this process are found in the VIIRS Sensor Specification Document [PS 154640-101] and the VIIRS Build SDR Module Level Software Architecture document [Y2479], and is further discussed in Section 3.2.5.

### 2.7.2 Top-of-Atmosphere Radiance

Calibrated top-of-atmosphere (TOA) radiance for all imagery bands will be produced in the Build-SDR module, following the system standards for VIIRS SDRs. An overview of the



process is given in Section 3.2.1. A full description of the process is documented in the VIIRS Radiometric Calibration ATBD [Y3261], the VIIRS Build SDR Module Level Software Architecture Document [Y2479] and the VIIRS Radiometric Calibration and Validation Plan [TP 154640-118].

### 2.7.3 Top-of-Atmosphere Reflectance

Digital numbers (DNs) in the daytime visible (DV) and daytime/nighttime visible (DNB) imagery band RDRs will be converted to top-of-atmosphere radiance, as described in the VIIRS Radiometric Calibration ATBD [Y3261].

### 2.7.4 Equivalent Blackbody Temperature

DNs in the Mid-Wave Infrared (MWIR) and Long-Wave Infrared (LWIR) imagery band RDRs will be converted to equivalent blackbody temperature, as described in the VIIRS Radiometric Calibration ATBD [Y3261].

### 2.7.5 Near Constant Contrast (NCC) Visible Imagery

The NCC visible imagery EDR will be generated from Daytime/Nighttime Visible Band (also called Day/Night Band or DNB) data. Calibrated top-of-atmosphere radiances in the 0.5-0.9  $\mu\text{m}$  band will be taken and converted to albedo to produce the NCC imagery. A description of the algorithm will be given in Section 3.3.

### 2.7.6 Manually-Generated Cloud Data

Our system solution produces radiance, reflectance, and equivalent blackbody temperature that are sufficient for an analyst to generate the cloud data products.

### 2.7.7 Sea Ice Data

Automated algorithms were used to flowdown the imagery requirements for the manually-generated ice edge location and ice concentration ARPs. Although these algorithms are not used to address the Imagery ARP requirements, they function in the Snow/Ice Module, as an integral part of the software architecture for producing Snow/Ice EDRs as well as Imagery Sea Ice ARPs [Y2477].

A description of the algorithm and its data flows will be given in section 3.5.

## 3.0 ALGORITHM DESCRIPTION

### 3.1 OVERVIEW

The imagery algorithm consists of four major processing functions:

1. The Explicit Imagery process
2. The NCC imagery product process
3. The manual cloud analysis product process
4. The sea ice data product process.

### 3.2 EXPLICIT IMAGERY PRODUCTION

#### 3.2.1 Processing Outline

VIIRS SDRs are computed from the VIIRS RDRs, as part of the Build-SDR module, which applies geolocation and calibration to the RDRs. The functionality of the Build-SDR module will allow it to produce SDRs which fully meet the explicit imagery requirements. The VIIRS EV\_375M SDR contains the TOA radiance for bands I1, I2, I3, I4, and I5, the TOA reflectance for bands I1, I2, and I3, and EBBT for bands I4, and I5, with associated geolocation and band quality flags. The Imagery algorithm obtains this data, and writes it to an output Imagery EDR file. The VIIRS EV\_DNB SDR contains the TOA radiance and TOA reflectance for the DNB. The Imagery algorithm obtains this data, and writes it to the Imagery EDR file. The process is documented in the Build-SDR Module Level Software Architecture Document [Y2479], the VIIRS Radiometric Calibration ATBD [Y3261], and the VIIRS Imagery Unit Level Detailed design Document [Y3273].

#### 3.2.2 Algorithm Input

The SDR algorithm requires the VIIRS RDRs for each imagery band. These RDRs are created by the ingest function of the NPOESS Interface Data Processor Segment (IDPS). The process is described in the Build-RDR Module Level Software Architecture Document [Y2478]. The Explicit Imagery algorithm requires the VIIRS SDRs for imagery resolution data (EV\_375M) and DNB data (EV\_DNB).

##### 3.2.2.1 VIIRS Data

The required VIIRS data are the VIIRS RDRs, which contain the basic DNs to be converted into radiance or reflectance by applying calibration coefficients. The calibration coefficients themselves are stored in calibration LUTs ([Y2490], [Y3261]).

##### 3.2.2.2 Non-VIIRS Data

No non-VIIRS data are required for the generation of Explicit Imagery.

### 3.2.3 Theoretical Description

The production of TOA radiance from application of calibration coefficients, TOA reflectance, and equivalent blackbody temperature is discussed in the VIIRS Radiometric Calibration ATBD [Y3261].

### 3.2.4 Archived Algorithm Output

The RDR to SDR process creates TOA radiance in all imagery bands, TOA reflectance in the daytime visible and daytime/nighttime visible bands, and equivalent blackbody temperature for the Mid Wave IR band and the Long Wave IR band. The Imagery algorithm stores these as fields in an Imagery EDR HDF file. All Explicit Imagery products shall be calibrated, geolocated, and reported for a set of earth locations forming an approximately rectangular lattice. The lattice spacing will be 742 meters +/- 5% for the DNB, and approximately equivalent to the HSR for the other imagery bands.

### 3.2.5 Performance of Explicit Imagery

The Explicit Imagery is obtained from the VIIRS EV\_375M SDR and the VIIRS EV\_DNB SDR. The SDRs are obtained from VIIRS RDRs by an RDR to SDR process. The RDRs are obtained by a rotating telescope scanning mechanism that minimizes the effects of solar impingement and scattered light. Figure 6 illustrates the design concept for VIIRS, designed and built by Raytheon Santa Barbara Remote Sensing (SBRS). VIIRS is essentially a combination of SeaWiFS foreoptics and an all-reflective modification of MODIS/THEMIS aft-optics. Calibration is performed onboard using a solar diffuser for short wavelengths and a blackbody source and deep space view for thermal wavelengths. A solar diffuser stability monitor (SDSM) is also included to track the performance of the solar diffuser. The VIIRS scan will extend to 56 degrees on either side of nadir, providing a swath of 3000 km for the nominal satellite altitude of 833 km.

The VIIRS SRD places explicit requirements on spatial resolution for the Imagery EDR. Specifically, the horizontal spatial resolution (HSR) of bands used to meet threshold Imagery EDR requirements must be no greater than 400 m at nadir and 800 m at the edge of the scan. This led to the development of a unique scanning approach which optimizes both spatial resolution and signal to noise ratio (SNR) across the scan. The concept is summarized in Figure 7 for the imagery (fine resolution) bands. The VIIRS detectors are rectangular, with the smaller dimension along the scan. At nadir, three detector footprints are aggregated to form a single VIIRS “pixel.” Moving along the scan away from nadir, the detector footprints become larger both along track and along scan, due to geometric effects and the curvature of the Earth. The effects are much larger along scan. At 31.59 degrees in scan angle, the aggregation scheme is changed from 3x1 to 2x1. A similar switch from 2x1 to 1x1 aggregation occurs at 44.68 degrees. The VIIRS scan consequently exhibits a pixel growth factor of only 2 both along track and along scan, compared with a growth factor of 6 along scan which would be realized without the use of the aggregation scheme. This scanning approach allows VIIRS to provide imagery at 800-m resolution or finer globally, with 375-m resolution at nadir. Additionally, due to the imagery requirements for VIIRS and the “sliver” detector design, MTF performance will be extremely sharp (0.5 at Nyquist).

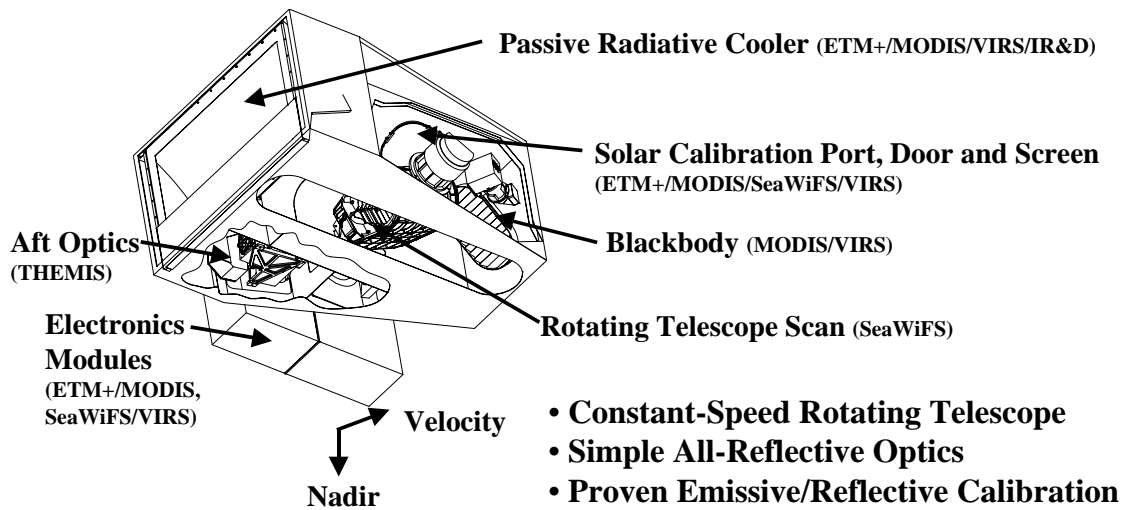


Figure 6. Summary of VIIRS design concepts and heritage.

## **Fine-Resolution Bands for Imagery**

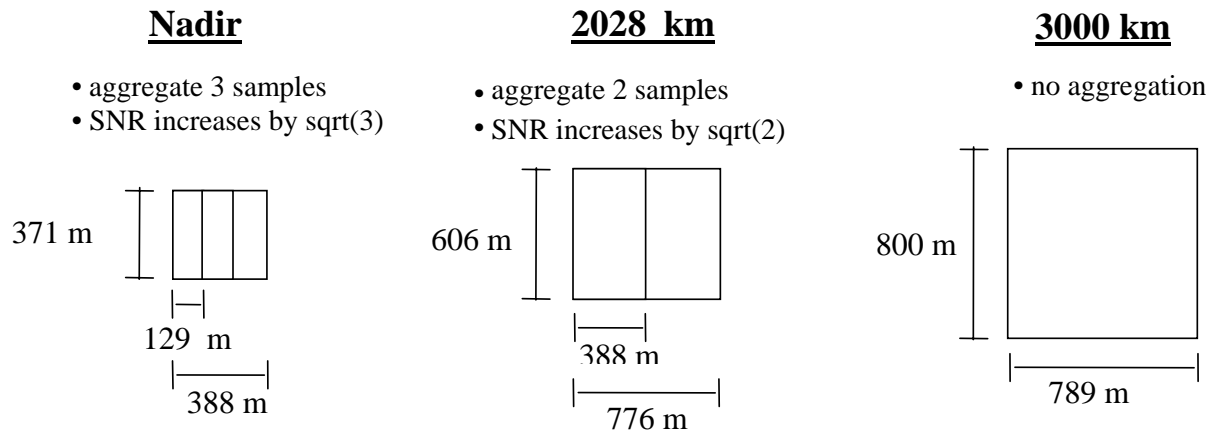
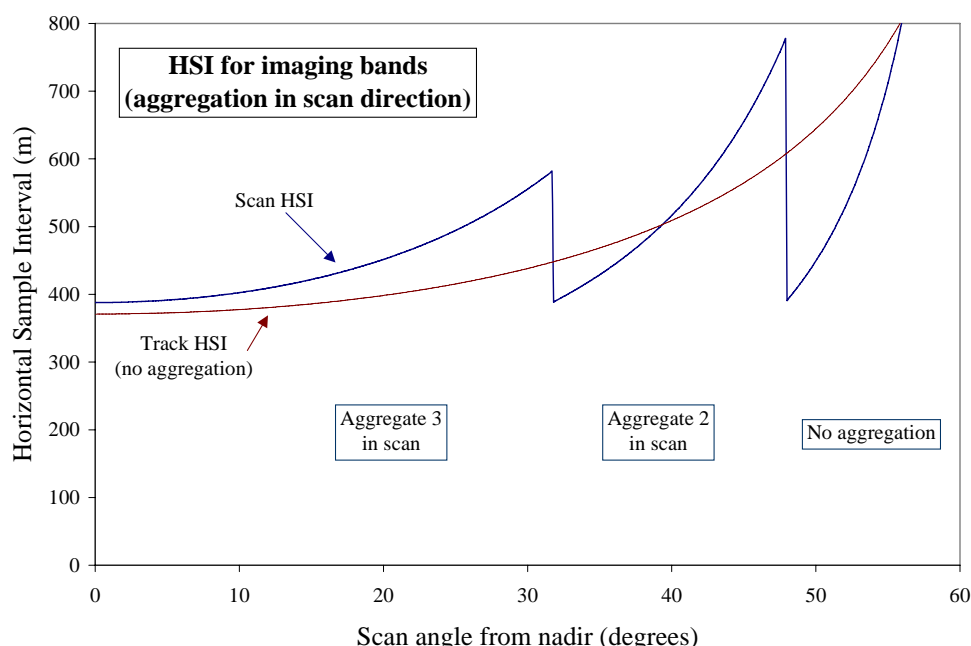


Figure 7. VIIRS detector footprint aggregation scheme for building Imagery “pixels”.

Figure 8, showing the Horizontal Sampling Interval (HSI) that results from the combination scan/aggregation scheme, illustrates the benefits of the aggregation scheme for spatial resolution.



**Figure 8. Horizontal Sampling Interval (HSI) for imagery bands (aggregation in scan direction).**

The HRI of the Daytime Visible (DV), Long-Wave Infrared (LWIR) and Mid-Wave Infrared (MWIR) imagery will be the HSI. The Modulation Transfer Function (MTF) specification is 0.5 at the sampling Nyquist frequency, resulting in HSR equal to HSI. Therefore, the specification for HRI is equivalent to the imagery HSR specification.

Even though the aggregation scheme greatly reduces the growth in HSI across the scan, there is still a factor of 2 growth resulting in a residual “bow tie” effect. We achieve an additional reduction in the bow tie by deleting 4 of the 32 detectors from the output data stream for the middle (Aggregate 2) part of the scan and 8 of the 32 detectors for the edge (No aggregation) part of the scan. Figure 9 illustrates the resultant additional bow tie deletion.

The sensitivity performance of the VIIRS imagery bands (c.f. Table 8 in Section 2.5) exceeds the Measurement Uncertainty specifications listed in Table 2 with margins > 30%.

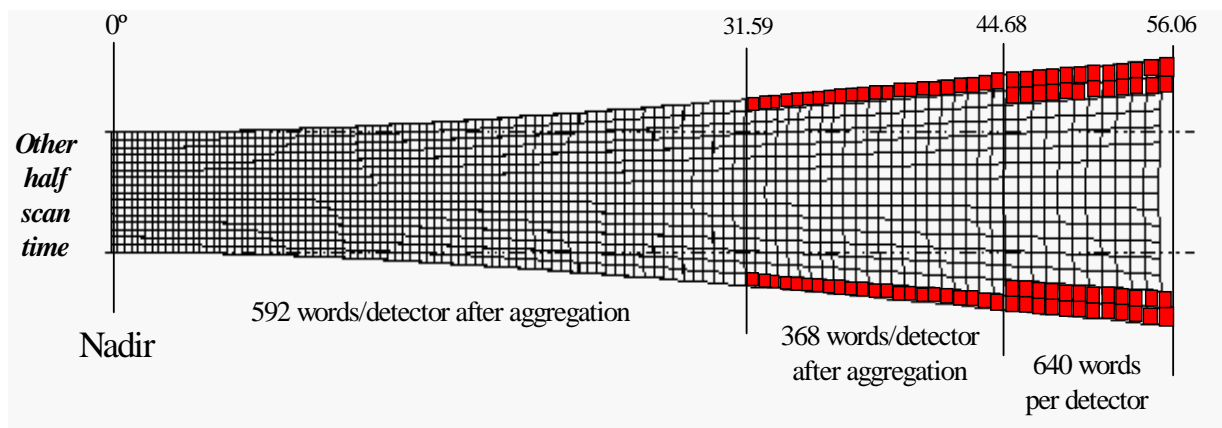


**Figure 9. VIIRS aggregation and bow tie pixel reduction.**

### 3.2.5.1 Daytime/Nighttime Visible Band

The TOA radiance and TOA reflectance are produced over the entire operating range of the DNB. The SNR performance of the DNB at nadir is shown in Figure 10. The performance at edge of scan is shown in Figure 11.

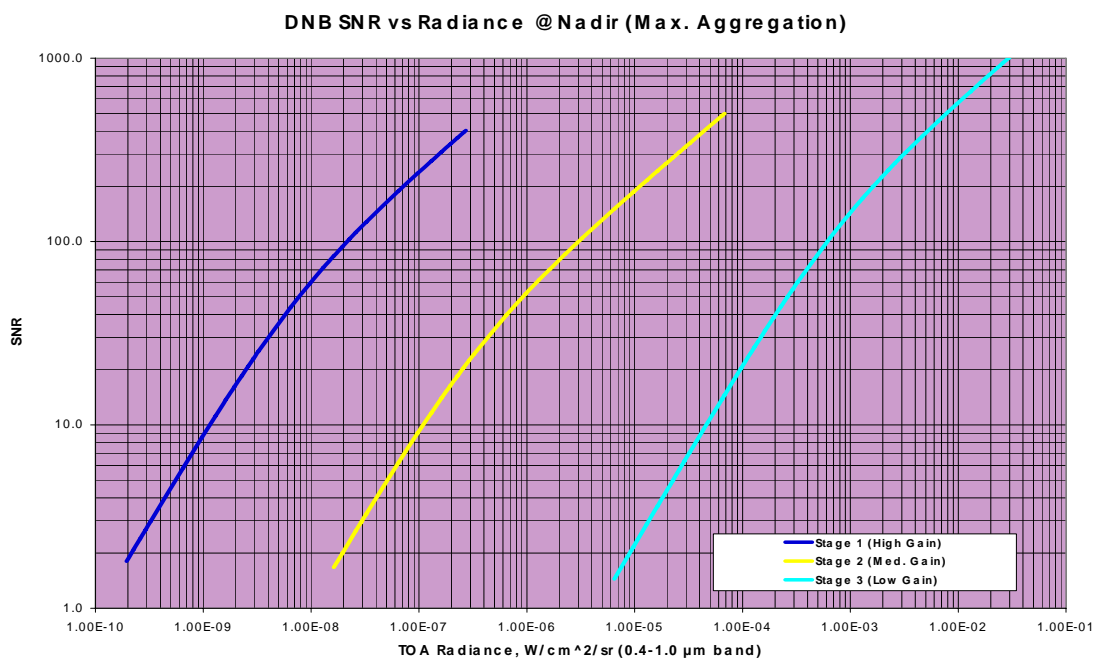


**Figure 10. Signal-to-noise performance of the Daytime/Nighttime Visible Imagery Band at nadir, for each of the three CCD gain stages. SNR performance over the specified measurement range ( $4.E-9$  –  $3.E-2$   $W/cm^2/sr$ ) is 30 to 1000. SNR greater than 3 is achieved at a radiance as low as  $3.2E-10$   $W/cm^2/sr$ .**

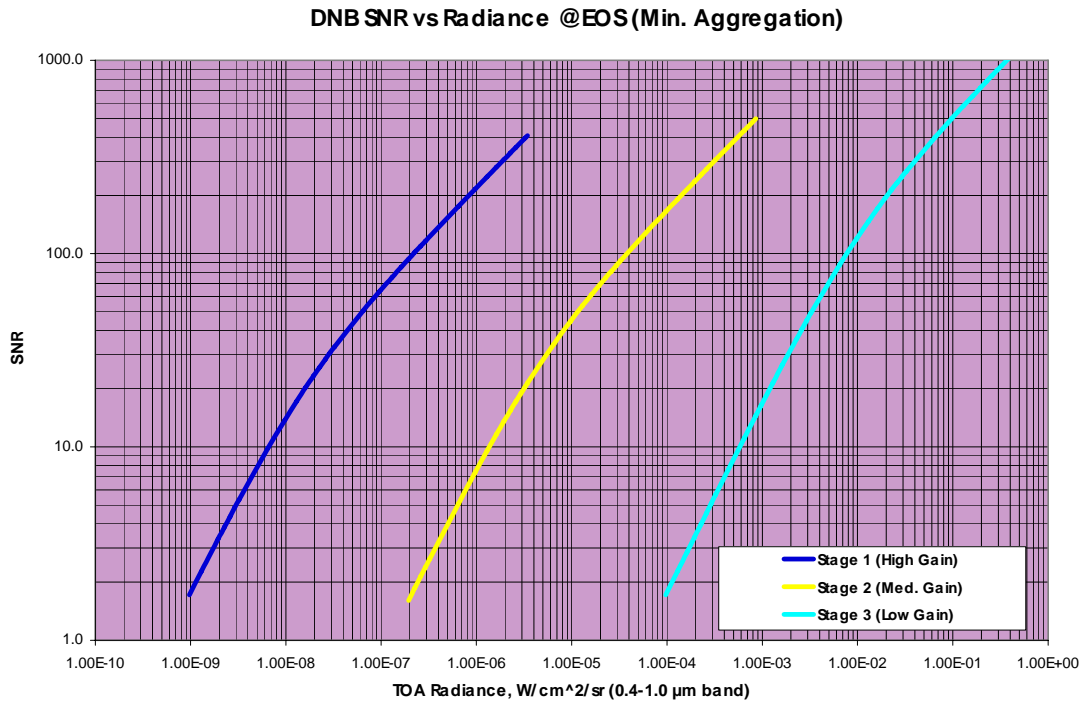


**Figure 11. Signal-to-noise performance of the Daytime/Nighttime Visible Imagery Band at edge of scan, for each of the three CCD gain stages. SNR performance over the specified measurement range ( $4.E-9 - 3.E-2 \text{ W/cm}^2/\text{sr}$ ) is 7 to 250. SNR greater than 3 is achieved at a radiance as low as  $1.8E-9 \text{ W/cm}^2/\text{sr}$ .**

The spectral response of the DNB has been designed to operate efficiently under lunar illumination conditions, as shown in Figure 12.

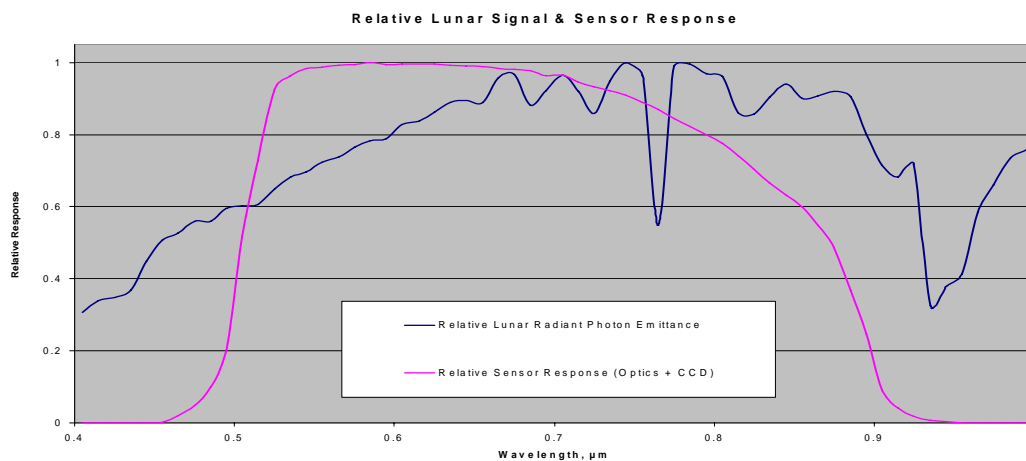


**Figure 12. Spectral Response of the Daytime/Nighttime Visible Imagery band, compared with the lunar signal.**

The spectral response of the DNB is designed to decline sharply at 0.5 microns, as can be seen in Figure 12. The purpose of the short-wave cut-off is to reduce contamination by atmospheric path radiance, which is more pronounced at shorter wavelengths. The design is compatible with OLS heritage.

SNR performance at night will vary with lunar phase, lunar elevation angle, and scan angle. An example for quarter moon phase is shown in Figure 13.

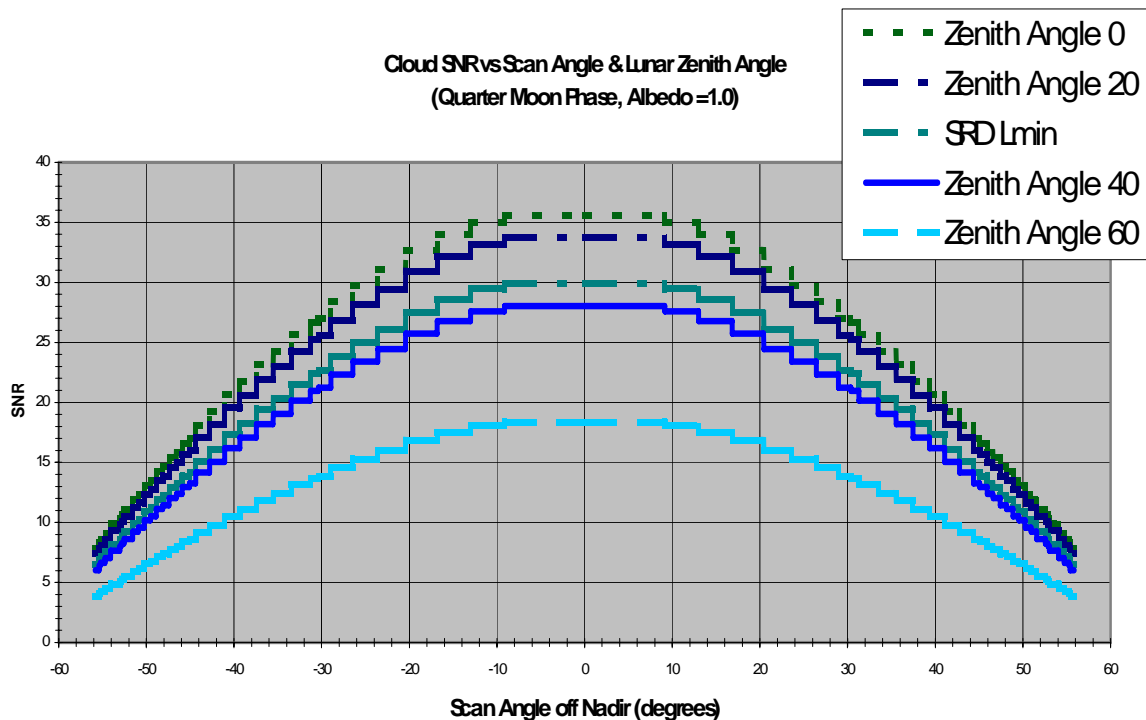


**Figure 13. SNR Performance of the Daytime/Nighttime Visible Imagery under quarter-moon illumination conditions, as a function of scan angle.**

The top two curves and bottom two curves represent lunar zenith angles of 0, 20, 40, and 60 degrees respectively. The middle curve corresponds to the minimum measurement range of  $4\text{E-}9 \text{ W/cm}^2/\text{sr}$ . SNR greater than 10 is achieved at the minimum radiance for almost the entire scan. SNR as high as 30 is achieved at the minimum radiance for a nadir view.

### 3.2.5.2 Other Imagery Bands

Performance characteristics for the Daytime Visible (DV), Long-Wave Infrared (LWIR), and Mid-Wave Infrared (MWIR) imagery bands meet specifications with comfortable margin (c.f. Figure 9, Table 7, and Table 8).



### 3.3 NCC VISIBLE IMAGERY PRODUCTION

#### 3.3.1 Processing Outline

This section describes the NCC Imagery EDR ground processing algorithm. The NCC algorithm takes calibrated and geolocated radiance as input. Thus, before the algorithm can be executed, a preprocessing step must be taken to convert the RDR to SDR [Y3261].

##### 3.3.1.1 Baseline Approach – Gain Management Algorithm

Our baseline approach is to adapt the OLS processing algorithm for terminator imagery. We have chosen this approach to ensure operational continuity between the DMSP and NPOESS missions.

The OLS terminator imagery is produced by a Gain Management Algorithm (GMA). The algorithm has been in use since the early 1980s. It is implemented by the OLS on-board analog signal processor (ASP). The function of the GMA is to adjust the on-board analog gain to compensate for the variable source signal radiance. The variable digital gain amplifier (VDGA) operates in the ASP. A detailed description of the process can be found in the OLS Technical Operating Report (Westinghouse, 1993). Summarizing from the report:

*“During active scan, the along scan gain control (ASGC) software controls the gain value presented to the VDGA. The computations performed for this control depend upon the spacecraft elevation, azimuth, and altitude, and the OLS scan angle. This computation produces the scene source elevation angle used to obtain a gain value from the gain value versus scene source elevation (GVVSSE) table. Thus, the software will cause the VDGA gain to follow the GVVSSE curve as defined by the GVVSSE table values.”*

Figure 14, created from data in the OLS Technical Operating Report, illustrates a typical GVVSSE curve.

BRDF corrections are applied as adjustments of the elevation angle in the GVVSSE table. There is a comparable table (GVVSLE) for a lunar source signal. Lunar BRDF and lunar phase corrections are applied as adjustments of the elevation angle in the GVVSLE table. The function of the GMA is to adjust the OLS ASP gain so that a signal from a reflecting surface (cloud or ground) with an albedo of 0.8 and the modeled BRDF will produce a 5 volt output signal from the L channel ASP. The GMA was designed to accommodate the capabilities of late 1970s processors, and is implemented on board the OLS. The implementation of the VIIRS NCC algorithm will occur on the ground, within the NPOESS IDPS. This approach will provide the flexibility to make algorithm and LUT modifications easily via ground software changes, and will take advantage of the superior computational capability of the IDPS. Our approach will preserve the OLS heritage by using LUTs that capture the gain and BRDF corrections applied on board the OLS.

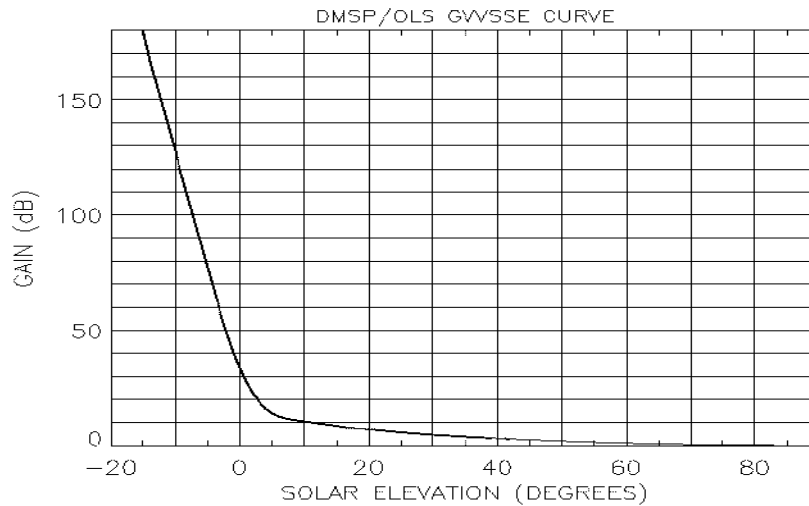


**Figure 14 – Typical Gain Value Versus Scene Source Elevation (GVVSSE) Curve for OLS on board variable gain control. The curve is designed so that a source with an albedo = 0.8 produces a 5 volt output signal from the L channel analog signal processor (Reference: OLS Technical Operating Report, March 1993).**

The VIIRS implementation operates as follows:

- 1) Read the 5 pre-constructed LUTs into memory. These are the GVVSSE LUT, the Solar BRDF LUT, the GVVSLE LUT, the Lunar BRDF LUT, and the Aerosol Correction LUT. Detailed descriptions of the LUTs can be found in [Y3273].
- 2) Obtain DNB TOA radiance from the VIIRS EV\_DNB SDR. The TOA radiance is stored as a 2-d array corresponding to each DNB pixel.
- 3) Obtain latitude/longitude, solar, lunar, and viewing angles, and lunar phase from the SDR.
- 4) For pixels where the solar source radiance is sufficient (determined by solar zenith angle), compute solar source radiance, using information in the GVVSSE and Solar BRDF LUTs.
- 5) For pixels where the lunar source radiance is sufficient (determined by lunar zenith angle), compute lunar source radiance, using information in the GVVSLE and Lunar BRDF LUTs.
- 6) If selected by a pre-set switch contained in the Aerosol Correction LUT, compute the expected path radiance at each pixel, using the Aerosol Optical Thickness IP and the Aerosol Correction LUT as input data. This step will require improved radiative transfer modeling, and in the baseline implementation, the switch is currently set to off..

- 7) Convert the observed TOA radiance at each pixel to albedo, using the solar source radiance, the lunar source radiance, and optionally the path radiance.
- 8) Write the albedo to the Imagery EDR file, along with quality flags.

The process flow for the algorithm is illustrated in Figure 15. The process flow operates on each DNB pixel.

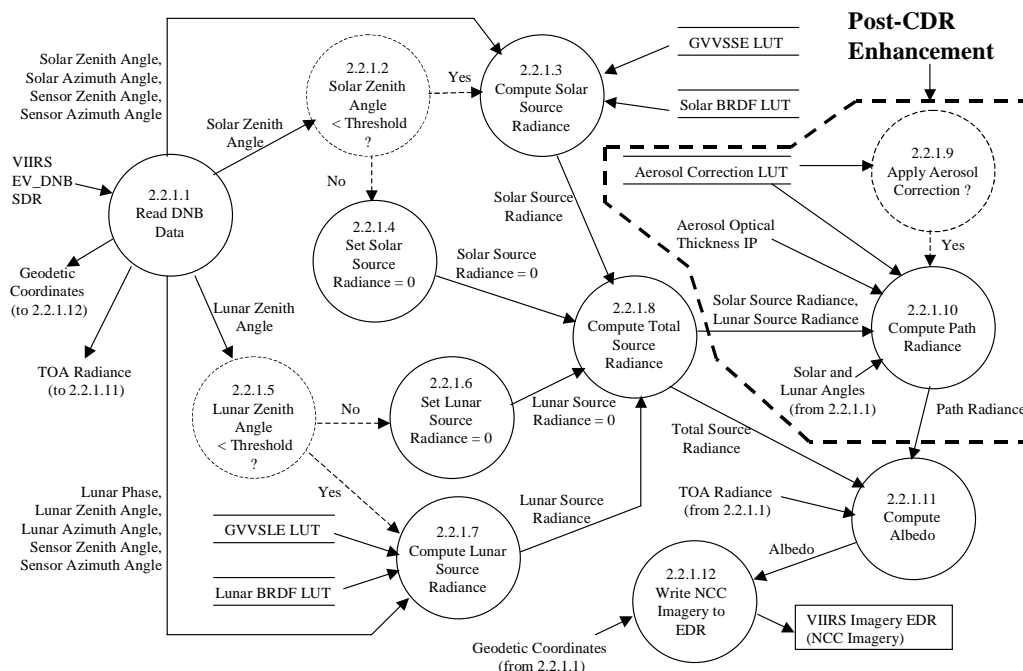


Figure 15. Process flow for the NCC Imagery algorithm.

### 3.3.1.2 Enhanced Algorithm Approach - Atmospheric Correction

As there are no explicit performance metrics for the NCC Imagery EDR, there is no requirement to provide NCC imagery that exceeds the performance of the OLS approach. However, there is value to the operational community in providing an NCC product superior to the terminator imagery currently provided by OLS. During Phase I, we developed an alternative NCC algorithm that promises to provide a superior NCC product. During Phase II, we have integrated the alternative algorithm with the OLS-based approach by adding step 6 to the common process flow. Implementation of steps 1-5 and 7 constitutes the OLS-based approach. Implementation of step 6 constitutes a post-CDR pre-planned product improvement (P<sup>3</sup>I). Implementation of all 7 steps constitutes the alternative approach of Phase I, as documented in the version 3 ATBD. The version 5 algorithm for NCC Imagery therefore preserves the OLS operational heritage and provides a framework for future implementation

of an atmospheric correction enhancement, when this is made feasible by improvements in radiative transfer models. When solar zenith angle is greater than 89.0 degrees, MODTRAN simulation (including version 4.0 and all previous versions) does not produce accurate TOA radiance. That is, the radiances calculated from MODTRAN are all the same for any surface conditions (i.e., from black surface with zero albedo to complete reflective surface with 1.0 albedo) and clouds. Thus, there is no cloud or surface signal in the simulated TOA radiance. A better RT model for the solar zenith angle range between 90 to 105 degrees is required for full implementation of the atmospheric correction enhancement to the algorithm. Alternatively, the atmospheric correction data could be derived from empirical measurements. The preferred approach remains to be determined. Although the OLS gain tables include zenith angles as large as 105 degrees, the solar signal will be smaller than the minimum of the DNB measurement range for solar zenith angle greater than 100 degrees. In practice, therefore, it is sufficient for the RT model to be accurate out to angles of 100 degrees. The atmospheric correction enhancement will also require that the GVVSSSE and GVVSSLE tables be revised to the VIIRS DNB specifications...

### 3.3.2 Algorithm Input

#### 3.3.2.1 VIIRS data

The algorithm requires the calibrated and geolocated day/night band radiance and the corresponding view/illumination geometry data. These are all supplied by the VIIRS EV\_DNB SDR. The optional atmospheric correction step also requires aerosol optical thickness, supplied by the VIIRS Aerosol Optical Thickness IP.

#### 3.3.2.2 Non VIIRS data

The algorithm requires five pre-constructed LUTs, described in [Y3273]. The GVVSSSE LUT will contain a solar gain function for a range of solar zenith angles (c.f. Figure 14). The GVVSSLE LUT will contain a lunar gain function for a range of lunar zenith angles, similar to the GVVSSSE function. The Solar BRDF LUT and Lunar BRDF LUT will contain BRDF correction factors, binned by zenith angle, viewing angle, and relative azimuth angle. The Aerosol Correction LUT will contain an atmospheric correction on/off switch and model path radiances, binned by AOT, source zenith angle, viewing angle, and relative azimuth angle. The Aerosol Correction LUT will be filled in the future, when feasible. The LUTs will be generated by the VIIRS Look up Table Generation Tool (LUTGT) [Y10810].

### 3.3.3 Theoretical Description

#### 3.3.3.1 Physics of the Problem

For decades, merged images (or “photo-mosaics”) were produced manually by “cut and paste” methods and by photo-manipulation. More recently, automated methods have been developed that compute the merged image. These methods typically create a new image on a line by line basis. Each line may take data from one image up to a given point; beyond that point, data comes from the second image. The region adjacent to the switchover point is called the “seam”.

An unintended feature of photo-mosaicing is the presence of visual artifacts that result from inherent differences between the two images that compose the merged image. The visual artifacts not only introduce potential confusion for the human analyst but can mask features of interest in the original images such as cloud type indicators or ice edge features. If one simply lines up two photos of the same scene taken at different times of day from the same vantage point and then cuts through the pair and tapes the opposite segments from the separate images together, one will immediately notice several artifacts. For example, if the contrast in one image does not match the contrast in the second or one is uniformly darker than the other (histogram mismatch), the analyst will notice an apparent edge at the seam joining the two halves. This seam is difficult to ignore since the eye responds preferentially to long straight features (e.g., edges, day/night texture changes, etc.).

Generically, artifacts can result from a number of inter-images differences. Some of these are content-related e.g., due to images taken at different times; some are sensor related, e.g., differences in dynamic range; some are platform-related, e.g., misregistration errors; and some result from a combination of content and platform e.g., uncorrected parallax errors. The algorithm must accomplish the seam-finding and image combination in such a way so as to minimize the introduction of artifacts and subsequently must minimize their visual impact.

A further occasion for artifacts occurs due to the special processing required for pixels lying within the solar terminator. For the purposes of this ATBD, we identify the terminator region as the zone that is neither astronomical night nor standard daytime. These pixels may be saturated in the high gain CCD stage while not being fully illuminated in the low gain stage. The choice of grayscale value for the image therefore must maintain available contrast without introducing confusing artifacts or false contrasts.

The NCC EDR does not correspond to a single consistent physical characteristic of the natural environment. The resultant data product is used to provide the analyst an image for visual interpretation. The product is derived from the DNB, which has a separate algorithmic production process that must conform to the system requirements. The requirements that pertain to the NCC EDR instead relate to its usability for manual interpretation.

The NCC EDR must adequately represent the surface and atmospheric (specifically, cloud) conditions across the terminator region to be analyzed without artifacts due to the significant radiance difference (on the order of  $1.e06$  to  $1.e07$ ).

Image quality in the terminator region is also degraded by atmospheric scattering. Because of the low sun angle, the radiation transmitted downward to a reflecting surface (cloud or ground) travels longer path lengths, thereby increasing the amount of path radiance relative to reflected radiance. This is undesirable, since the primary purpose of image analysis is to detect the reflecting sources. Excessive path radiance washes out the image. An example of this effect can be seen in Figure 16. In principle, atmospheric correction can remove the path radiance, thereby recovering the contrast between various reflecting surfaces. In practice, current RT models (e.g. MODTRAN 4.0) are not capable of achieving satisfactory path radiance removal in the terminator region (c.f. Section 3.3.1.2).

### 3.3.3.2 Mathematical Description of the Algorithm

The alternative algorithm of Phase I includes all of the planned processing steps, and therefore provides the most complete mathematical description.

The general procedures of the alternative algorithm can be expressed using the following:

- a) In the terminator region, the radiance of the day/night band (retrieved from the digital number using the calibration coefficients) is resultant from either solar or lunar illumination or both. If the lunar zenith angle,  $\theta_{\text{moon}} > \theta_{\text{moon\_max}}$ , it assumes that lunar radiance is zero. Currently  $\theta_{\text{moon\_max}}$  is set to the limit of the GVVSL, 105 degrees. Also at night, where  $\theta_{\text{sun}} > \theta_{\text{sun\_max}}$ , it assumes the solar radiance is zero. Currently  $\theta_{\text{sun\_max}}$  is set to the limit of the GVVSS, 105 degrees. Other sources of radiance (e.g. city lights) are not considered here. The combined radiance can then be expressed as the following:

$$L = L_{\text{sun}} + L_{\text{moon}} \quad (3.3.3.2.1)$$

- b) The radiance components can be decomposed to those from atmospheric path and those from the target (surface or clouds):

$$L = L_{\text{sun\_p}} + L_{\text{moon\_p}} + L_{\text{sun\_t}} + L_{\text{moon\_t}} \quad (3.3.3.2.2)$$

The target radiances,  $L_{\text{sun\_t}}$  and  $L_{\text{moon\_t}}$ , are the radiances on the ground or at the top of clouds.

- c) The path radiance reduction procedure is to remove the path radiance from the total radiance, i.e., subtract the total radiance by the path radiance simulated from model atmosphere. The resultant radiance becomes:

$$L' = L - (L_{\text{sun\_p}} + L_{\text{moon\_p}}) = L_{\text{sun\_t}} + L_{\text{moon\_t}} \quad (3.3.3.2.3)$$

Note that the path radiances are set to zero in the baseline approach.

- d) The normalization procedure is to divide this new radiance by the reference radiance of a reference surface

$$L_{\text{norm}} = L' / L_{\text{ref}} = (L_{\text{sun\_t}} + L_{\text{moon\_t}}) / (L_{\text{ref\_sun\_t}} + L_{\text{ref\_moon\_t}}) \quad (3.3.3.2.4)$$

Where:

$$L_{\text{ref\_sun\_t}} = \rho_{\text{sarf}} \cdot E_{\text{sun}} / \pi / G_{\text{sun}}(\theta_{\text{sun}}) \quad (3.3.3.2.5)$$

$$L_{\text{ref\_moon\_t}} = \rho_{\text{larf}} \cdot E_{\text{moon}} / \pi / G_{\text{moon}}(\theta_{\text{moon}}) \quad (3.3.3.2.6)$$

The solar BRDF lookup table provides the solar ARF,  $\rho_{\text{sarf}}$ , and the lunar BRDF lookup table provides the lunar ARF,  $\rho_{\text{larf}}$ . The GVVSSSE lookup table provides the solar gain function  $G_{\text{sun}}(\theta_{\text{sun}})$  and the GVVSSLE lookup table provides the lunar gain function  $G_{\text{moon}}(\theta_{\text{moon}})$ .

The GVVSSSE and GVVSSLE look up tables for the OLS system are empirically based. The baseline approach for NCC is to continue to use empirically based tables, since the MODTRAN RT model is not reliable for solar or lunar zenith angles near the terminator. Empirically based LUTs should be used until such time as a dependable RT model becomes available.

The significant radiance difference across the terminator due to illumination irradiance difference is normalized in  $L_{\text{norm}}$  and the resultant image product will present near constant contrast across the scene.

Atmospheric effects due to absorption and scattering by aerosols are included in the empirical solar and lunar gain functions. Since these functions represent averaged aerosol conditions, they do not allow for AOT dependent adjustments. The purpose of the atmospheric correction enhancement (c.f. Section 3.3.1.2) is to allow for removal of path radiance, which includes an AOT dependent adjustment through RT modeling. The model must include angularly dependent and AOT dependent path radiance and gain functions. The atmospheric correction enhancement is not enabled in the current version of the algorithm, because the Aerosol Correction LUT is empty. Because atmospheric correction is not activated, the mathematical description of the details of its radiative transfer is therefore deferred.

### 3.3.4 Archived Algorithm Output

The NCC algorithm output is a visible image at the resolution of the DNB Horizontal Reporting Interval of 742 meters +/- 5%. It will be stored in the Imagery EDR as a field in the Imagery HDF file, along with associated quality flags.

### 3.3.5 Performance of NCC Visible Imagery

#### 3.3.5.1 Baseline Algorithm

Our baseline algorithm is designed to capture the on board OLS GMA within the data processing architecture of the VIIRS Ground Segment. We therefore expect baseline radiometric performance to be comparable to that of the OLS process. Figure 16 is an example of typical OLS terminator imagery.

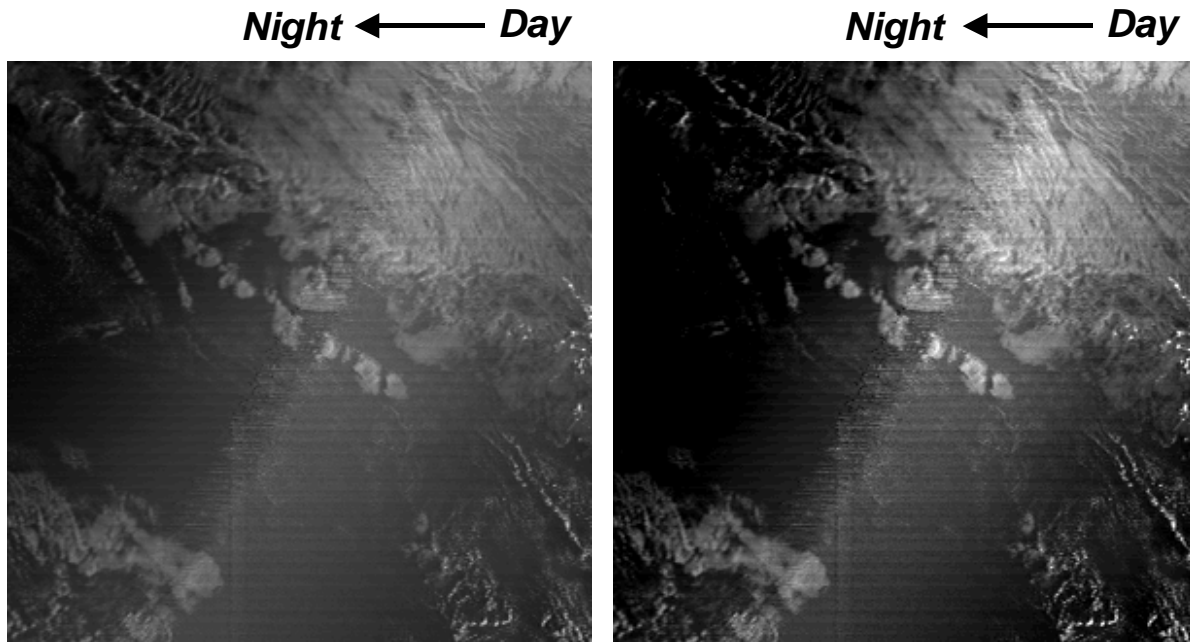


**Figure 16 – F13 OLS Visible (HRD) image for the first terminator crossing of the July 20, 2001 1131 UT orbit.**

The image in Figure 16 displays 300 SDS scan lines for a scan angle range of  $24^{\circ} - 47^{\circ}$ . The daytime/nighttime sides are indicated. The full dynamic range is displayed in the LEFT image. The RIGHT image is contrast-enhanced to highlight the terminator crossing effects (e.g., path radiance from atmospheric scattering). Figure 16 demonstrates how well the OLS algorithm works. Because the image processing occurs on board, we have no pre-processed image with which to compare it. The image shown in Figure 17 is a good indicator of how Figure 16 would appear if the OLS analog signal was not processed by the OLS GMA.

The NCC imagery will have a spatial resolution of 0.74 km everywhere in the swath. This is a significant improvement over the OLS terminator imagery, which has a spatial resolution of 2.7 km at nadir.

### 3.3.5.2 Atmospheric Correction Enhancement

The atmospheric correction algorithm is designed to improve the NCC imagery by removing the path radiance caused by atmospheric scattering. The analysis of algorithm performance performed during Phase I was based on MODTRAN 4.0 simulation. When the SZA is greater than  $89.0^{\circ}$  degrees, MODTRAN simulation (including version 4.0 and all previous versions) does not produce accurate TOA radiance. That is, the radiance calculated from MODTRAN is the same for any surface or cloud albedo. Thus, there is no cloud and surface signal in the simulated TOA radiance except for the path radiance which only changes with illumination and viewing geometry at given atmosphere.



For a noise-free simulation, the path radiance is 100% removed using the LUT because the simulated image and the LUT were generated using the same MODTRAN model. Therefore, when the SZA is greater than 89 degrees, the solar (path) radiance is completely removed and the retrieved image preserves the cloud and surface contrast. In a real situation, because the solar path radiance cannot be completely removed, the algorithm's performance in the region where SZA ranges from 89 to 100 degrees will of course not be as good as a simulated noise-free result.

An improved radiation transfer (RT) model for the SZA range between 90 and 100 degrees is required to test algorithm performance on real sensor data. We discuss this matter further in the section on algorithm initialization and validation (Section 3.3.6.3). Another option is to produce the path radiance LUT based on empirical measurements.

Also, the algorithm would need to be changed to allow for the dependence of  $L_{\text{ref}_{\text{sun}_t}}$  and  $L_{\text{ref}_{\text{moon}_t}}$  on aerosol optical thickness. Determining these dependences would also require either an improved RT model or empirical data to generate GVVSSSE and GVVSLLE that are a function of AOT. To implement this enhancement, it would also require that the NCC GMA be revised to allow for the effects of atmospheric attenuation. The current implementation does not have GVVSSSE and GVVSLLE dependence on AOT.

However, it is not necessarily desirable to remove the effect of aerosols, because aerosols (e.g. blowing dust) provides useful meteorological information. It may simply be sufficient to remove the effect of Rayleigh scattering. In this case, the AOT path radiance does not need to be removed, and so aerosols would still be visible in the imagery. This simplifies implementation of atmospheric correction as well, since the GVVSSSE and GVVSLLE would not need a dependence on AOT.

Figure 17 is a simulated radiance image at the terminator area using the Amazon TERCAT scene provided by the IPO. Due to the significant irradiance change across the terminator, features in the nighttime side of the scene are not visible. Figure 18 shows the output from a prototype of the NCC alternative algorithm given the inputs from Figure 17, for an ideal noise-free sensor input and ideal atmosphere / BRDF correction. It is included as an example of the quality of NCC imagery that we aspire to achieve with our algorithm.

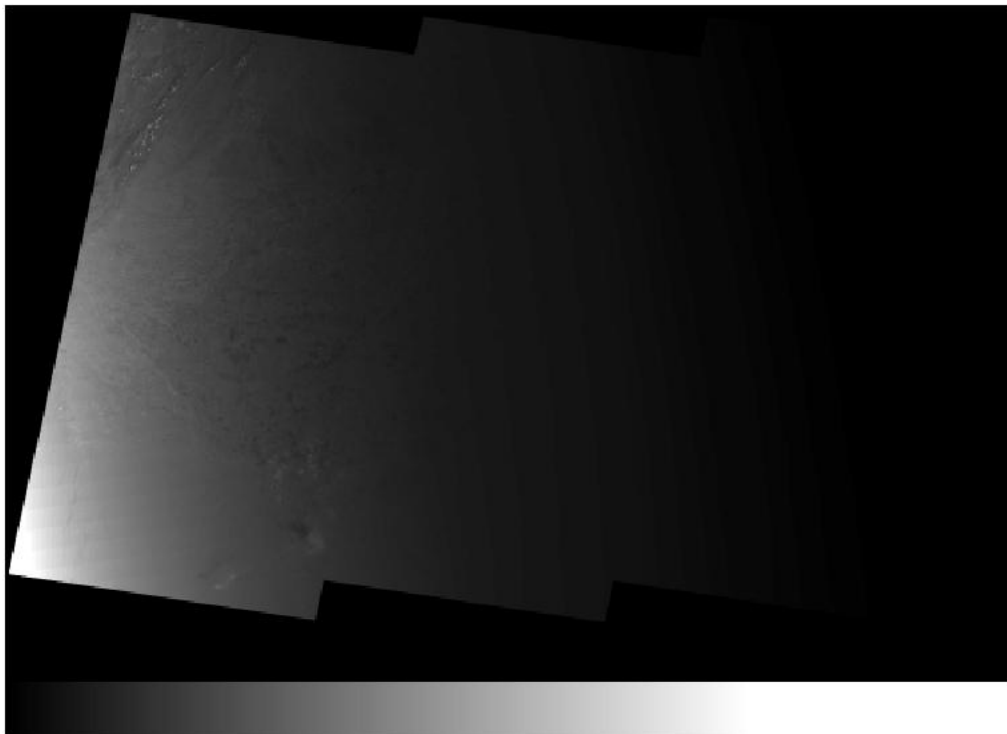


Figure 17. Input radiance image to the NCC algorithm

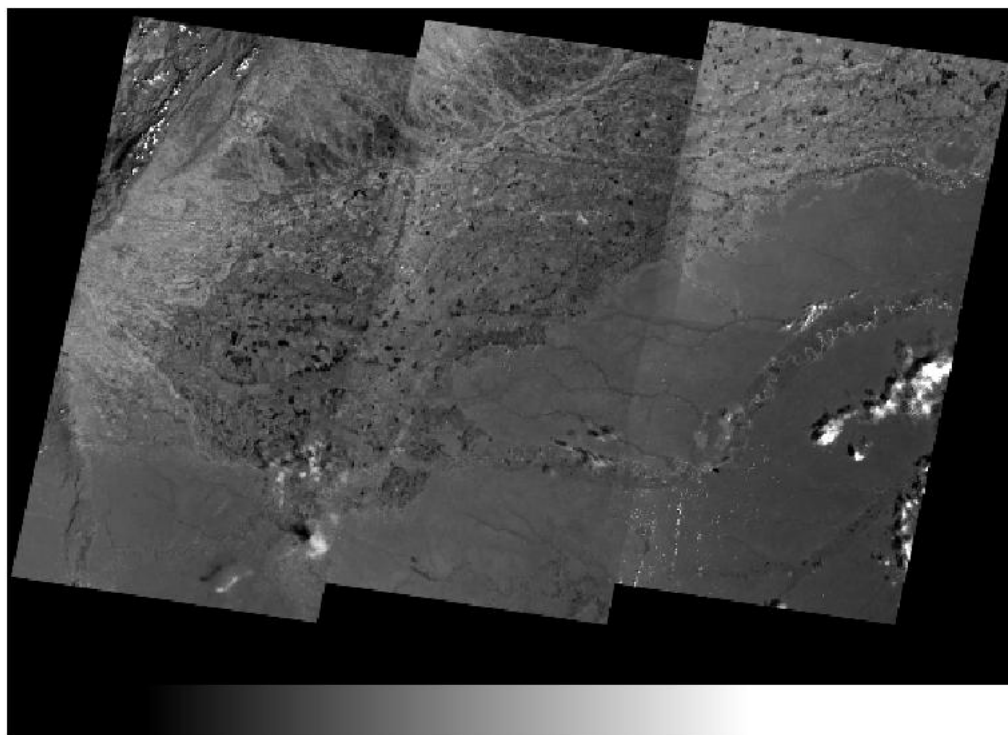


Figure 18. NCC Algorithm Output

### 3.3.6 Initialization and Validation

#### 3.3.6.1 Initialization

The baseline algorithm is based on proven OLS heritage. The LUTs used by the algorithm will be generated offline by the LUTGT, using OLS gain and BRDF values to preserve continuity. The atmospheric correction LUT will also be generated by the LUTGT, using the best available forward model.

#### 3.3.6.2 Pre-Launch Characterization

Our pre-launch plan is to test both the baseline algorithm and the enhancement algorithm on OLS imagery obtained from the National Geophysical Data Center (NGDC), and make any algorithm adjustments that improve the terminator imagery. Algorithm run time performance will be assessed with regard to the requirement to produce NCC Visible imagery in near real time at field terminals. The algorithm uses standard, straightforward interpolation of relatively simple LUTs. Therefore, we do not anticipate run time problems (c.f. Section 3.3.7.1).

#### 3.3.6.3 Validation

Following NPP launch, NCC algorithm performance will be tested on VIIRS DNB terminator imagery. Validation will be by manual inspection of the NCC processed terminator imagery. Trained analysts can readily determine whether the imagery provides a near constant contrast across the terminator. The baseline algorithm, adapted from the heritage OLS technique, will be used operationally unless and until it is determined that the atmospheric correction enhancement produces a superior product. If atmospheric correction LUTs are developed prior to NPP launch, we can re-process the identical granule off-line with the atmospheric correction applied. Trained analysts can compare both sets of NCC imagery to determine whether atmospheric correction produces a superior product.

### 3.3.7 Practical Considerations

#### 3.3.7.1 Numerical Computation Considerations

The baseline algorithm is already operational on the DMSP, and poses no numerical computation problems. The solar and lunar gain values are obtained from direct interpolation of 1-d LUT arrays, with no inversion, iteration, or search window functions. The BRDF values are also obtained from direct interpolation of LUT arrays. Though these are multi-dimensional, their size will be kept small enough to allow rapid processing.

The atmospheric correction algorithm should run as quickly, since it involves a similar process of acquiring values from a pre-set LUT for each pixel. The size of the path radiance LUT depends on the numbers of geometry nodes and atmospheric models. The actual computation for each output pixel is relatively simple and the total computation time is largely dependent on the size of the input LUT. As with the BRDF LUTs, the size of the path radiance array will be kept small enough to allow rapid processing.

### 3.3.7.2 Programming and Procedural Considerations

All procedures are automatic, to perform in the operational environment. All LUTs will be generated off-line.

### 3.3.7.3 Configuration of Retrievals

The NCC algorithm requires the VIIRS day/night band SDR, the VIIRS Aerosol Optical Thickness IP, and five VIIRS LUTs as input. The output of this algorithm is for analyst manual interpretation and does not serve as quantitative input to any other EDRs. The NPOESS processing configuration is designed to satisfy these expectations.

### 3.3.7.4 Quality Assessment and Diagnostics

In general, the NCC image should resemble its constituent imagery products. If these products are insufficient to support manual analysis, then the NCC product is unlikely to serve the analyst any better. Thus, if there is little moonlight, contrast at the terminator and on the dark side will be poor. Sun glint will also impair manual analysis. If helpful to analysts, it is possible to flag imagery that might show sun or moon glint. The algorithm software is designed to set NCC quality flags for each DNB pixel. The flags are set if there is a processing problem with the solar gain, solar BRDF, lunar gain, lunar BRDF, and/or path radiance derivations. If either the observed DNB TOA radiance or the computed source radiance for a given pixel is less than a minimum threshold (currently set as the measurement range minimum of  $4 \cdot 10^{-9} \text{ W/cm}^2/\text{sr}$ ), a low radiance quality flag will be set for that pixel.

### 3.3.8 Algorithm Watch List

Following its review of the Version 3 ATBDs, the VIIRS Operational Algorithm Team (VOAT) has produced a list of items requiring attention. One of these, item 13: NCC Algorithm Products, directly affects the NCC Imagery EDR.

During discussions with the VOAT, it was clear that the reason for this item was the concern over the alternative algorithm. Following our clarification that the baseline algorithm would be adapted from the current OLS algorithm, this item was cancelled. Our NCC algorithm development plan, as described in Sections 3.3.1 and 3.3.6, is now low risk. We will continue to work with the IPO and the VOAT to ensure a low risk implementation of the NCC algorithm.

## 3.4 GROUND-TRACK MERCATOR IMAGERY PRODUCT DESCRIPTION

The purpose of the VIIRS GTM Imagery algorithm is to map VIIRS Imagery (I) channel and Moderate (M) channel data onto GTM coordinates. The GTM layout is a grid of pixels, where rows are at right angles to the ground track and columns are parallel to the ground track. This GTM layout does not have the “bow-tie” effect. The GTM Imagery EDR products are primarily used for visual snow/ice analysis and to display for human viewing.

The GTM is not a map projection, i.e., it does not have an exact set of unchanging transformation equations. Rather, a numerical integration process allows a latitude/longitude calculation of a row/column (X, Y) position on the map plane, or vice versa. The actual ground track of the spacecraft establishes the map plane; consequently, the map plane is different for every orbit. The GTM map has an advantage of always having the ground track in the center of the map plane. Furthermore, multiple granules of satellite data can be concatenated without having to switch from one orbit path map to another.

NPOESS creates two kinds of GTM maps: Fine and Coarse. The Fine GTM map has a pixel-center spacing of 375 meters, which is close to the nadir sample distance of the VIIRS Imagery resolution data. The Coarse GTM map has a pixel-center spacing of 750 meters, which is close to the nadir sample distance of the VIIRS M-band resolution data. The pixel spacing in the along track direction is equal to the pixel spacing in the cross track direction. The maximum variation, in both conformality and area per pixel, is about one percent. The X-coordinate on the GTM map increases in the direction of spacecraft motion along the ground track. The X axis is precisely on the ground track. The Y axis of the map is at a right angle to the X axis. That is, the rows of the GTM map are always at an exact right angle to the ground track. The time attached to each row of the map is the time the spacecraft passes over the nadir point of that row. See Figure 19.

A 3090-kilometer GTM swath was chosen to accommodate a maximum satellite altitude of 850 kilometers. There are 1541 rows and 8241 columns in the fine resolution GTM layout. The row size was chosen to accommodate the minimum altitude (maximum distance of a granule) of the satellite. There can be a variable number of empty columns on the edges of the swath, due to a larger area of the Earth's surface seen near the poles and less near the equator. Rows pull together slightly at the swath edges due to Earth curvature and horizontal size of the GTM swath. There are also a variable number of empty rows at the bottom of the GTM rectangle, due to the fixed horizontal sample distance and forward ground motion of the spacecraft. This layout allows concatenation of an unlimited number of EDR granules without any discontinuities, even at the poles.

The center column of the coarse map exactly follows the center column of the fine map. The pixel centers of the coarse map center column are the same as every other pixel of the fine map center column. Similarly, the pixel centers to the left and right of the center column on the coarse map have the same centers as every other pixel on the corresponding row of the fine map. So the scaling from the coarse map to the fine map is always an exact factor of two. Once the locations of the Fine GTM map are established, the locations of the Coarse GTM map are determined by a simple 2x2 decimation. In Figure 20 each dot represents a pixel center on the GTM Fine Map. The emphasized dots represent coarse pixels on the Fine Map.

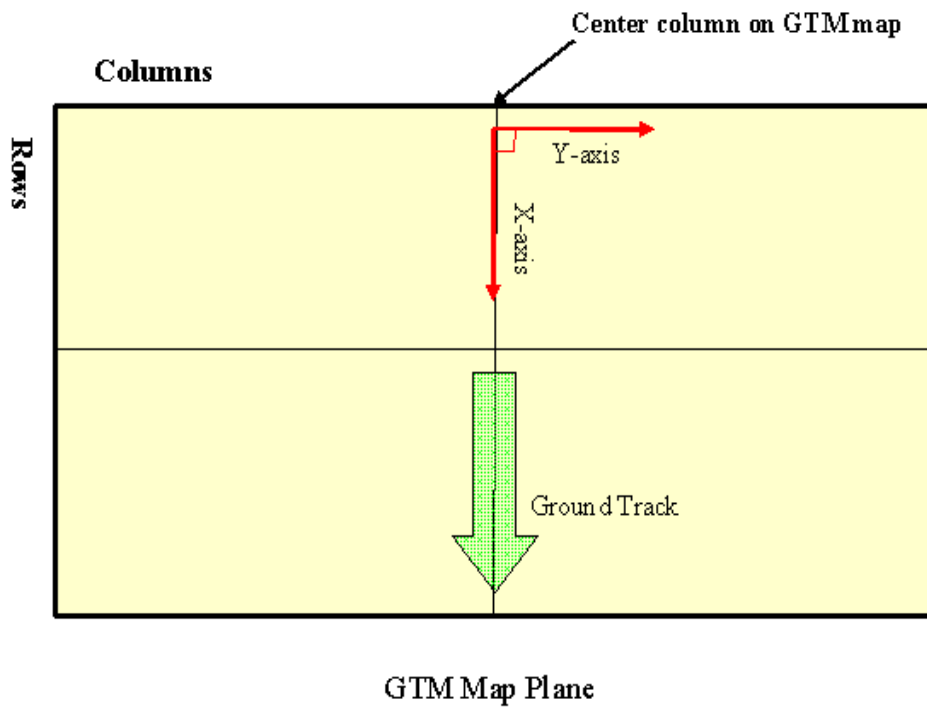


Figure 19. GTM Map Attributes

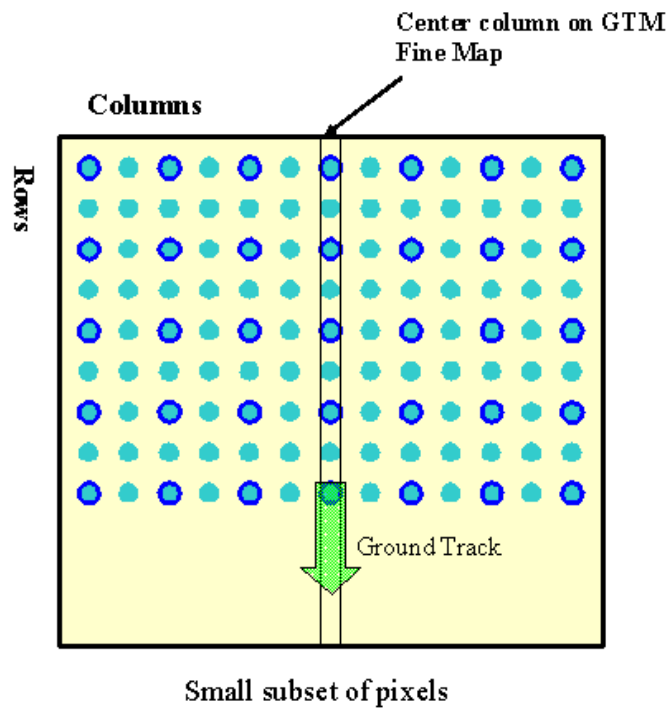


Figure 20. Fine Map Pixels with Emphasized Coarse Pixels

Even though the characteristics of the VIIRS sensor have been used to establish the parameters of the GTM maps, any kind of data can be remapped to the GTM maps. This makes it possible to form matching overlays from any number of data sources.

### 3.4.1 Processing Outline

The first step in creating the GTM map data for an NPOESS granule is to obtain the ground track from the NPOESS Common Geolocation software. Common Geolocation functions provide the geodetic latitude, longitude, and direction of ground track motion, at least once per second. The basis of this ground track data is the ephemeris data reported by the GPS sensor on the spacecraft. This data comes down in the Ephemeris and Attitude data packets (these packets are also called "spacecraft diary" packets). Notice the direction of ground track motion is in the ECR system of the rotating Earth. This means the direction of ground track motion accounts for the rotation of the Earth as well as the inertial motion of the spacecraft.

Once the locations of the ground track column pixels are established, it is possible to calculate the locations of the pixels along the rows by a simple application of spherical trigonometry. The geodetic latitude and longitude of the center pixel are used along with the radius of the Earth at that geodetic latitude. The direction from the center pixel to another pixel in the row is exactly 90 degrees to the left or right of the direction of ground track motion, which means the row is at an exact right angle to the ground track. All the pixels in one row of the map are theoretically at the same time as the center pixel, so there is no spacecraft motion or Earth rotation to account for along each row. The fact that the Earth is not an exact sphere is not a problem, since the objective is a reproducible map where there is a "one-to-one and onto" relationship between the surface of the Earth and the GTM map. In summary, great circle distance and spherical trigonometry, location of the pixel in the center of each row, and direction of ground track motion are used to establish the location of each pixel along the row.

### 3.4.2 Algorithm Input

The GTM algorithm uses a relatively small, single set of data: 1) the ephemeris data recorded by the GPS sensor on the spacecraft during the time span of the granule, 2) the deterministic granule boundaries (start and stop time of each granule) of the spacecraft, and 3) the 375 meter Earth surface distance between each pixel of the Fine GTM map. VIIRS I-Channel Imagery algorithm requires several types of data to perform mapping to the GTM layout, summarized in Table 9.

**Table 9. VIIRS I-Channel Imagery EDR Inputs**

Name	Description
Spacecraft Diary RDRs	Attitude and ephemeris data for the granule.
VIIRS Band I1, I2, and I3 SDRs	Radiances and reflectances, granule boundary times and granule mode. Used for day and mixed mode granules.

Name	Description
VIIRS Band I4 and I5 SDRs	Brightness temperatures and radiances, granule boundary times and granule mode. Used for day, mixed and night mode granules.
VIIRS IMG Geolocation	Geolocation data for every pixel in the granule.
VIIRS IMG Gridded Geolocation	Map grid row and column values for every pixel in the granule and the granule MDS.
Band I1-I5 EDR DQTTs	Data Quality Threshold Tables used for performing data quality checks on the EDR outputs. These are optional inputs.

### 3.4.3 Theoretical Description

Common Geolocation is used to calculate the ground track points for the start time and end time of the granule. Then a combination of spherical trigonometry and Common Geolocation functions are used to space the rows of the Fine GTM map as close to 375 meters as possible, and to put the center of the map precisely on the ground track. For the present granule size of about 85.752 seconds, there are about 1536 rows for Image resolution and 768 rows for Moderate resolution. The number of rows varies slightly because the granule size is a fixed number of seconds, and the ground track speed of the spacecraft varies slightly. The maximum variation in row spacing at nadir is 375 meters, +/- about 0.7 meters. Careful location of the first and last row in one granule means the GTM map of one granule always precisely concatenates with the GTM maps of the neighboring granules. Thus, the centers of each row of the GTM map, the ground track pixels, are located by equal distance spacing of the pixels precisely on the ground track.

The operational software only does full calculations for every 10<sup>th</sup> row and column, and then does quadratic interpolation of the pixels between. So, the calculation of a full set of latitudes and longitudes for a map is a relatively fast process.

The process of converting row and column to latitude and longitude, and vice versa, can be done by two methods. Method 1 is based on the fast search of a full set of geolocation data for the GTM map. Method 2 works from only the ground track data and works by an iterative search of the ground track, followed by a spherical trigonometry calculation along the row. Method 2 is slightly faster and the difference between the results is always less than one meter (the size of floating point round-off to 32 bits). The Nearest Neighbor method is used for filling pixels in order to preserve contrast and sharpness for human viewing. If full geolocation accuracy of the Sensor Data Record (SDR) is needed, the SDR should be used and not the GTM Imagery EDR.

Based on mode (day, mixed, or night) of the granule, data from either two or five image resolution channels are mapped onto the GTM map. In other words, two or five separate EDRs are created along with geolocation data for a given granule. Radiance and reflectance



values for channels I1 through I3, along with radiance and brightness temperature values for channels I4 and I5, are processed for “day” and “mixed” mode granules. Radiance and brightness temperature values for channels I4 and I5 are processed for “night” mode granules. Currently, only six of the 16 moderate resolution channels are mapped onto the GTM map. The selection of which six channels to create is determined by a configuration file (see Section 2.3.7). It is the responsibility of the operator to select the appropriate bands for the mode of the granule day, mixed, or night) that is to be processed. Six EDRs are created using the shortnames VIIRS-M1ST-IMG-EDR through VIIRS-M6TH-IMG-EDR. The EDR metadata can be read to determine the Band ID used to generate the EDR. The Day Night Band (DNB) is processed by the Near Constant Contrast (NCC) Imagery algorithm to produce an EDR mapped to GTM. See the VIIRS NEAR CONSTANT CONTRAST IMAGERY EDR OAD, D36814, for more information. VIIRS GTM Imagery EDRs are not corrected for height.

### 3.4.4 Archived Algorithm Output

VIIRS I-Channel Imagery EDRs are summarized in Tables 10-11. Note that the I1 – I3 band EDRs have a reflectance field where as the I4 and I5 band EDRs have a brightness temperature field. The VIIRS I-Channel Imagery GEO is summarized in Tables 12-14. Similar tables exist for M-bands as shown in the VIIRS GTM Operational Algorithm Description Document, D42815 (2009).

**Table 10. VIIRS I-Channel Imagery EDR Outputs**

Output	Type	Description	Units / Range
radiance	Uint16 * [1541 * 8241]	Top of Atmosphere radiances for the I1-I5 Bands	W/(m <sup>2</sup> ·sr·μm) / -1.2 – 87.0
reflectance (I1 – I3 EDRs only)	Uint16 * [1541 * 8241]	Top of Atmosphere Reflectances (Daytime only) for the I1 - I3-Bands	Unitless / 0.0 – 1.6
brightTemp (I4, I5 EDRs only)	Uint16 * [1541 * 8241]	Top of Atmosphere Equivalent Blackbody Brightness Temperatures for the I4, I5-Bands	Degree / 208 - 367
pixelQuality	Uint8 * [1541 * 8241]	Pixel-level quality flags	See Table 16
radScale	Float32	Scale for scaled radiance	Unitless
radOff	Float32	Offset for scaled radiance	Unitless
refl/btScale	Float32	Scale for Reflectance / Brightness Temp	Unitless
refl/btOff	Float32	Offset for Reflectance / Brightness Temp	Unitless

**Table 11. VIIRS I-Channel Imagery EDR Pixel Level Quality Flags**

Byte	Bits	Description	Values
Byte 0	0-1	Imagery Quality (Pixel Quality as determined by the SDR Calibration Quality. Dead Pixel Replacement: Individual bad pixels caused by a bad detector are filled as an average of the two adjacent detector pixels. Bad edge-of-scan	0: Good 1: Poor 2: No Calibration 3: Dead pixel replacement

Byte	Bits	Description	Values
		pixels use the adjacent pixel value. (If two adjacent pixels are dead, a fill value is used for each pixel.)	
	2	Pixel is saturated	0: False 1: True
	3-4	Missing Data (Data required for calibration processing is not available for processing)	0: All data present 1: EV missing 2: Cal data missing 3: Therm data missing
	5-6	Out of range	0: Good 1: Radiance out of range 2: Reflectance or EBBT out of range 3: Both out of range
	7	Spare	

Table 12. VIIRS I-Channel Imagery GEO Outputs

Output	Type	Description	Units / Range
rowTime	Int64 * [1541]	Time of the nadir point of the GTM row in IET (1/1/1958). Represents the time of the nadir point of the GTM row.	Microsecond / 1483228832000000 - 2272147232000000
Latitude	Float32 * [1541 * 8241]	Latitude of each pixel (positive North)	Degree / -90 - 90
Longitude	Float32 * [1541 * 8241]	Longitude of each pixel (positive East)	Degree / -180 - 180
sunZenith	Float32 * [1541 * 8241]	Zenith angle of sun at each pixel position	Degree / 0 - 180
sunAzimuth	Float32 * [1541 * 8241]	Azimuth angle of sun (measured clockwise positive from North) at each pixel position	Degree / -180 - 180
sensorZenith	Float32 * [1541 * 8241]	Zenith angle to Satellite at each pixel position	Degree / 0 - 180
sensorAzimuth	Float32 * [1541 * 8241]	Azimuth angle (measured clockwise positive from North) to Satellite at each pixel position	Degree / -180 - 180
terrainHeight	Int16 * [1541 * 8241]	Ellipsoid-Geoid separation	Meter / -500 - 8300
satRange	Float32 * [1541 * 8241]	Line of sight distance from the ellipsoid intersection to the satellite	Meter / 820,000 -1,900,000
pixelQuality	UInt8 * [1541 * 8241]	Pixel Level Geolocation Quality Flags	Refer to Table 18
scanQuality	UInt8 * [48]	Scan Level Geolocation Quality Flags	Refer to Table 19
sdrRow	UInt16 * [1541]	Imagery SDR pixel row index number	Unitless

Output	Type	Description	Units / Range
	* 8241]	that was remapped to this GTM pixel (row numbering begins with zero)	
sdrCol	UInt16 * [1541 * 8241]	Imagery SDR pixel column index number that was remapped to this GTM pixel (column numbering begins with zero)	Unitless

**Table 13. VIIRS I-Channel Imagery GEO Pixel Level Quality Flags**

Byte	Bits	Description	Values
Byte 0	0-1	SDR Pixel Mapping Coordinate (GTM to SDR). Indicates whether this pixel originated from the previous, current, or next granule in the SDR Imagery Resolution Geolocation.	0: Error 1: Previous Granule 2: Current Granule 3: Next Granule
	2-7	Spare	

**Table 14. VIIRS I-Channel Imagery GEO Scan Level Quality Flags**

Byte	Bits	Description	Values
Byte 0	0	Solar Eclipse	0: No Solar Eclipse 1: Solar Eclipse
	1-7	Spare	

### 3.4.5 Practical Considerations

#### 3.4.5.1 Graceful Degradation

There is one case where input graceful degradation is indicated in the VIIRS GTM Imagery EDR: An input retrieved for the algorithm had its N\_Graceful\_Degradation metadata field set to YES (propagation).

#### 3.4.5.2 Exception Handling

Missing sensor data caused by bad detectors are replaced during pre-processing of the GTM algorithm as follows: For edge of scan, the radiance value of the adjacent pixel is copied into the missing pixel. For non-edge of scan, the radiances are averaged using the two adjacent pixels and copied into the missing pixel. Missing data points are left as the initialization fill value in the GTM Imagery EDRs. Additionally, the VIIRS GTM Imagery software is designed to handle a wide variety of processing problems. Any exceptions or errors are reported to IDPS using the appropriate INF API.

### 3.5 MANUAL CLOUD ANALYSIS ARP DESCRIPTION

#### 3.5.1 Processing Outline

Manual cloud analysis products are not produced by the VIIRS operational system. They are expected to be produced at various locations by trained analysts, using the VIIRS Imagery as input data. Different analysts may wish to use different techniques. The specifications for the VIIRS sensor have been developed by analysis using the techniques described below, which we refer to as the VIIRS Manually-Generated Cloud Data algorithm (VMCD). The first version of a User's Guide to assist an analyst in implementing the techniques is included as an Appendix to this document. A more recent text, based upon this document, has been published under the title, VIIRS – A New Operational Cloud Imager by Hutchison and Cracknell (2006).

#### 3.5.2 Algorithm Input

Ancillary data, both VIIRS and non-VIIRS, are useful for manual cloud analysis. We have assessed the relative importance of the various sources of ancillary data. A prioritized list is presented as Table 15.

**Table 15. Ancillary data to augment manual cloud analysis.**

Prioritized Item	Application	Utility assessment
1) Cloud mask/ Cloud Cover	Used to speed manual analysis by providing a mostly-correct first guess	Crucial. Manual analysis cannot be accomplished without this. Analysis timelines do not permit analyst to determine the cloud state of every pixel or even horizontal cell individually.
2) Geographic/ physio-graphic data, oceanic currents	Identifies clear-scene structural and textural details for comparison	Very important, but difficult to assess contribution. Analysts have varying degrees of initial geographic knowledge
3) Raw Vis/Day-Night Vis/IR imagery (contrast enhanced)	Presents a less processed view of the scene. Processing artifacts, pseudo-colors, etc., are removed, allowing analysts to make an independent assessment of the scene.	Important but difficult to assess contribution. Perform manual cloud analysis with and without these data using different teams of analysts; compare results to ground truth [Manual comparison method]
4) Cloud Mask diagnostics (TBR)	Flags that indicate whether ambiguous results occurred from the several cloud tests. Manual attention concentrates on these locations	Will be important but difficult to assess contribution. Perform manual cloud analysis w/ and w/o, compare results to ground truth
5) Snow/Ice fields	Draws analyst attention to suspect snow/ice areas for confirmation.	Important. Manual comparison method
6) Conventional Surface observer cloud reports from nearest hourly/synoptic time	Provides independent on-the-spot assessment of cloud conditions	Less important. Manual comparison method
7) Aerosols	Analyst can judge whether imagery	Less important. Manual comparison method

Prioritized Item	Application	Utility assessment
	effects are from clouds or aerosols	
8) Cloud Top T, p, z	Could be of use but is likely to overload an already stressed analyst. Would be better to design one product that would roll this and the next three items together and ideally merge with cloud mask.	Given a reliable product this could take on greater importance.
9) Optical depth, Effective Particle Size	See Cloud Top T, p, z	See Cloud Top T, p, z
10) MIS* soundings	See Cloud Top T, p, z	See Cloud Top T, p, z

\* Conical Scanning Microwave Imager/Sounder

It is important to not overwhelm an analyst with an abundance of information. Manual cloud analysis accuracy is not the bottleneck. Decreasing the amount of time required to review and correct the automated analysis to a given level of accuracy is more important than further increasing accuracy, once the objective performance level is met. Additional information can greatly decrease manual analysis throughput. Cloud analysts are generally mass producers, not craftsmen or artisans.

Given that, we could focus our thoughts on a “new” product that would synthesize many of the items presented in the table into one product that could be easily used by an analyst to improve his analysis.

### 3.5.2.1 VIIRS Data

The VMCD algorithm requires SDRs for each VIIRS imagery channel and several imagery assist channels. The Imagery channels include the daytime/nighttime visible band, the 0.64  $\mu\text{m}$  daytime visible band, the 3.74  $\mu\text{m}$  band, and the 11.45  $\mu\text{m}$  band. The imagery assist channels include the 0.412  $\mu\text{m}$ , 0.858  $\mu\text{m}$ , 1.38  $\mu\text{m}$ , 1.61  $\mu\text{m}$ , 4.05  $\mu\text{m}$ , 8.55  $\mu\text{m}$ , and the 10.8  $\mu\text{m}$  bands. It is assumed that these data are accurately calibrated, earth-located, and co-registered.

### 3.5.2.2 Non-VIIRS Data

AFWA has two major functions that use VIIRS capabilities to generate cloud data (1) QC, Bogus of the cloud data base, discussed in Section 2.3.1, and (2) contingency support, e.g. understanding the contents of a scene – e.g. Kosovo. Ancillary data requirements for both functions include:

- a. Automated cloud analyses (cloud cover, cloud top height, etc.)
- b. Surface type maps (geography) of area covered by imagery
- c. Surface elevation and terrain maps

- d. Conventional weather observations as available (surface reports, aircraft reports, and radiosonde observations)

### 3.5.3 Theoretical Description

#### 3.5.3.1 Physics of the Problem

The ability to manually identify clouds in any given spectral band is based upon the contrast, measured in radiance, between the cloud and the surrounding cloud-free background. More precisely:

$$C = I_v(\text{TOA})_{\text{cloud}} / I_v(\text{TOA})_{\text{background}} \quad (3.5.3.1.1)$$

The measured or satellite observed radiance,  $I_v(\text{TOA})$ , may be composed of reflected solar radiation and resultant albedos, thermal radiation emitted by or brightness temperatures of the terrestrial feature, or both when observations are made in the 3-5 micron wavelength interval.

The monochromatic, upwelling infrared radiance measured at the sensor aperture in a cloud-free atmosphere is given by (Liou, 1980, p. 247):

$$I_v(0) = \varepsilon_v B_v[T_s] T_v(p_s) + \int_{p_s}^0 B_v[T(p)] \frac{\partial T_v(p)}{\partial p} dp + (1 - \varepsilon_v) \int_0^{p_s} B_v[T(p)] \frac{\partial T_v(p)}{\partial p} dp \quad (3.5.3.1.2)$$

where:  $\nu$  = wavenumber of emission

$B_\nu[T(p)]$  = Planck function at wavenumber ( $\nu$ ) for temperature ( $T$ )

$\varepsilon_\nu$  = emissivity of surface at wavenumber ( $\nu$ )

$T_v(p_s)$  = atmospheric transmittance between pressure level ( $p_s$ ) and space

$I_v(0)$  = monochromatic radiance arriving at satellite.

$P_s$  = surface pressure

$T_s$  = surface temperature

For imaging sensors, the atmospheric transmittance between pressure levels and space is very small and Equation 3.5.3.1.2 is closely approximated by Equation 3.5.3.1.3, which shows that the radiance arriving at the satellite sensor is a function of the emissivity of the surface, the surface temperature, and the transmission from the surface to the sensor:

$$I_v(0) = \varepsilon_v B_v[T_s] T_v(p_s) \quad (3.5.3.1.3)$$

Thus, the capability to manually detect a cloud in infrared imagery is enhanced not only by temperature contrasts between the features but also by observing the features in spectral bands where emissivity contrasts exist or in bandpasses which effect atmospheric transmissivity as is the case with the 1.378 micron channel which suppresses the signatures of low-level features, including clouds and cloud-free surface thus enhancing the signatures of higher level clouds.

The amount of solar radiation reflected by the Earth-atmosphere system into the sensor aperture is given by (Liou, 1980, p. 25):

$$I(0; \mu, \phi) = I(\tau_1; \mu, \phi) e^{-\tau_1/\mu} + \int_0^{\tau_1} J(\tau'; \mu, \phi) e^{-\tau_1/\mu} \frac{d\tau'}{\mu}, \quad (3.5.3.1.4)$$

	Term A	Term B
where:	$I_\nu(0)$	= monochromatic radiance arriving at satellite
	$\tau$	= optical depth of each $\tau'$ layer, while the atmosphere is $\tau_1$
thick	Term A	= surface energy contribution attenuated to space
	Term B	= internal atmospheric contributions attenuated to space
	$\mu$	= cosine of angle between radiation stream and local zenith
angle	$\phi$	= azimuth angle.

The complexity of this calculation lies in the source function term,  $J(\tau; \mu, \phi)$ , which is given for solar radiation by Equation 3.5.3.1.5.

$$J(\tau; \mu, \phi) = \frac{\tilde{\omega}}{4\pi} \int_0^{2\pi} \int_{-1}^1 I(\tau; \mu', \phi') P(\mu, \phi; \mu', \phi') d\mu' d\phi' \quad (3.5.3.1.5)$$

$$+ \frac{\tilde{\omega}}{4\pi} \pi F_0 P(\mu, \phi; -\mu_0, \phi_0) e^{-\tau/\mu_0}$$

	Term C
where:	Term C = multiple scattering of diffuse (scattered) energy
	Term D = single scattering of direct solar irradiance, $F_0$ .

And:

$\omega$	= single scattering albedo
$P$	= phase function
$F_0$	= solar irradiance
$\mu_0$	= cosine of solar zenith angle
$\phi_0$	= solar azimuth angle

Thus, the capability to manually detect a cloud in visible and near-infrared imagery is enhanced by viewing in spectral bands where contrasts in the reflectivities of the features are known to exist. In reality, monochromatic radiation does not exist because of line broadening from natural, pressure (collision), and Doppler (thermal velocity) effects. Also, since an instrument can distinguish only a finite bandwidth, the upwelling radiance measured by the satellite is integrated over the sensor transmission filter, which is also called the sensor response function, and is given by Equation 3.5.3.1.6.

$$I_v(0) = \left[ \int_{v_1}^{v_2} I_v(0) \phi_v dv \right] / \int \phi_v dv \quad (3.5.3.1.6)$$

where:  $\phi_v$  = filter (sensor) response function at wavenumber ( $v$ )  
 $v_1, v_2$  = wavenumber range of filter response

### 3.5.3.2 Image Processing to Enhance Cloud Detection in Multispectral Imagery

The manual interpretation of clouds and background features in multispectral imagery is facilitated by the use of false color composite images that are made by assigning a different spectral band to each gun of a cathode ray tube (CRT; d'Entremont *et al.*, 1987). The hue of the false color composite emphasizes the gun in which the feature has the strongest signature, i.e., has the larger radiance arriving at the satellite sensor. Equal contributions from each channel in the CRT results in a feature appearing as a (white through black) gray shade in the false color composite, with the shade of gray depending upon the strength of albedos or brightness temperatures of the feature in the spectral bands.

In current operational AVHRR imagery, the signature of vegetated land is more pronounced in the 0.9- $\mu\text{m}$  channel than the 0.6- $\mu\text{m}$  band while water clouds are similar in both the 0.6- $\mu\text{m}$  and 0.9- $\mu\text{m}$  channels as seen in Panels A(1) and A(2) in Figure 21, respectively. Thus, a false color composite of the scene shown in Panel A(3) shows highly vegetated areas in green, less-vegetated areas as brown, and clouds as white (Hutchison *et al.*, 1997). In addition, the land-sea boundary is seen distinctly in the color composite since the land near the ocean's edge is densely vegetated while the ocean has a low albedo in both spectral bands.

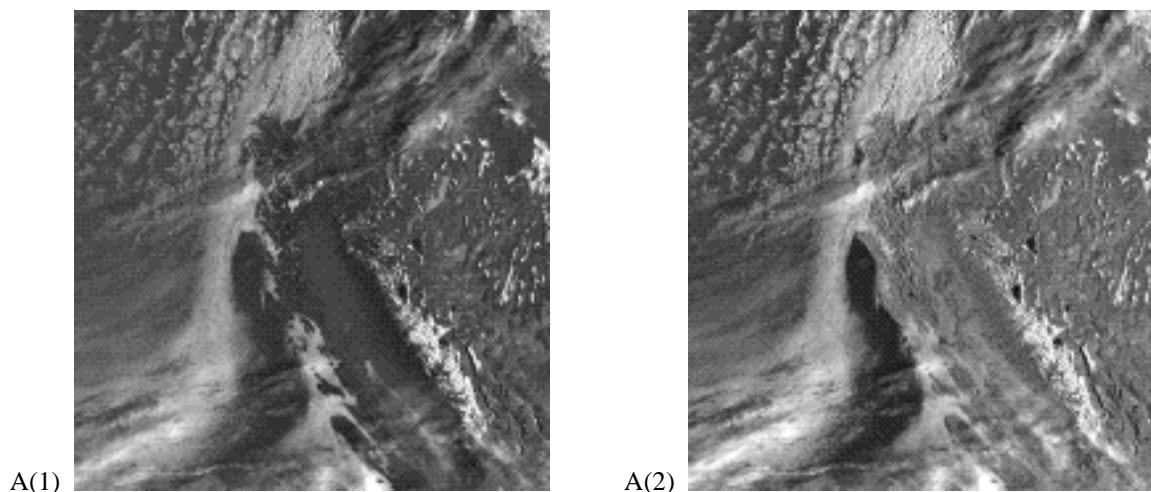
Additional false color composites can be created to emphasize other features in the scene. For example, high water clouds may be differentiated from lower-level water clouds by including 3.7- $\mu\text{m}$  and/or the 12.0- $\mu\text{m}$  infrared bands shown in Panels A(1) and A(2) respectively in Figure 20. This process is demonstrated in Panel A(3) where the 0.6- $\mu\text{m}$  image assigned to the blue gun in Figure 19 has been replaced with the 12.0- $\mu\text{m}$  channel. Colder clouds appear bluish in the composite in Panel A(3) of Figure 22 while warmer clouds have a yellow-greenish hue.

Care must be taken using this false color composite to avoid misclassifying optical thin, cirrus clouds as lower-level clouds. This is accomplished using another color composite described in Figure 23.

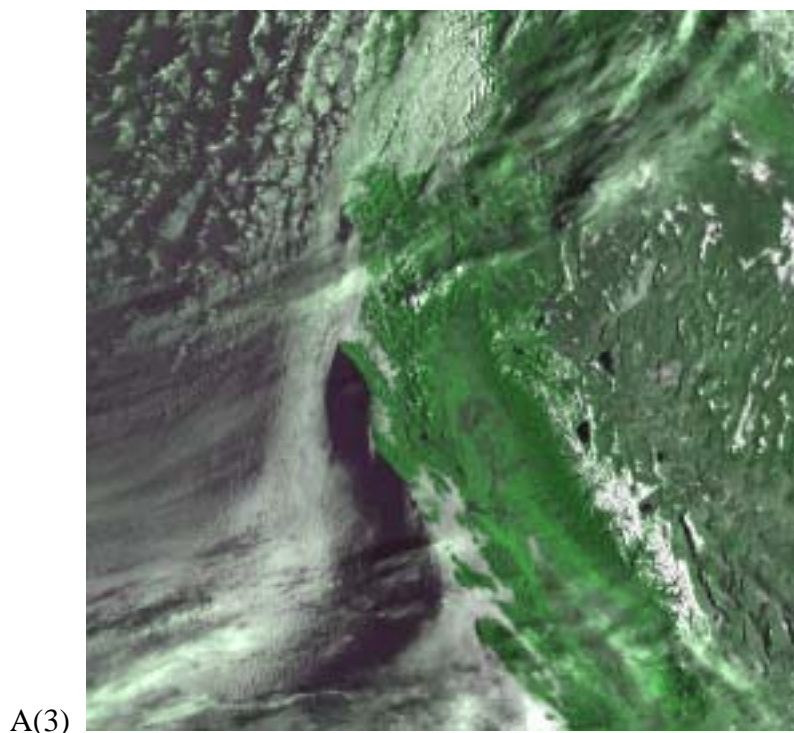


First, a method is described to differentiate between snow and water clouds in daytime imagery. The contrast between snow and water clouds is greatly enhanced by including the 1.6- $\mu\text{m}$  channel in the false color composite, since water clouds are highly reflective in this band while snow and ice (clouds) reflect poorly (Valovcin, 1978). Alternatively, the reflectivity of snow in the 3.7- $\mu\text{m}$  band is also very small and can be used to simulate the signatures in a 1.6- $\mu\text{m}$  channel by removing the thermal component of the radiation from the observed satellite radiances (Hutchison *et al.*, 1997; Allen, Durkee, and Walsh, 1990) to create an image which facilitates the manual distinction between snow and water clouds as shown in Figure 23.

A benefit of using the 3.7- $\mu\text{m}$  albedo channel, rather than the 1.6- $\mu\text{m}$  imagery to manually discriminate between snow and water clouds, is that the former simultaneously enhances the contrast between snow and thin cirrus clouds as well as the contrast between water clouds and snow. In fact, the spectral signature of optically thin cirrus in the derived 3.7- $\mu\text{m}$  albedo image is actually enhanced over that present in the 12.0- $\mu\text{m}$  imagery (Hutchison *et al.*, 1997) as seen in Panels A(1) and A(2) of Figure 24. This stronger signature of cirrus in the 3.7- $\mu\text{m}$  albedo image over the 12.0- $\mu\text{m}$  imagery results from the methodology used to create the former, which in effect produces a 3.7 minus 12.0- $\mu\text{m}$  brightness temperature difference image that enhances the signature of thin cirrus.

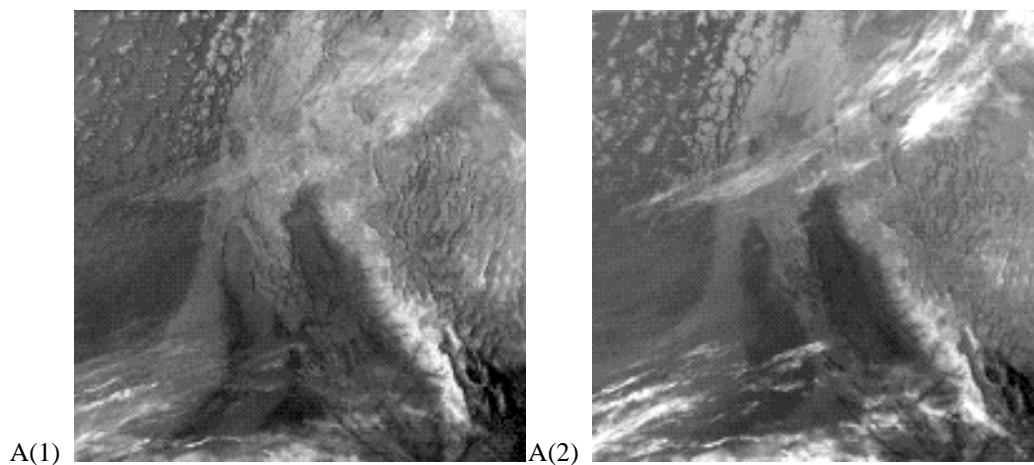


Panels A. Highly reflective snow and water clouds are visible in AVHRR Channel 1, A(1), while coastline and inland lakes become more discernible in Channel 2, A(2). Snow is bright in both channels.

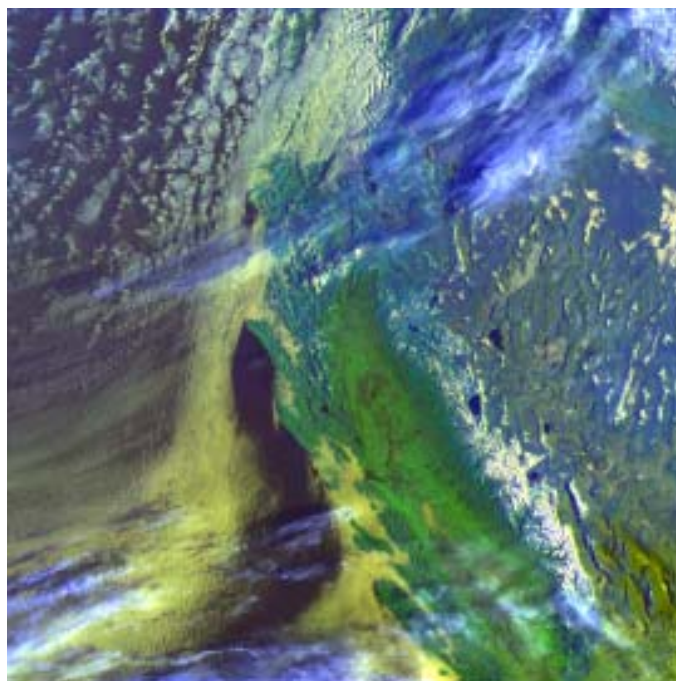


Panel A(3). False color composite of NOAA-12 AVHRR imagery, created by assigning Channel 1 to the red and blue guns and Channel 2 to the green gun of a CRT. This false color composite is useful for manually distinguishing between densely vegetated (rich green hue) and more sparsely vegetated (brownish hue) land as well as the water-land boundaries. Snow and clouds both appear bright in this color composite.

**Figure 21. NOAA-12 AVHRR Channel 1 and Channel 2 imagery collected over western U.S. at 1505 GMT on March 19, 1996.**

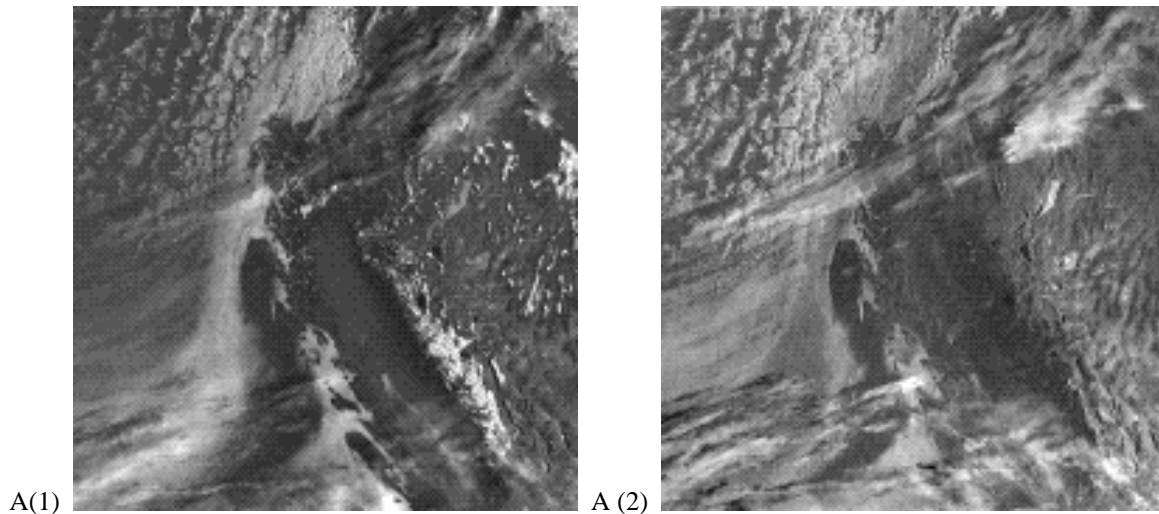


Panels A. Ice clouds and snow along the Sierra Mountain range, lower right quadrant, have a similar (bright) appearance in AVHRR channel 3, A(1), and channel 5, A(2), which makes distinguishing between them difficult.



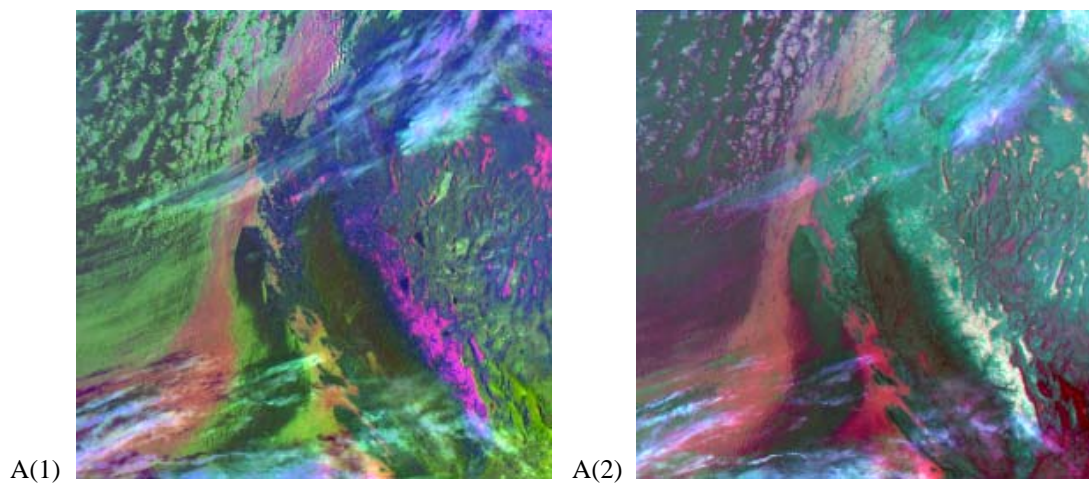
Panel A(3). The false color composite in A(3), created by assigning AVHRR Channel 1 to the red and blue guns and Channel 2 to the green gun of a CRT, is used to manually distinguish between densely (rich green hue) and more sparsely (brownish hue) vegetated land as well as the water-land boundaries. Snow clouds both appear bright in this color composite.

**Figure 22. NOAA-12 AVHRR Channel 3 and Channel 5 imagery collected over western U.S. at 1505 GMT on March 19, 1996.**



Panels A. The contrast between snow is greatly enhanced by correcting the 3.7- $\mu\text{m}$  band for thermal emissions as seen by comparing the 0.6- $\mu\text{m}$  band, A(1), with the 3.7-micron albedo data in A(2), and the brightness temperature difference image of channel 3 minus channel 5, C(2).

**Figure 23. NOAA-12 AVHRR Channel 1 and the derived 3.7- $\mu\text{m}$  (albedo) data for the scene collected 1505 GMT on March 19, 1996.**



Panels A. The false color composite in A(1), created by assigning AVHRR Channel 1 to the red, the derived Channel 3a (albedo) to the green, and Channel 5 to blue gun of a CRT while Channel 3 replaces Channel 3a in A(2).

**Figure 24. Color composite of NOAA-12 AVHRR imagery created by assigning Channels 1, 3, and 5 to the red, green and blue guns of a CRT.**

The enhanced spectral signatures in channel 3a (albedo) greatly assist in manually distinguishing between ice clouds (blue) and snow (purple) in Panel A(2) of Figure 24. The



clear distinction between thin cirrus and the snow-covered mountains in the lower-right quadrant results from the spectral signatures of these features being very different in channels 1, 3a, and 5. In fact, it was found that the signature of snow in Panel A(1) of Figure 24 from the red and blue guns was nearly an order-of-magnitude greater than its signature in the green gun; thus, snow appears purple in the false color image, indicating nearly equal energy coming from the red and blue guns (channels 1 and 5). On the other hand, the signature of snow in Panel A(2) from the red, green, and blue guns is nearly the same for channels 1, 3, and 5; since equal contributions from each gun produces a gray shade rather than a color, snow appears white in this figure. Thin cirrus appears bluish in both panels because ice has its strongest signature in channel 5. However, it is important to note that more thin cirrus is evident in Panel A(1) than A(2) because the signature of thin cirrus in the combination of channel 3a and channel 5 is greater than its signature in channel 3 and channel 5. Finally, the large difference in the signature of snow between channel 3a and channel 1, shown in the false color composite of Panel A(1), means it is possible to positively identify snow-covered surfaces using an automated algorithm based upon the bi-spectral reflectance ratio between these two channels. It appears that the low clouds in Panel A(1), shown as red and occurring in the left half of the image, have a similar spectral signature to that of snow and therefore could be misclassified; however, this is not the case. In channel 3a, the spectral signature of snow is much weaker, by a factor of nearly 5, than the signature of low-level water clouds. In addition, the relative signature of warmer, water clouds is only slightly larger in channel 1 (the red gun) than in channel 5 (the blue gun) and this difference becomes smaller as the cloud tops become colder, i.e. the clouds change from low to middle level clouds. On the other hand, while the spectral signature of snow is much lower in channel 3a (the green gun) than the channel 1 (the red gun), it is even lower when compared to channel 5 (the blue gun) since snow-covered surfaces appear cold in channel 5. Thus, the channel 1, 3a, and 5 false color composite is a robust display for the manual identification of snow and thin cirrus in multispectral imagery (Hutchison *et al.*, 1997; Hutchison and Locke, 1997). Therefore, the threshold requirements for manual cloud detection and cloud typing in daytime imagery are satisfied using only the DV, MWIR, and LWIR imagery bands along with image processing techniques..

### 3.5.3.3 Mathematical Description of the Algorithm

The most important step in creating the manual Cloud-No Cloud (CNC) analysis is the accurate interpretation of all cloudy and cloud-free features in the multispectral images using (1) the principle set forth in Eq. 3.5.3.1.1, (2) image enhancement techniques, and (3) false color composites as previously described while (4) following guidelines that are well documented in the literature (Scorer, 1990). Once these features are identified, the manual cloud-no cloud (CNC) analyses are created from the analysis of individual bands of the multispectral imagery where these features, included edges, are most distinct. The cloud ground truth analysis (CGTA) software allows analysts to compare the spectral signatures of clouds and cloud-free surfaces in all spectral bands and use iterative techniques over subimage regions to create CNC analyses. Individual CNC analyses may be created from a single band or composited from as many as five spectral bands into a total CNC analysis. The operator may draw polygons around areas of interest in each channel and set threshold levels for declaring pixels in that area cloudy; thus, the need for strong contrasts between clouds and

background features becomes apparent. Additionally, a composite (total cloud) analysis from one set of five channels for a scene can be updated with CNC analyses of another five bands of the same scene, e.g., if working with hyperspectral imagery, to extend the total CNC analysis to include all clouds in 10 spectral bands and so forth. Thus, in theory, there is no limit to the number of spectral bands that may be used to create the manual CNC. In practice, only a couple of bands are needed for skilled analysts to interpret features in a scene and create the manual CNC analysis with a repeatability of about 1-2 percent. Additionally, the accuracy of the manual CNC analysis is limited by image quality, i.e., clouds smaller than the sensor HSR may not be included in the manual analysis. Cloud Type ground truth (cirrus, stratus, cumulus) analyses are accomplished in a similar manner using only the areas already declared cloudy in the composite CNC mask as described in Hutchison *et al.* (1997).

#### 3.5.3.4 VIIRS Imagery and Imagery Assist Color Composites

The Raytheon VIIRS design calls for a flowdown of imagery “sensing” requirements necessary to meet threshold Application-Related Requirements for the Imagery EDR. A minimum of three imagery channels are required to satisfy threshold requirements for the Manually-Generated Cloud Data (Hutchison, 1998). These are the daytime visible (DV) band, the Mid-Wave Infrared (MWIR) band, and the Long-Wave Infrared (LWIR) band.

Our VIIRS design also calls for imagery assist channels to be used with imagery channels to push toward NPOESS VIIRS Objectives. In the case of the Manually-Generated Cloud Data, this is readily accomplished using (1) false color composites and (2) the CGTA software concepts. The Imagery Risk Reduction Plan identifies the attributes of each Manually-Generated Cloud Data ARP for which pushing toward objective requirements is feasible (Hutchison, 1999). The performance summary for the Manually-Generated Cloud Data Product ARPs is provided in Section 3.5.4.

This section identifies the color composites recommended for the manual analysis of cloud cover and types with VIIRS imagery and imagery assist bands and discusses the colors present in the color composites. The approach assumed is one of “peeling an onion” in which information about the scene is gained incrementally as more VIIRS channels are used in color composites. While this approach may not ultimately be used in the time-constrained environment of a weather central, it is useful for training analysts in the interpretation of multispectral satellite meteorology. Training programs that incorporate imagery and the identification of cloud ARPs in the VIIRS User’s Guide are planned, although not included here due to the size of these color imagery files based upon MODIS Airborne Simulator (MAS) data. Information from this section and Section 3.5.3.3 form the basis for the VIIRS User’s Guide, which is included as an appendix to this version of the Imagery ATBD.

The generation of these color composites was done with MAS imagery. The methodology was discussed in the Imagery Technical Interchange Meeting (TIM; [Y4963]). This methodology is depicted in Figure 25.

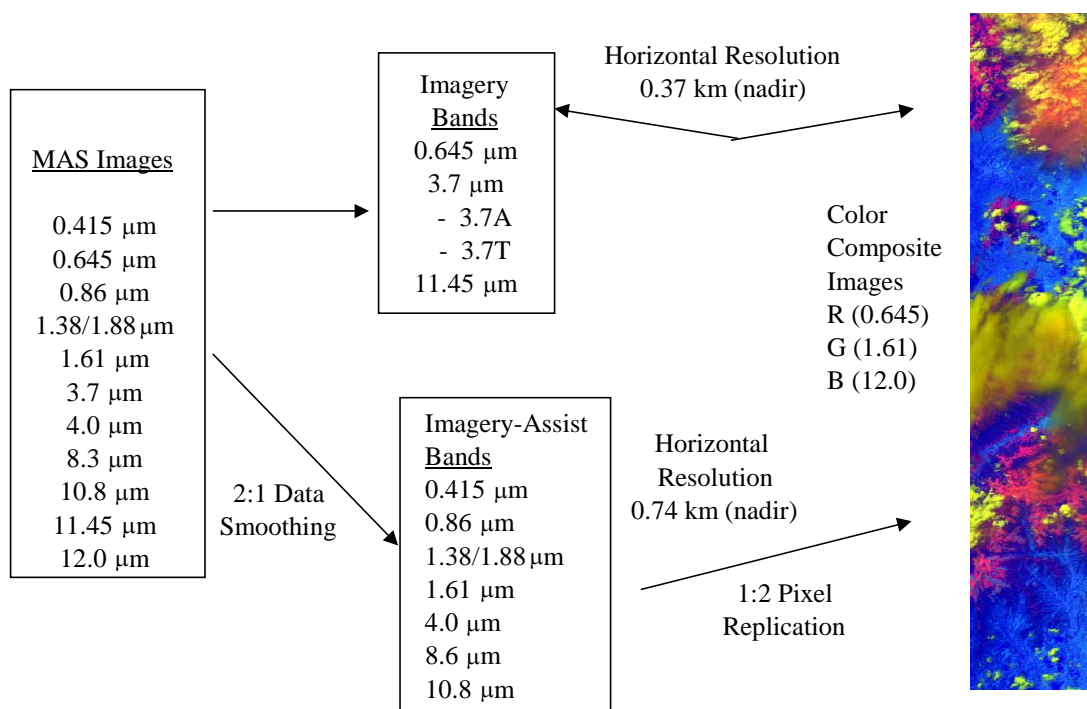


**Figure 25. Methodology illustrated in using MAS data to construct Color Composites using Imagery and Imagery Assist bands.**

VIIRS bands at 0.86 and 1.6  $\mu\text{m}$  are also available at the resolution of the imagery bands. The analyst can use these with unsmoothed imagery bands to obtain some RGB color composites at imagery resolution.

Initially the MAS bands most spectrally similar to VIIRS were considered with reflectance determined for the Solar and NIR bands and brightness temperatures (BTs) determined for the thermal and crossover region bands. The imagery bands underwent no data smoothing, while the imagery assist bands went through 2:1 data smoothing. The final bandset used in the Color Composite generation was decided based upon the spectral information content of the bands used, and what distinct spectral features the cloud analyst wished to from the imagery. Note, this methodology is usable by VIIRS due to the spectral similarities that exist between the VIIRS and MAS/MODIS band sets.

Eighteen color composites were constructed from the VIIRS bandset after a careful survey of the spectral information content. All 18 Composites are included in the Appendix. Eight of these are discussed in this section.

1. Daytime Composite #1 – RGB (0.64, 1.61, 10.8./11.45): Figure 26

A traditional RGB composite that highlights a rich array of cloud and surface detail.

Feature Identification: Highlight differences between water clouds and snow

–Snow is rose – purple

–Low clouds are yellow;

–Higher (water) clouds range from yellow through green to light blue as the cloud temperature decreases.

Assists in separating low, middle, and high-level water clouds as a cloud typing objective

Ambiguities: Cirrus and snow are similar but can be differentiated

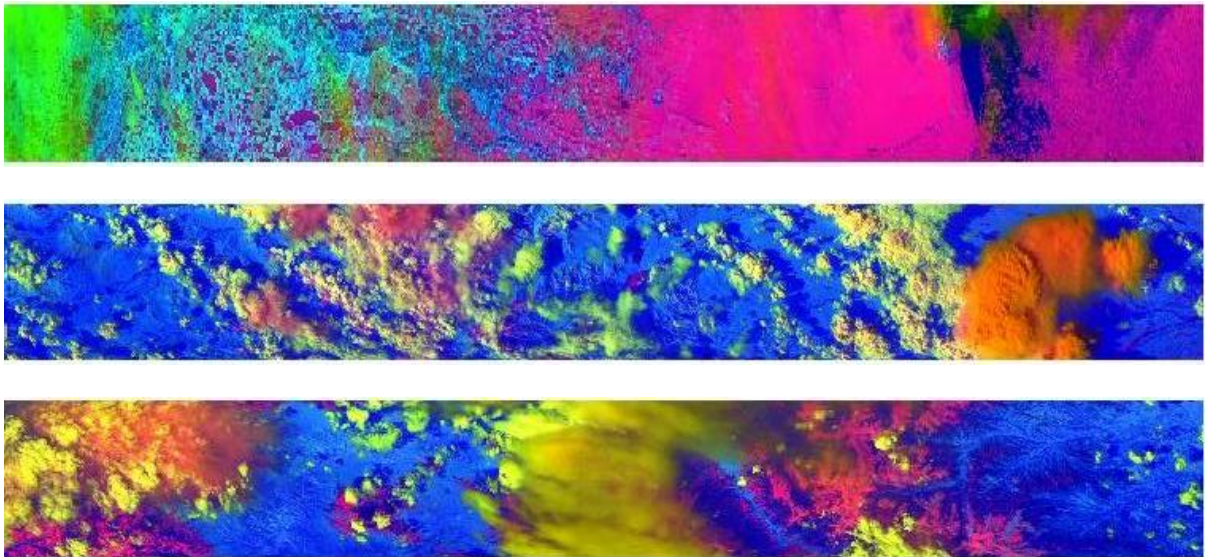


**Figure 26. RGB Composites of bands (0.64, 1.61, 10.8./11.45)**



2. Daytime Composite #2 - - RGB (1.38[1.88], 1.61, 11.45): Figure 27.

This composite brings out additional detail.

Feature Identification: Clear Distinction between cirrus and snow/ice fields

- Snow/ice fields are masked in 1.38  $\mu\text{m}$  imagery
- The 11.45  $\mu\text{m}$  imagery channel provides useful information on cloud top temperatures, when coupled with the 1.38  $\mu\text{m}$  channel can be used to differentiate between cirrus and other cloud types
- Optically-thin cirrus has a deep bluish hue
- Lower-level water clouds appear greenish
- Optically thick cirrus are more golden and in some cases purple
- Overshooting tops, e.g. thunderstorms, appear orange or white-lavender (objective requirement)

Ambiguities: Little detail on snow and surface features. This composite may not provide great detail on cloud top temperatures, i.e. cloud heights, if large temperature variations exist in the scene.

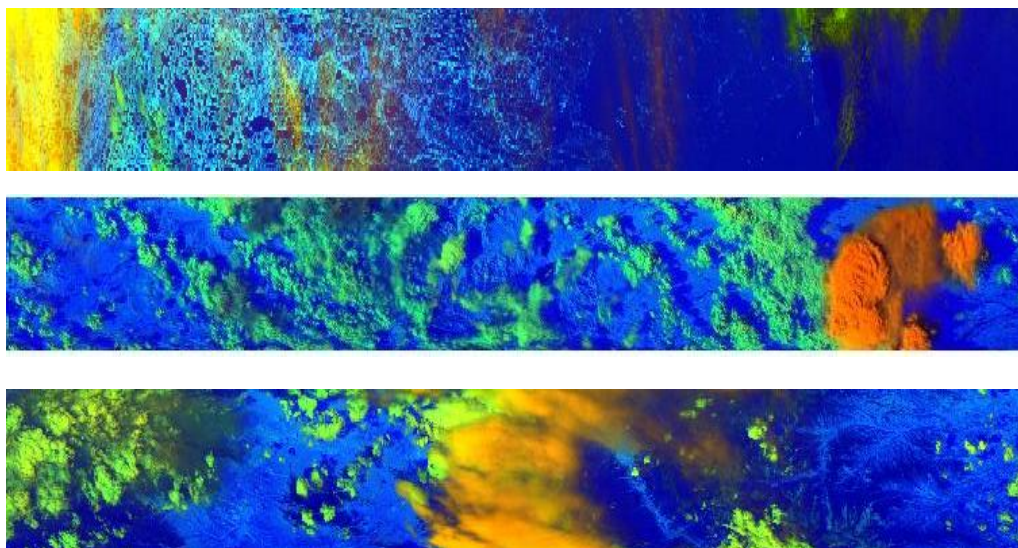


**Figure 27. RGB Composites of bands RGB (1.38[1.88], 1.61,11.45)**

3. Daytime Composite #3 - - RGB (1.61, Invert BT8.6, 0.64): Figure 28.

This composite brings out additional detail.

Feature Identification: Distinction between lower level Cumulus and upper level Cirrus and snow/ice fields

- Snow/ice fields are blue from 0.64  $\mu\text{m}$  imagery
- Optically-thin cirrus has a greenish – turquoise hue due to contribution emissions at 8.6  $\mu\text{m}$
- Lower-level water clouds are rose to white
- Overlaying water clouds are darker blue

Ambiguities: Cirrus and snow may in some cases be the same color

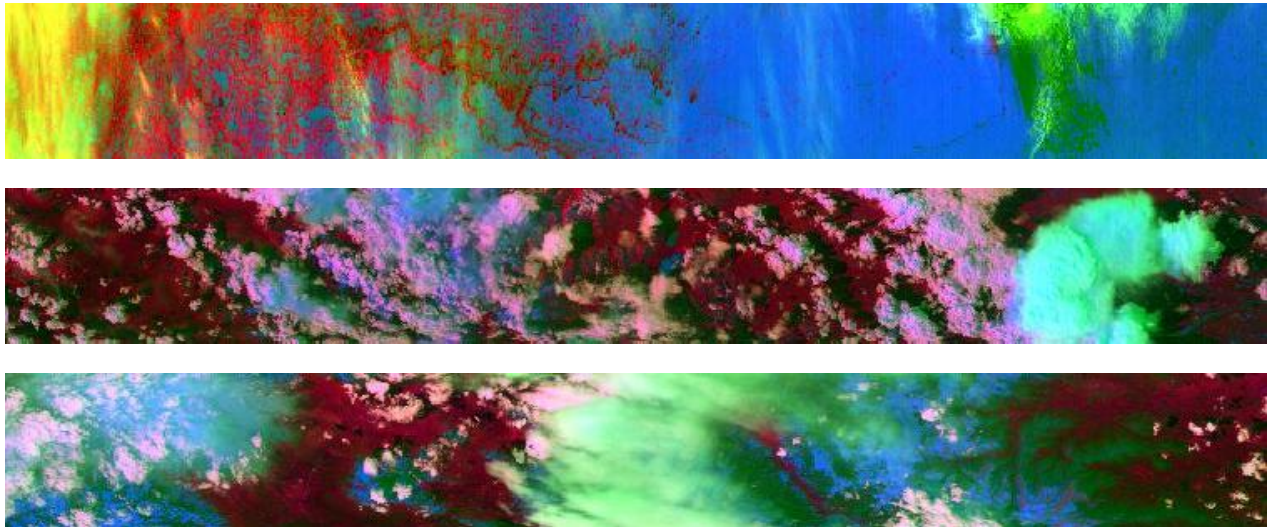


**Figure 28. RGB Composites of bands RGB (1.61, Invert BT8.6, 0.64)**

4. **Day/Night Composite #4** – RGB (BT11.45, BT8.6, BT3.75): Figure 29

This composite brings out additional detail.

Feature Identification: Distinction between lower level Cumulus and upper level Cirrus and snow/ice fields

- Snow/ice fields are olive-green from Thermal imagery
- Optically-thin cirrus has a deep blue-blackish hue over land and blue over ice
- Lower-level water clouds appear dark blue
- Vegetated regions tend to be white
- Overshooting tops, e.g. thunderstorms, appear black with dark clearly defined boundaries, and cellular structure clearly visible (objective requirement)

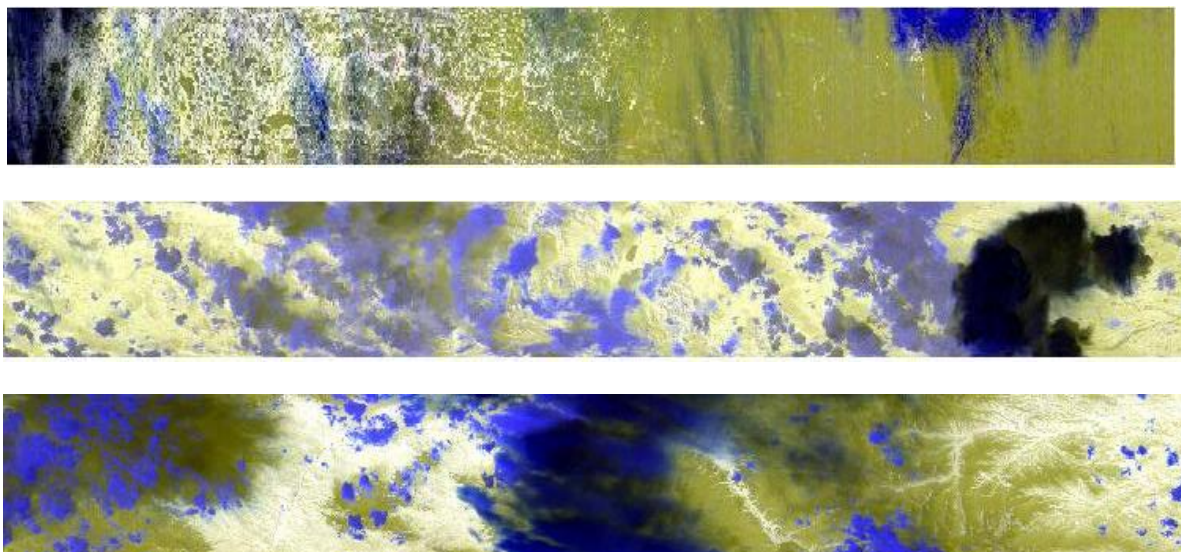


**Figure 29. Day/Night Composite #4 – RGB (BT11.45, BT8.6, BT3.75)**

5. Daytime Composite #5 – RGB (0.64, 0.858, 0.64), Figure 30.

**Feature Identification:** This is the well-known color composite design to highlight “vegetation” because vegetated regions are more highly reflective in the longer wavelengths that make these regions appear “green” in the false color composite. Separation of land and water surfaces is also readily accomplished with this composite that uses the 0.64  $\mu\text{m}$  imagery channel with the 0.858  $\mu\text{m}$  imagery assist channel.

**Ambiguities:** Several features appear gray shaded in this composite and might be ambiguous. For example, snow, water clouds, and non-vegetated regions may all appear as a shade of gray with snow and clouds being particularly difficult to separate.



**Figure 30. Color composite of MAS data collected over Denver, CO  
[RGB= (0.64  $\mu\text{m}$ , 0.858  $\mu\text{m}$ , 0.64  $\mu\text{m}$ )].**



6. Daytime Composite #6 – RGB (0.64, 1.61, 10.8), Figure 31.

**Feature Identification:** This is a relatively new color composite designed to highlight differences between water clouds and snow in newly acquired data from NOAA-15. The process renders the snow and ice white and most other surface features in natural colors. Low clouds are yellow; higher clouds range from yellow through green to light blue as the cloud temperature decreases. This composite assists in separating low, middle, and high-level water clouds as a cloud typing objective.

**Ambiguities:** Differentiation between snow/ice and cirrus clouds may be difficult, especially when they are approximately the same temperature in the 10.8  $\mu\text{m}$  imagery channel, since these clouds are relatively transparent in the 0.64  $\mu\text{m}$  imagery band, and both reflect poorly at 1.61  $\mu\text{m}$  imagery assist channel. (These data were taken from the NOAA website at <http://www.osei.noaa.gov/Events/Snow/NOAA15new> for the gtrlks.jpg example. Cirrus clouds are evident along with snow south of Lake Michigan but both appear white.)

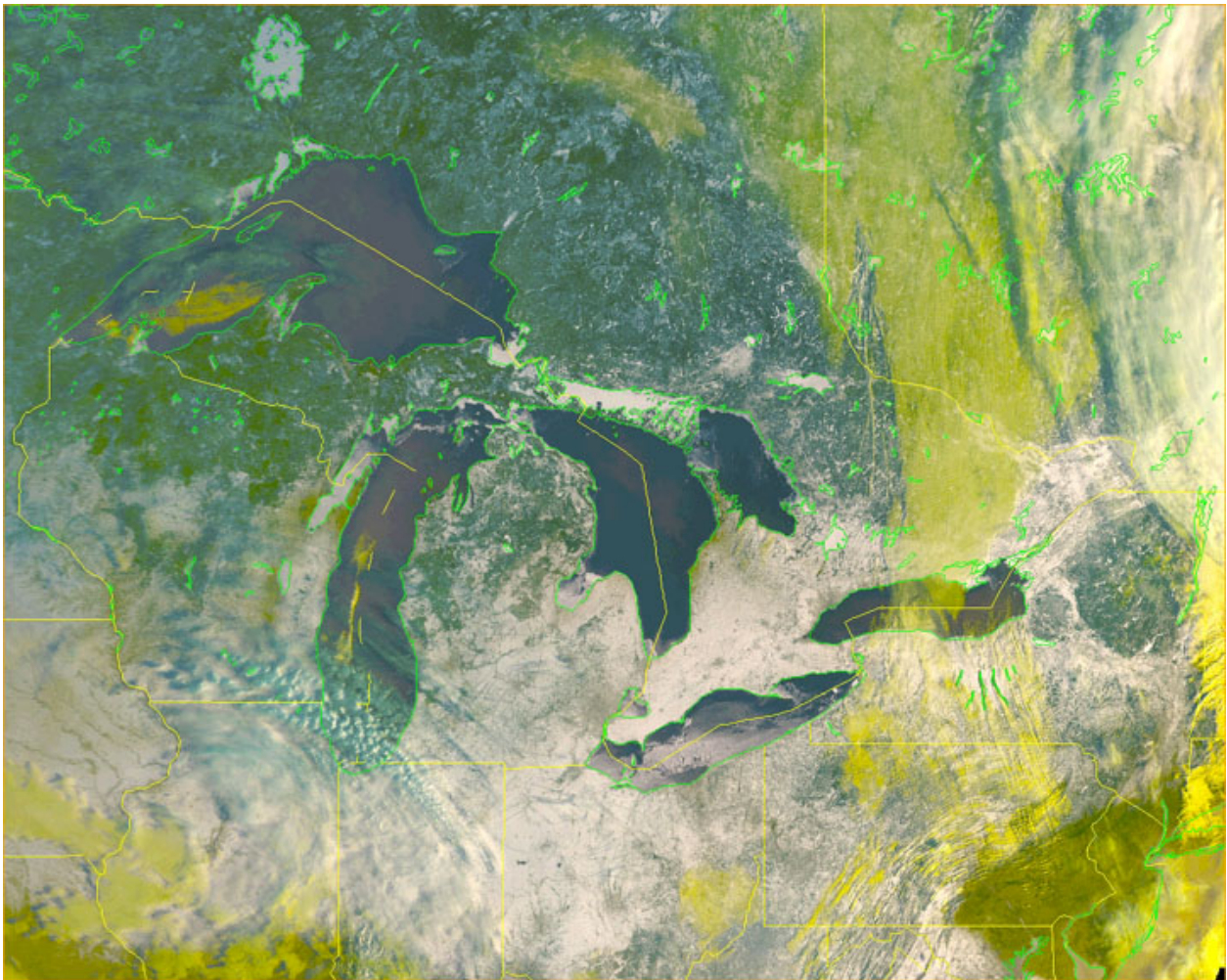


**Figure 31. Color composite of NOAA-15 AVHRR imagery created by assigning the 0.64  $\mu\text{m}$ , 1.61  $\mu\text{m}$ , 10.8  $\mu\text{m}$  channels to the red, green and blue guns of a CRT.**

7. Daytime Composite #7 alternative – RGB (0.64, 1.61, 3.75 albedo), Figure 32a.

Feature Identification: This color composite is also designed to highlight differences between water clouds and snow but provides better differentiation between optically-thin cirrus clouds and snow/ice since the 3.75  $\mu\text{m}$  albedo imagery channel has the appearance of a 3.75  $\mu\text{m}$  minus 10.8  $\mu\text{m}$  brightness temperature difference fields. Therefore, the cloud/cloud discrimination is more accurate. Vegetated land appears green, snow fields are red, optically thick clouds appear yellow to white, while optically thin water (edges) clouds appear bluish. Thin cirrus clouds appear a deep orange because their signatures is more strongly suppressed in the 3.75  $\mu\text{m}$  albedo band than in the 1.61  $\mu\text{m}$  imagery assist channel while thick cirrus appears reddish since it is highly reflective in the 0.64  $\mu\text{m}$  imagery channel while nearly equal in the other two channels.

Ambiguities: This composite provides no information on cloud top temperatures as does the RGB (0.64, 1.61, 3.75) since the process renders the snow and ice white and most other surface features in natural colors. Care must be taken in this composite since the 3.75  $\mu\text{m}$  channel measures optical thickness, not temperatures. Therefore, edges of a stratocumulus cloud, for example, may be a different color than pixels located at center of the cloud.

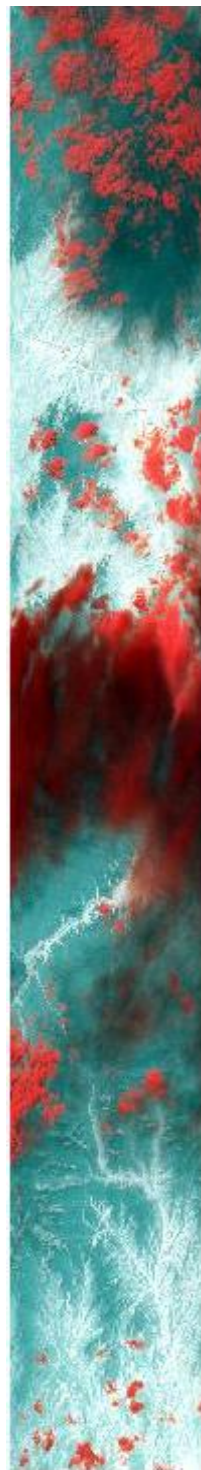
8. Nighttime Composite #9 – RGB (3.75, 10.8, 11.45), Figure 32b.

Feature Identification: This is the well-known color composite design to highlight stratus clouds (which appear reddish due to their lowest emissivity in the 3.75  $\mu\text{m}$  imagery) and optically-thin cirrus clouds, which appear bluish due to their coldest temperatures in the 11.45  $\mu\text{m}$  imagery channel.

Ambiguities: This composite may not provide great detail on cloud top temperatures, i.e. cloud heights, if large temperature variations exist in the scene.



(a)



(b)

**Figure 32 (a.) Color Composite of MAS imagery over Denver, CO [RGB (0.64, 1.61, 3.75 albedo] (b.) [RGB (3.75, 10.8,11.45)]**

Generation of these RGB composites greatly assists the manual analyst in determining cloud type and also to increase confidence in the cloud cover determination. Use of RGB composites will result in fewer Quality Control (QC) bogus operations and assist the manual cloud analyst in determining cloud type for many of the objective cloud types. The biggest improvement will be in the fact that the manual analyst will have improvements in meeting critical time schedules by using RGB composites.

The Raytheon VIIRS team has identified the need for a “VIIRS User’s Guide” for the interpretation of imagery and has developed the structure of this publication. It is needed because:

Current OLS & AVHRR sensors are spectral content limited. Analysts using these data are accustomed to “seeing” clouds and different backgrounds in only five spectral bands. VIIRS extends MODIS a leap forward into an operational context. MODIS contains 36 spectral bands but these data are only used in a research environment. VIIRS will provide all the value of MODIS for manual cloud analyses in the operational environment within a 20 minute time frame.

Algorithm technology and user knowledge must be brought forward to fully realize value of true multispectral VIIRS measurements. The VIIRS automated cloud analysis algorithms exploited the spectral signatures of these data to generate the cloud cover product. It is therefore essential that those who perform manual quality control of these automated products be expert in the knowledge of spectral signatures in these bands. Thus, it becomes necessary to educate the users of the VIIRS data. A VIIRS User’s Guide is the one highly beneficial approach to help facilitate this education process

### 3.5.3.5 VIIRS Cloud Mask for Imagery

In addition to the Imagery and Imagery assist bands the analyst will also have access to the Cloud Mask Intermediate Product (IP). The Cloud Mask is an automated algorithm done within the VIIRS Data Processing Architecture. A full description of this algorithm is available in the VIIRS Cloud Mask (VCM) Algorithm Theoretical Basis Document ATBD (ref Y2412).

### 3.5.4 Performance of Manually-Generated Cloud Data

The performance of manually-generated cloud data with respect to the VIIRS requirements and the system specification (c.f. Tables 3 and 4) is reviewed in this section.

The performance analysis was conducted as part of the SRD requirements flowdown to the sensor, as documented by Hutchison (1998). A brief overview of the methodology is provided here.



VIIRS sensing requirements were established using a series of simulations. To define these requirements for the manually generated cloud data product, the following simulation scenarios were defined and results of the simulations are shown in the Appendix:

- Case 1: Stratus at Night
- Case 2: Daytime and Nighttime Cirrus
- Case 3: Cloud Typing (Stratus versus Cirrus)
- Case 4: Cumulus
- Case 5: Daytime Obscurations

All simulations were performed over a variety of surface backgrounds, as shown in Figure 34, including ocean, sand, fresh snow, and mixed vegetation. Values for spectral reflectivities and absorptivities were taken from the data base in the Space-Based Infrared System (SBIRS) toolkit. Later, it was verified that identical values were used in MOSART once this software package was released by the NPOESS IPO to Raytheon. Radiative transfer computations were made within PACEOS<sup>TM</sup>, which can generate imagery scenes using MODTRAN 3.5 and later MODTRAN 3.7, after it was released by the IPO.

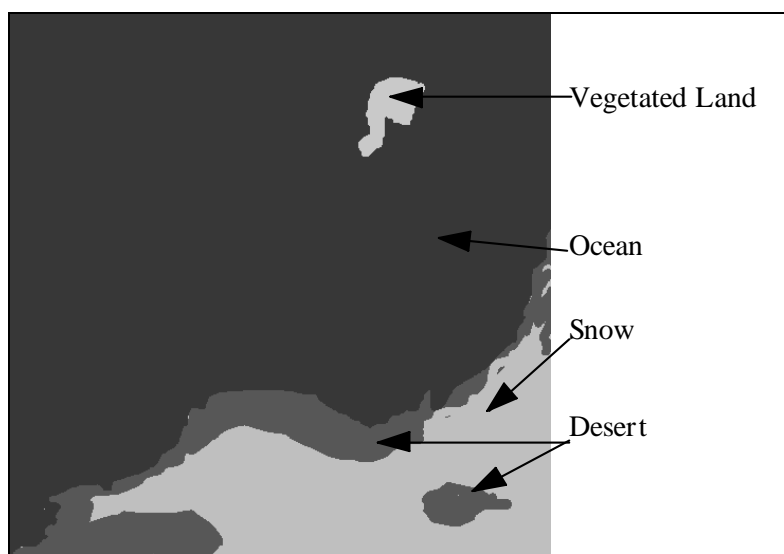


**Figure 34. VIIRS sensing requirements were based upon a variety of surface classifications.**

Recommended values for TBRs and TBDs were created by running a series of simulations using results of manual cloud analyses on simulated clouds of different optical thickness. Statistics were developed between the manual analyses and the binary cloud maps (ground truth or a priori analyses) input into PACEOS<sup>TM</sup> at the start of each simulation.

Results are shown for cirrus clouds. The detection and typing of cirrus clouds (Case 2) is a driving requirement for VIIRS imagery. This case was simulated using four different visible optical depths, i.e. 0.003, 0.008, 0.015, and 0.030 along with models for sensor noise generated by Santa Barbara Remote Sensing (SBRS). All analyses were performed using only the simulated 12.0- $\mu\text{m}$  VIIRS imagery channel. Manual cloud cover analyses were created from the synthetic imagery and compared against the binary cloud map which was input PACEOS<sup>TM</sup> to generate the simulations. Results were then summarized using definitions of measurement accuracy, precision, and uncertainty as defined in Appendix A of the NPOESS SRD dated April 17, 1997.

Figure 35 illustrates the results of a simulation that satisfies the requirements for cloud cover Measurement Uncertainty.

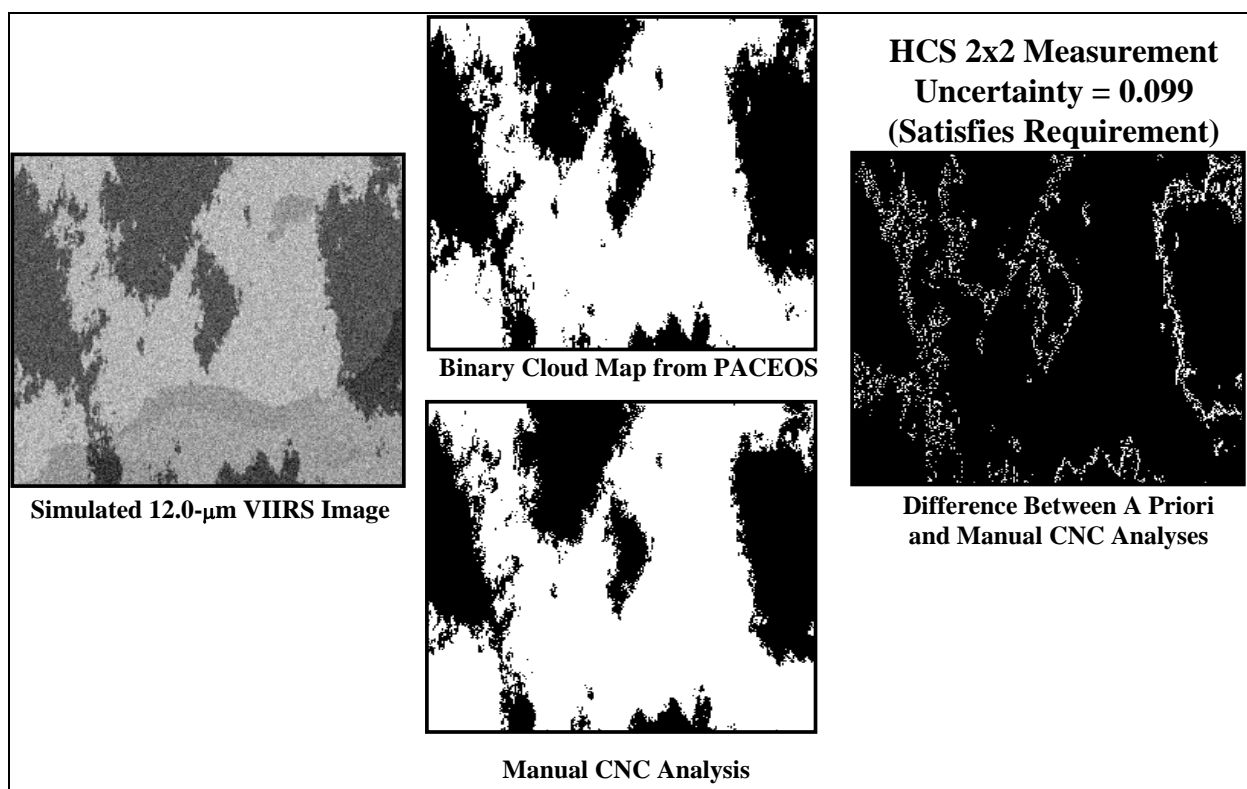


**Figure 35. Measurement uncertainty based upon manually-generated cloud analysis of simulated VIIRS 12.0- $\mu\text{m}$  imagery created for cirrus optical depth 0.03.**

### 3.5.4.1 Cloud Cover

The sensor noise model used for the simulation shown in Figure 33 is noisier than the sensor specification. As a result, the specification provides margin against the requirement. Table 16 shows the Cloud Cover measurement uncertainty errors, determined using the procedures described above, stratified by cloud type. Performance is for a horizontal cell 3 times the

imagery HSR, and is based on the sensor noise specification. Actual sensor performance is expected to be better than the specification.

**Table 16. Cloud Cover Measurement Uncertainty**

Cloud Type	Status (Nighttime)	Cirrus	Cumulus (Daytime)	Obscured Not Cloudy
Measurement Uncertainty	0.027	0.078	0.04	0.041

These results demonstrate that the predicted performance satisfies threshold requirements with margin, even for the driving case of thin cirrus.

Additional analyses were also completed to determine the capability of the human analyst to satisfy VIIRS Objective Requirements for the manually-generated cloud cover ARP. Results are based upon the manual detection of cirrus clouds, which is the worst case scenario. These results are shown in Table 17 and demonstrate that the measurement uncertainty remains below 0.1 for HCS 2 times HSR, which is the only attribute that changes between the VIIRS Threshold Requirement and Objective Requirement for the manually-generated cloud cover ARP. Therefore, the imagery channels selected for the VIIRS sensor also allow the analyst to satisfy the VIIRS Objective Requirements for manually-generated cloud cover, even though there is little margin. (Blue denotes VIIRS Objective Requirements are satisfied for this ARP.)

The threshold HCS requirement, shaded green, is 3 x 3 pixels. The objective HCS requirement, shaded blue, is 2 x 2 pixels. The results shown in Table 12 were obtained with the LWIR band, using a sensor model with more noise than the current specification (c.f. Section 2.2, Table 2).

Table 17 also shows the relationship between HCS and measurement uncertainty of manually-generated cloud cover analyses (Blue denotes success in meeting Objective Requirements; Green is success in meeting Threshold Requirements). VIIRS pixels are classified as either completely cloudy or completely cloud-free by the human analyst, which makes the distributions completely bi-modal at the HSR level. As these pixel data are aggregated to the reporting interval, these distributions become less bi-modal as the HCS size increases. Thus, the larger the HCS, the less likely it is to be perfectly correct but more important they are also less likely to be completely in error when compared to the a priori cloud map used to build the simulated VIIRS imager. The result is that the Root Mean Square Error (RMSE) measurement uncertainty becomes smaller as the HCS becomes larger. At HCS 2x2 HSR, the measurement uncertainty for the manually-generated analysis of cirrus in simulated VIIRS imagery using only the LWIR band is 0.099. The Objective requirement is 0.1 at this HCS; therefore, the objective requirement is satisfied.

**Table 17. Measurement Uncertainty versus HCS from manual analysis of cirrus with visible optical depth of 0.03.**

HCS	NUMBER OF HCS PIXELS IN SIMULATONS			BI-MODAL	UNCERTAINTY
(2 x 2 pixels)	Total	Clear	Overcast	(Percent)	(Fraction)
Truth	16,129	10,363	4677	93.25	n/a
Analysis	16,129	10,124	4969	93.58	0.099
(3 x 3 pixels)					
Truth	7140	4417	1890	88.33	n/a
Analysis	7140	4364	2010	89.27	0.078
(4 x 4 pixels)					
Truth	3969	2389	967	84.56	n/a
Analysis	3969	2373	1049	86.22	0.069
(8 x 8 pixels)					
Truth	961	528	170	72.63	n/a
Analysis	961	529	194	75.23	0.050
(25 x 25 pixels)					
Truth	100	40	3	43.00	n/a
Analysis	100	40	6	46.00	0.032

### 3.5.4.2 Cloud Type

Three characteristics of clouds are considered by the human analyst in creating the Manually-Generated Cloud Type ARP. These characteristics include:

(1) Cloud spectral signatures: in general, stratus clouds are colder in the 3.75 micron band than the 11.45 micron band while the reverse is true for thin cirrus clouds.

(2) Cloud top temperatures: in general, water clouds can be segregated into lower level and higher level clouds based upon their temperatures in the 11.45 micron band. For example, comparison of the cloud top temperature to cloud-free surface temperatures of the neighbor regions allows the analyst to estimate cloud top height, using the general rule that temperature decreases approximately 6 degrees Kelvin for every kilometer in the troposphere. This approach allows stratocumulus (low clouds) to be readily differentiated from altocumulus (middle clouds).

(3) Texture: in general, cumuliform clouds are readily differentiated from stratiform clouds and cirrus clouds are identified by texture. For example, cirrocumulus associated with the jet stream is famous for its “fishbone” appearance.

These characteristics can be combined to identify additional cloud types. For example, texture allows standing lenticular clouds to be identified and cloud top temperatures allow stratocumulus standing lenticular clouds to be separated from altocumulus standing lenticular clouds while spectral signatures allow cirrocumulus standing lenticular clouds to be identified.

Based upon the spectral signatures, cloud top temperatures, and the Raytheon VIIRS imager design, we believe it is possible to positively identify 18 of the 17 cloud types listed as

Objective Requirements for the Cloud Type ARP, including all cloud types listed as Threshold Requirements. This list and techniques used for positive identification are shown in Table 13. Examples of the applications of these techniques are contained in Appendix A.

**Table 18. Approach to the positive identification of cloud types by human analysts using VIIRS imagery and imagery assist bands.**

Cloud Type	Abbreviation	Approach to Accurate Classification			Comments
		Spectral Signature	Shape/Texture	Temperature Contrast (cloud top vs cloud-free)	
Alto cumulus	AC		x	x	
Alto cumulus Castellanus	ACCAS				small scale features
Alto cumulus (Standing Lenticular)	ACSL		x	x	
Alto stratus	AS		x	x	
Cirrocumulus	CC	x	x	x	
Cirrocumulus (Standing Lenticular)	CCSL	x	x	x	
Cirrostratus	CS	x	x	x	
Cirrus	CI	x	x	x	
Cumulonimbus	CB	x	x	x	
Cumulus	CU		x	x	
Cumulus Fractus	CUFRA				small scale features
Towering Cumulus	TCU		x	x	
Stratus Fractus	STFRA				small scale features
Nimbostratus	NS				requires ancillary precipitation data
Stratocumulus	SC		x	x	
Stratocumulus (Standing Lenticular)	SCSL		x	x	
Stratus	ST	x		x	
Obscured/Not Cloudy	OBS	x	x		
Clear	CLR	x			

Cloud types achieved for Threshold Requirements are shaded green. Cloud types achieved for Objective Requirements are shaded blue. Unshaded cloud types are unachieved objective requirements.

The imagery channels chosen to satisfy the requirements for cloud cover also allow the threshold cloud types, listed in the table, to be identified with little or no ambiguity based upon unique spectral signatures, texture, and shape. Therefore, the minimum cloud typing can be completed with very high (>95%) probability of being correct.

The four cloud types that cannot be identified directly with VIIRS imagery and imagery assist bands are nimbostratus, cumulus fractus, stratus fractus, and altocumulus castellanus. Nimbostratus is only differentiated from altostratus by the occurrence of rain, which cannot be positively identified by the VIIRS alone. The other unidentifiable cloud types involve all fractus-type clouds that are identified by small scale features indicative of atmospheric instabilities. The small scale features are observable by the human on the ground but not by a satellite with a 400 meter horizontal spatial resolution at 833 km in space.

### 3.5.5 Initialization and Validation

Initialization and validation activities can best be accomplished in coordination with the U.S. Air Force Weather Agency (AFWA), which is the primary customer for the manual and automated cloud data product EDRs. The purpose of these activities is to assure that:

- (1) VIIRS data products can be incorporated into the automated Cloud Depiction and Forecast System (CDFS)
- (2) Human analysts have the necessary skills to fully exploit the VIIRS imagery in the quality control (BOGUS) process. This initialization and validation process assumes that the CDFS program will provide AFWA with the capability to construct color composites and that there exists an interactive environment which allow analysts to exploit these color composites in the quality control process to ensure the benefits of an operational test and evaluation program are fully achieved in an operational setting prior to the launch of the first VIIRS sensor.

While the development of such a test and evaluation program will require the participation of numerous agencies (including the NPOESS IPO, AFWA, and Raytheon VIIRS team), the proposed approach could utilize MODIS imagery and automated cloud data products (i.e. automated cloud cover and cloud top EDRs as test data sets for initialization of the CDFS software environment. Analysts would be given access to MODIS imagery. Training on the exploitation of these data sources could be based upon the VIIRS User's Guide. The User's Guide, which has been further developed in Phase II, is included as an appendix to this document. This approach to an initialization and verification program is highly desirable since it would leverage existing software at AFWA and the analysts needed to provide an independent assessment of the VIIRS imagery.

The pre-launch characterization and post-launch validation plan for the VIIRS Cloud EDRs will be extended to the Manually Generated Cloud Data. Details are discussed in the VIIRS System Verification and Validation Plan Document [TP 154640-001].

## 3.6 MANUAL SEA ICE ANALYSIS ARP DESCRIPTION

### 3.6.1 Processing Outline

Manual sea ice analysis products are not produced by the VIIRS operational system. They are expected to be produced at various locations by trained analysts, using the VIIRS Imagery as input data. Different analysts may wish to use different techniques. The manual sea ice data Application Related Products (ARP) requirements for ice edge location and ice concentration are discussed in sections 2.5.3 and 2.5.4. Enhanced imagery of VIIRS visible (640 nm) and near infrared (865 nm) reflectance bands may be visualized to assist in determination of ice edges for day and surface temperature derived from the VIIRS imagery resolution thermal band (11.45  $\mu\text{m}$ ) for night. Available microwave sensors such as AMSR-E or (MIS in the NPOESS timeframe) should assist in analysis of sea ice concentration and ice edge location, particularly for night. Geolocation associated with ice edges is determined by referencing the latitudes and longitudes in the 375 m terrain corrected Geolocation SDR associated with ice edge pixels. A VIIRS Manual Ice Concentration may be derived by application of a tie point method, such as described in the VIIRS Sea Ice Characterization ATBD (D41063.) The fraction of ice cover for each imagery pixel is retrieved and reported as the VIIRS Sea Ice Concentration Intermediate product. Gridded ice fraction at imagery resolution may be used to assist in determination of the VIIRS Manual Ice Edge Location.

### 3.6.2 Algorithm Input

An assessment of the importance of various data (VIIRS and other data sources) to augment VIIRS Imagery data are listed in Table 19.

**Table 19. Data to Augment Manual Analysis of Sea Ice Concentration and Ice Edge Location**

Prioritized Item	Application	Utility assessment
1) VIIRS Sea Ice Concentration IP	Allows analyst direct visualization of sea ice concentration and provides basis for ice edge detection.	Very important. Manual comparison method. VIIRS Ice Concentration IP is a non-deliverable Retained Intermediate Product.
2) VIIRS Surface Temperature IP	Allows analyst direct visualization of surface temperatures to assist in discrimination of ice from ice free regions.	Very important. Manual comparison method. VIIRS Surface Temperature IP is a non-deliverable Retained Intermediate Product.
3) Raw Vis/Day-Night Vis/IR imagery (contrast enhanced)	Presents a less processed view of the scene. Processing artifacts, pseudo-colors, etc., are removed, allowing analysts to make an independent assessment of the scene.	Important but difficult to assess contribution. Perform manual sea ice analysis and compare results to ground truth [Manual comparison method]
4) Microwave sensor data	Draws analyst attention sea ice regions. Can judge whether imagery effects are from clouds or sea ice. Provides independent assessment of the scene.	Important. Manual comparison method

Prioritized Item	Application	Utility assessment
6) Sea Ice Age EDR	Draws analyst attention sea ice regions at VIIRS moderate resolution (750 m @ nadir)	Important. Manual comparison method
7) Cloud mask/ Cloud Cover	Used to discriminate clouds from sea ice by providing details on pixel cloud confidence, thin cirrus, and cloud phase.	Important. Manual analysis to assist discrimination of sea ice and clouds.
8) Geographic latitude, longitude, and solar zenith angle	Identifies latitude, longitude and solar zenith angle determination of location and identification of terminator transition regions	Important. Manual analysis to determine pixel locations and terminator region
9) Aerosols	Analyst can judge whether imagery effects are from clouds or aerosols	Less important. Manual comparison method

### *Geographic Latitude/longitude, Solar Zenith and Sensor Zenith Angles*

The VIIRS EV\_375M SDR will contain geodetic latitude, longitude and solar zenith angle of each imagery resolution pixel. The SDR coordinates will be used to report the latitude and longitude coordinate of each pixel. The solar zenith angle will be used to determine terminator transition regions. The sensor zenith angle will be used to assess the quality or reject analysis of pixels residing near the edge of scan.

### *Aerosol Optical Thickness*

Aerosol optical thickness (AOT) is obtained at moderate pixel resolution from the Aerosol Optical Thickness IP. It is used to assess pixel quality.

### *Surface Temperature*

Surface temperature is needed for ice concentration retrieval at night, and is often useful for daytime retrievals.

The VIIRS Surface Temperature IP algorithm [D43761] will determine the surface temperature for each imaged pixel, which will be supplied as a Surface Temperature IP [Y10880].

### *Cloud Mask*

The VIIRS cloud mask [Y2412] is expected to derive a status of confident clear / probably clear / probably cloudy / confident cloudy for each pixel, building on MODIS cloud mask heritage (Ackerman *et al.*, 1997). The VIIRS cloud mask contains information about the cloud phase and includes a land water mask at moderate resolution.



### 3.6.2.1 VIIRS Data

VIIRS data will be in the form of two-dimensional pixelized images of visible surface reflectance, NIR surface reflectance and thermal infrared brightness temperature. A summary of VIIRS imagery resolution bands applicable to sea ice concentration and ice edge location is presented in Table 20. The 0.64, and 11.45  $\mu\text{m}$  imagery bands are sufficient to meet SRD requirements with margin. The 0.865, 1.610 and 3.74  $\mu\text{m}$  imagery-assist bands provide extra margin.

**Table 19. Sea Ice Manual ARP Analysis Input Imagery Data Summary.**

$\lambda$ ( $\mu\text{m}$ )	$\Delta\lambda$ ( $\mu\text{m}$ )	GSD (m) at Nadir (Track x Scan)	HCS (m) at Nadir (Track x Scan)	GSD (m) at Edge of Scan (Track x Scan)	HCS (m) at Edge of Scan (Track x Scan)
0.64	0.080	371 x 131	371 x 393	800 x 800	800 x 800
0.865	0.039	371 x 131	371 x 393	800 x 800	800 x 800
1.610	0.06	371 x 131	371 x 393	800 x 800	800 x 800
3.740	0.38	371 x 131	371 x 383	800 x 800	800 x 800
11.45	1.90	371 x 131	371 x 393	800 x 800	800 x 800

### 3.6.2.2 Non-VIIRS Data

The algorithms for Imagery (Sea Ice Data) require no ancillary data from outside of the VIIRS system. Available microwave sensor imagery from AMSR-E or the Microwave Imager/Sounder (MIS) in the NPOESS timeframe will be required to supplement analysis based on VIIRS Imagery SDR data, particularly for analysis for terminator and night conditions.

## 3.6.3 Theoretical Description of the Retrieval

In the following sections, the mathematical background of the processes outlined in Section 3.6.1 is described.

### 3.6.3.1 Physics of the Problem

#### *Ice reflectance*

Remote sensing and *in situ* studies of sea ice are relatively widespread and are of significant potential benefit. The wide range in spectral albedo observed in sea ice of various types and thickness is a well-established characteristic of sea ice (Grenfell and Maykutt, 1977; Grenfell and Perovich, 1984).

Spectral reflectance curves differ for different ice type. Each ice type has its own characteristic spectral signature. Spectral albedo of sea ice at various bands undergoes significant changes depending upon ice thickness, structure, and the state of the ice surface.

Reflectance from ice surfaces differs from snow reflectance because the ice consists of sheets rather than grains. Clear ice slabs are highly transmitting (Bolsenga, 1983). Reflectance occurs by scattering from impurities, such as brine pockets and air bubbles. Therefore, the reflectance observed from natural ice surfaces is highly variable, depending on the condition of impurities for a given ice sheet. Given the wide variety of ice conditions in nature, ice reflectance is not as well determined as snow reflectance. Snow reflectance is amenable to the Mie scattering theory (Warren, 1982). In contrast, studies of ice reflectance tend to be empirical.

One well-established characteristic of sea ice is the wide range in albedos observed in first-year ice of various types and thickness (Grenfell and Maykutt, 1977; Grenfell and Perovich, 1984). This characteristic is an important limiting factor in reflectance-based retrieval of ice concentration in the absence of snow cover (Massom and Comiso, 1994).

Visible and NIR reflectance is a useful ice/water discriminator, as water reflectance in this spectral range is lower than the reflectance from all but the thinnest ice surfaces.

### *Snow reflectance*

The reflectance characteristics of sea ice surfaces are influenced by accumulated snow cover. Pure snow is a distinctive target across a part of the solar spectrum. It is among the brightest of natural substances in the visible and near-infrared part of the spectrum, but it is also often the darkest in the shortwave infrared (Dozier, 1989). The spectral albedo of snow depends on wavelength, and this dependency is controlled by the imaginary part ( $k$ ) of the complex refractive index. This reaches a minimum at a wavelength of about 0.46 microns, and increases by a factor of  $10^6 - 10^7$  as wavelength increases out to 2.5 microns (Warren, 1982; Dozier, 1989). Light transmission decays exponentially in snow across a distance ( $d$ ) as  $\exp(-4\pi kd/\lambda)$ . The  $e$ -folding distance for snow (the distance over which transmittance is reduced to  $1/e$ ) decreases from more than 20 m in the 0.4 – 0.5 micron range to less than 1 mm at 1.6 microns.

Light in snow is scattered primarily by refraction through, not reflection from, the ice grains. Photons are scattered at the grain surfaces, but absorbed while traversing the grain interiors. Only about 3 percent of the light scattered by an ice grain is reflected from the external surface. Nearly 89 percent is refracted through the grain, and 8 percent is scattered after internal reflections (Bohren and Barkstrom, 1974). Because ice is so transparent to visible radiation, snow reflectance is insensitive to grain size in bands below 0.7 microns, but sensitive to absorbing impurities in the snow (Wiscombe and Warren, 1980; Grenfell *et al.*, 1981). Because absorption by ice is much stronger in bands above 1.4 microns, reflectance at these wavelengths is insensitive to absorbing impurities, but sensitive to grain size. Absorbing particulates affect snow reflectance out to 0.9 microns (Grenfell *et al.*, 1981; Warren and

Wiscombe, 1980), so the 0.86 micron band is sensitive to both absorbing impurities and grain size. All values in this paragraph are determined from geometric optics for a sphere.

The spectral signature of snow is unique among common substances. Clouds and snow are both bright across the visible and near-infrared region, but clouds are much brighter than snow in the shortwave infrared. This is because the smaller size of the scatterers in clouds decreases the probability of absorption in this spectral region where ice and water are moderately absorptive (Crane and Anderson, 1984; Dozier, 1984, 1989). Conversely, bodies of open water are dark at all wavelengths.

Visible and NIR reflectance is a useful ice/water discriminator when there is snow cover on the ice, as water reflectance in this spectral range is lower than snow reflectance.

The physical basis of snow reflectance is also discussed in the VIIRS Snow Cover/Depth ATBD [D43758].

### *Surface temperature*

During a great part of the seasonal cycle, infrared bands will be the only available information to retrieve ice fraction. Infrared radiance allows us to calculate surface temperature.

Ice surface temperature is a good indicator of ice state for ice with thickness less than 1 meter. The surface temperature varies in a large range of magnitude depending on the stage of ice development or ice age (thickness). Thus, surface temperature is an indicator of ice age.

Changes in sea ice surface temperature are governed by the joint influence of vertical heat fluxes of different origin. The intensity of turbulent exchange by heat between the atmosphere and underlying ice surface, as well as the surface balance of long-wave radiation, directly depend on ice surface temperature. Vertical heat flux through ice cover is an explicit function of the vertical ice temperature profile, which depends on ice surface temperature. Thus, all main components of heat exchange between the atmosphere and the underlying ice surface (except short-wave radiation fluxes) are explicit functions of ice surface temperature.

In wintertime, heat flux between the atmosphere and ice is compensated by ice growth at the underside of the ice. There are no vertical changes in heat flux at the boundary between air and ice surface. At the same time, many components of heat flux depend on ice surface temperature. Therefore, conditions of conservation of vertical heat flux at the surface can be fulfilled only if ice surface temperature is adjusted to varying influencing environmental conditions.

Ice thickness is the main factor determining vertical heat flux through the ice under specified atmospheric conditions. Thus, a general conclusion about the relation between ice surface temperature and thermodynamic processes in ice cover and atmospheric boundary layer can be formulated. Ice surface temperature is determined by the processes of vertical heat exchange and is a distinctive indicator of ice thickness.

Surface temperature is a useful ice/water discriminator, as water temperature is higher than the temperature of all but the thinnest ice surfaces.

### 3.6.3.2 Mathematical Description of the Sea Ice Algorithms

#### 3.6.3.2.1 Image Processing for Sea Ice ARP Analysis

Manual interpretation of sea ice extent, concentration and ice edges in multispectral imagery is facilitated by use of false color composite images of the VIIRS Imagery reflectance and brightness temperature imagery bands listed in table 19. Histogram equalization and other image processing contrast enhancement techniques can be utilized to increase contrast of ice features associated with ice edges and regions of ice concentration less than 100%. Ice edges between pure open water and ice pixels during day may be detected by manual analysis of enhanced Red, Green, Blue (RGB) imagery of the following band combinations: 1.6  $\mu\text{m}$  (red), 0.865  $\mu\text{m}$  (Green), 0.64  $\mu\text{m}$  band (Blue). Night detection of ice edges will require utilization of both enhanced grey shade images and pseudo color images of the VIIRS imagery resolution 11.45  $\mu\text{m}$  and 3.7  $\mu\text{m}$  thermal bands. Pseudo coloring is a standard image processing technique in which selected ranges of values in an image (temperatures) are assigned to specific colors. Regions above the freezing point temperature of sea water may be assigned a color such as red. Availability of a Surface Temperature IP product would allow visualization of pseudo colored surface temperature imagery and allow for more accurate discrimination of regions above and below sea water freezing temperature. Direct enhancement of grey shade thermal imagery also will be required to distinguish ice from ice free regions in VIIRS night imagery. Pseudo color image enhancement of available microwave sensor (MIS) based surface temperatures and ice concentration products will provide valuable supplemental information, particularly for terminator and night conditions as well as cloud obscured regions.

Figure 36 is enhanced MODIS proxy day scene of the Bering Strait. The imagery for the VIIRS 1.6, 0.865, and 0.64  $\mu\text{m}$  bands were enhanced by performing a histogram equalization contrast enhancement and combined into an RGB image. Ice free oceans appear dark blue and clouds appear white or blue/white. Land cover with no snow appears green. Snow covered land as bright yellow and sea ice surfaces appear as light yellow. St Lawrence Island is in the center of the scene. Zoomed imagery shown in Figure 37 may be enhanced individually (Figure 38) to further assist in distinguishing ice edges from ice free ocean.

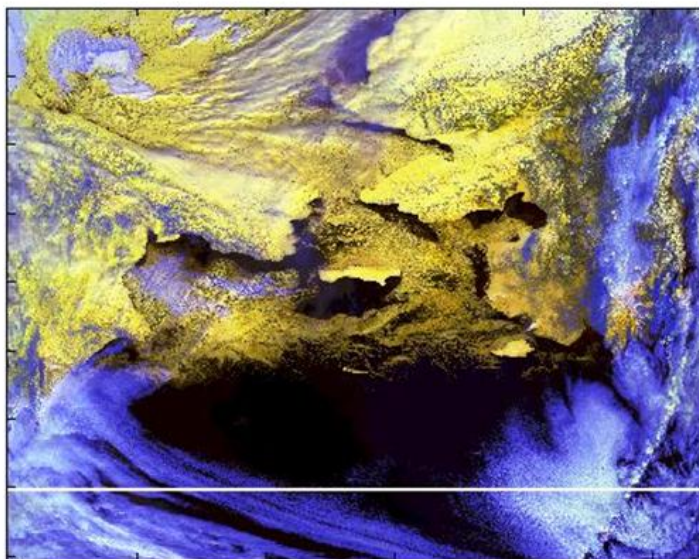


**Figure 36. Enhanced VIIRS Imagery SDR RGB (1.6, 0.865, 0.64  $\mu\text{m}$ ) image of Bering Strait.**

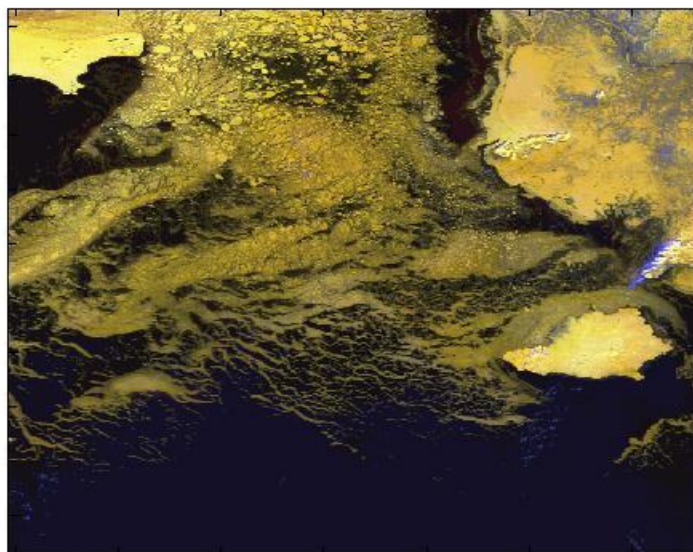


**Figure 37. Zoomed region of VIIRS Imagery SDR RGB (1.6, 0.865, 0.64  $\mu\text{m}$ ) imagery.**

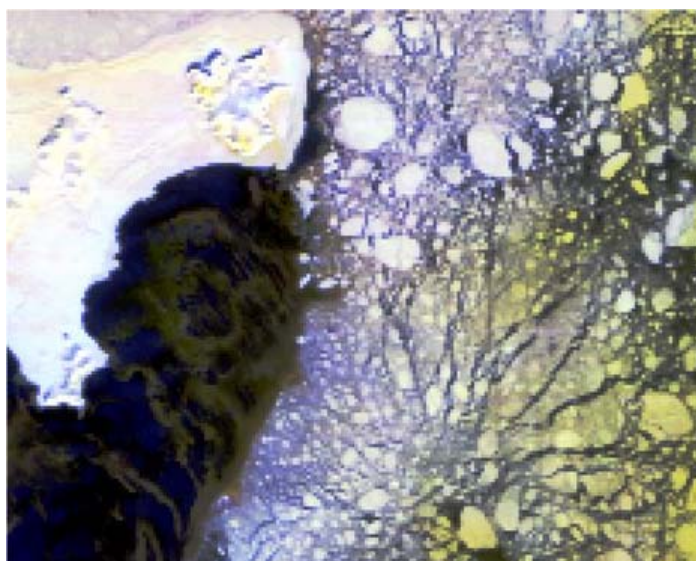


**Figure 38. Progressive zooms of VIIRS Imagery SDR RGB (1.6, 0.865, 0.64  $\mu\text{m}$ ) showing St. Lawrence Island region.**

Figure 38 shows details of ice edge near St Lawrence Island using localized histogram equalization contrast enhancement.



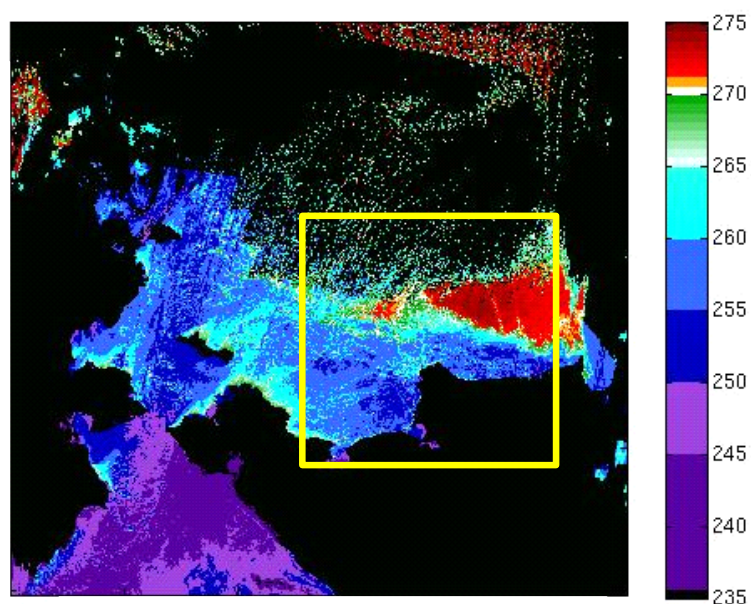


Figure 39. VIIRS Surface Temperature IP Bering Strait night scene for March 27, 2001 09:15 UTC.

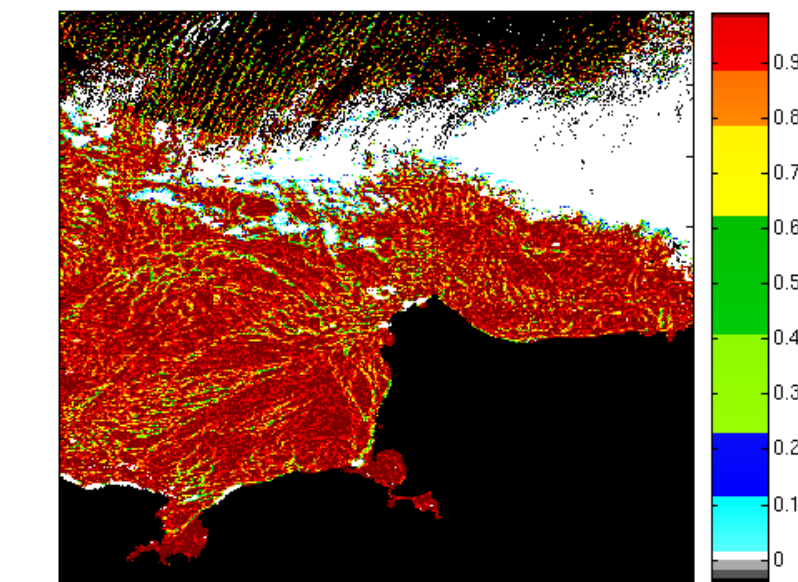
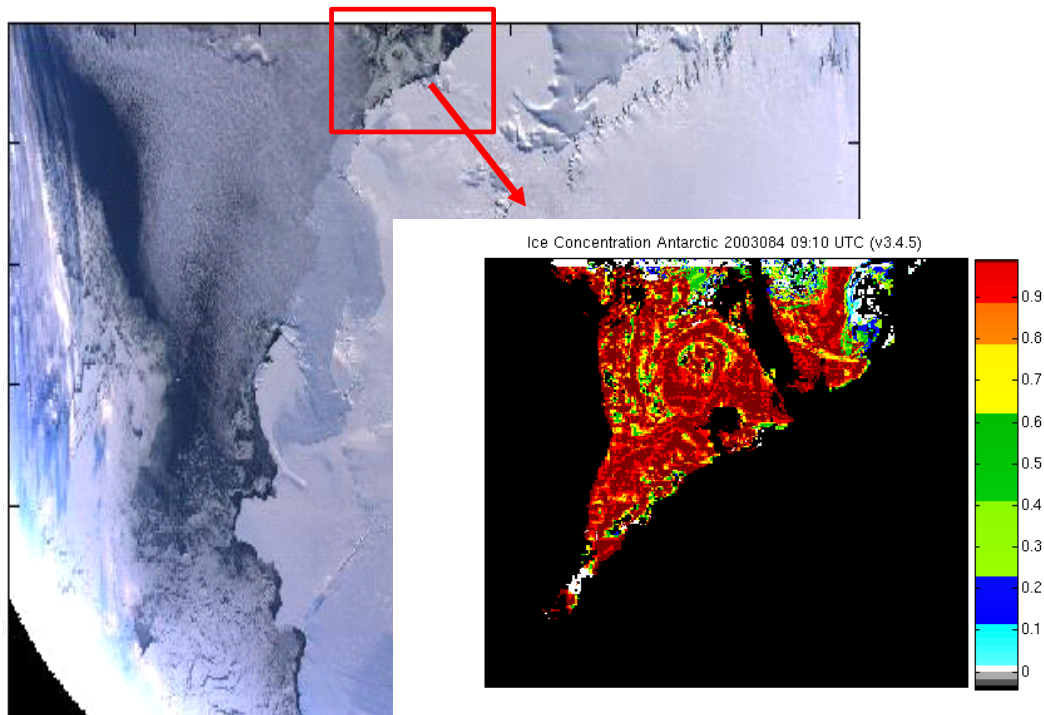


Figure 40. VIIRS Sea Ice Concentration IP zoom of boxed region in figure 39.

VIIRS Surface Temperature IP shown in Figure 39 is derived from the VIIRS Imagery SDR 11.45  $\mu\text{m}$  band. The temperature scale ranges from 235 K to 275 K. Land and clouds are masked black. Ice fractions shown in Figure 40 were derived from VIIRS Surface Temperature IP data. Scale shows ice fraction. Land and clouds are masked black.



**Figure 41. Antarctica scene March 25, 2003 09:10 UTC, MODIS Proxy VIIRS Imagery SDR RGB (1.6, 0.865, 0.64  $\mu\text{m}$ ) with zoom window showing Sea Ice Concentration IP.**

### 3.6.3.2.2 Ice Concentration from Tie Points

Under conditions where there is a predominant ice type in a local area, ice fraction for each imaged pixel can be retrieved by the direct application of a tie point method. The tie point is a special case of spectral mixture analysis, restricted to two end-members. The end-member signatures are derived from identifying pure pixels in the scene. The mathematical basis of the approach is discussed in the VIIRS Sea Ice Characterization ATBD [D41063] and is the basis of the VIIRS Sea Ice Concentration Intermediate Product. Examples of the VIIRS Sea Ice Concentration IP imagery are shown in Figures 40 and 41.



### 3.6.3.2.3 Ice Edge Location

Sea ice edge location may be performed by manual analysis of enhanced VIIRS Imagery SDR reflectances and brightness temperatures. In addition pseudo color imagery of VIIRS Surface Temperature IP and VIIRS Sea Ice Concentration IP data will further assist detection of ice edges if these Intermediate Products are made available to the analyst. Geographic locations of the ice edge may be determined by referencing the VIIRS Geolocation SDR latitudes and longitudes. Gridded ice fraction at imagery resolution may further assist in manual analysis of ice edge location [Y2506]. A pixel may be tagged as a possible ice edge pixel if one of the following conditions is met:

(1) It has ice concentration greater than 0.1 and at least one neighboring pixel has ice concentration less than 0.1

(2) It has ice concentration less than 0.1 and at least one neighboring pixel has ice concentration greater than 0.1

The set of tagged pixels are examined to derive an edge/no edge binary map and ice edge coordinates. Each neighboring pair of tagged pixels will produce an edge coordinate and an edge pixel. The edge pixel will be that member of the pair whose concentration is closer to the 0.1 edge value. The edge latitude/longitude coordinate is derived by a weighted linear interpolation of the pixel coordinates. The interpolation is to a concentration value of 0.5, as a pixel containing a compact ice edge located at the pixel center will have a concentration of 0.5.

$$\text{Lat} = (\text{Lat})_1 + ((C_1 - 0.5) \times ((\text{Lat})_2 - (\text{Lat})_1) / (C_1 - C_2)) \quad (3.6.3.2.2.1)$$

$$\text{Lon} = (\text{Lon})_1 + ((C_1 - 0.5) \times ((\text{Lon})_2 - (\text{Lon})_1) / (C_1 - C_2)) \quad (3.6.3.2.2.2)$$

where:  $C_1$  = measured ice concentration for pixel with greater concentration

$C_2$  = measured ice concentration for pixel with lesser concentration

$(\text{Lat})_1$  = latitude for pixel with greater concentration,

$(\text{Lat})_2$  = latitude for pixel with lesser concentration,

$(\text{Lon})_1$  = longitude for pixel with greater concentration,

$(\text{Lon})_2$  = longitude for pixel with lesser concentration,

and the coordinates apply to the pixel centers, as supplied by the geo-location algorithm [Y3258].

### 3.6.3.2.4 Supplemental Microwave Sensor Image Analysis

Available microwave sensor imagery from AMSR-E or the Microwave Imager/Sounder (MIS) in the NPOESS timeframe will supplement sea ice data analysis based on VIIRS Imagery SDR data, particularly for analysis for terminator, night and cloud obscured regions. Pseudo color image enhancement of available microwave sensor (MIS) based surface temperatures (brightness temperatures) and ice concentration products will provide valuable supplemental information. Examples of AQUA/AMSR-E sea ice concentration and brightness temperature products are available from the National Snow Ice Data Center on-line ([http://nsidc.org/data/amsre/data\\_summaries.html](http://nsidc.org/data/amsre/data_summaries.html)).

### 3.6.4 Performance of Sea Ice Data

The performance of the algorithms with respect to the VIIRS requirements and the System Specification. Truth data for sea ice concentration and sea ice edge are not available at comparable resolution to the VIIRS Imagery SDR imagery resolution products. Qualitative assessments of performance were performed based on MODIS MOD 29 data.

#### 3.6.4.1.1 Ice Concentration

Performance has been qualitatively estimated by comparison against MODIS MOD29 sea ice extent aggregated to 5 km resolution to obtain ice fraction. Results are shown in Figure 42.

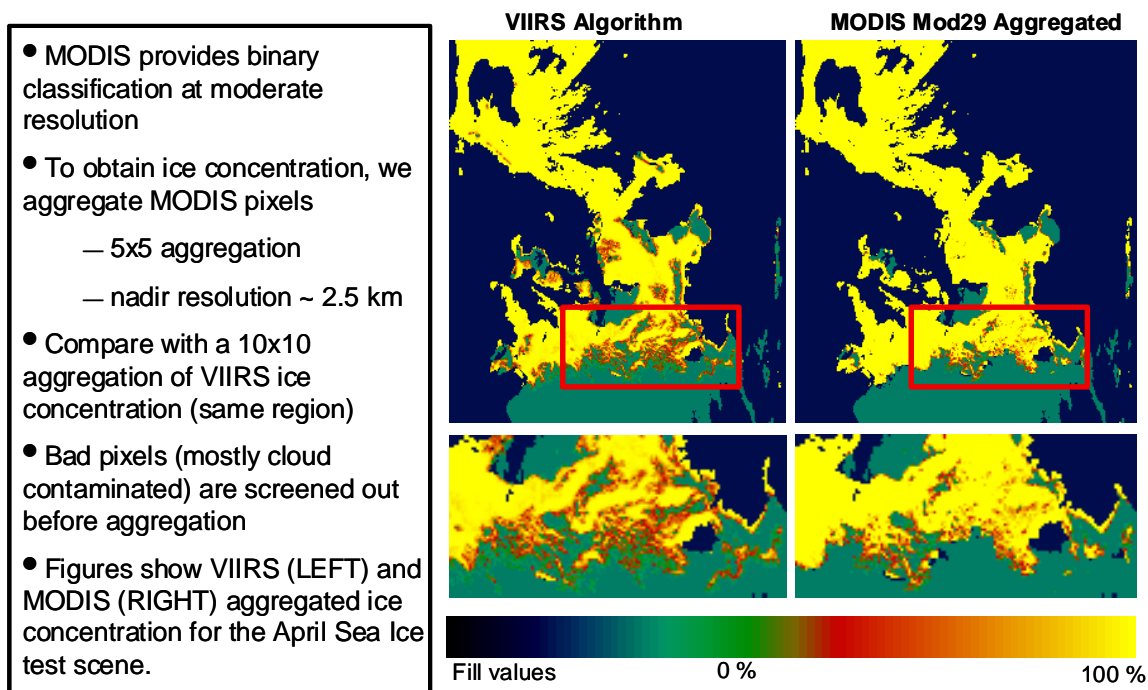


**Figure 42. Comparison of VIIRS Ice Concentration IP with MODIS MOD29 derived ice concentrations.**

Ice concentration from the VIIRS Sea Ice Concentration IP for the Bering Strait scene of April 24, 2001 23:05 UTC were aggregated to 10x10 to 5 km resolution and compared with

ice fractions derived by aggregating MODIS MOD29 sea ice extent to 5 x 5 km resolution. The ice fractions qualitatively compare well but differences exist due to the fact that the day MODIS MOD29 sea ice extents are based on an NDSI algorithm whereas the VIIRS Sea Ice Concentration IP is based on a tie point methodology. Performance of the manual analyzed sea ice concentration ARP must be performed using on orbit data.

### 3.6.4.1.2 Ice Edge Location

The quality of the VIIRS Imagery SDR has been demonstrated to allow detection of sea ice edge location based upon trial runs of a non-operational automated edge detection algorithm for the April 24, 2001 day scene. Contours of ice edge location are shown in Figure 43.

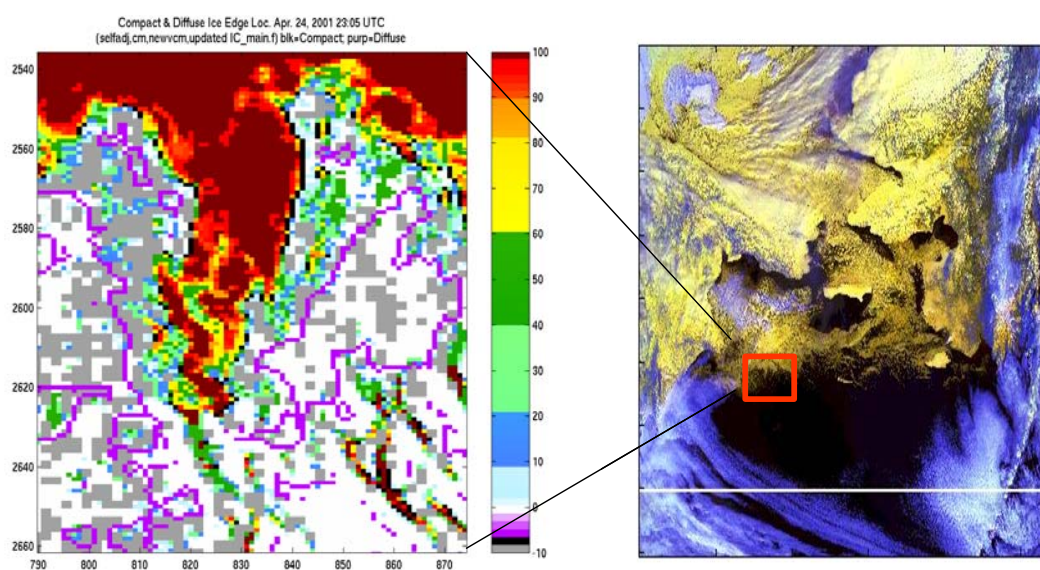


**Figure 43. Comparison of sea ice edge location with enhanced VIIRS imagery SDR enhanced reflectance imagery.**

Figure 43 shows the Bering Strait scene for April 24, 2001 23:05 UTC. The right panel shows enhanced RGB imagery of VIIRS Imagery SDR 1.6, 0.865 and 6.4  $\mu\text{m}$  reflectance bands. Contours of Sea Ice edge locations are shown in the left panel for the zoomed box region superposed on ice concentration. Black contours are compact ice edge locations. Diffuse ice edge location contours are shown as purple. Night time analysis will require use of supplemental microwave data products.

## 3.7 PRACTICAL CONSIDERATIONS

### 3.7.1 Numerical Computation Considerations

Paragraph SRDV3.2.1.5.4-1 of the VIIRS SRD states the following:

*“The scientific SDR and EDR algorithms delivered by the VIIRS contractor shall be convertible into operational code that is compatible with a 20 minute maximum processing time at either the DoD Centrals or DoD field terminals for the conversion of all pertinent RDRs into all required EDRs for the site or terminal, including those based wholly or in part on data from other sensor suites.”*

RDR here stands for Raw Data Record. This essentially means that any and all EDRs must be completely processed from VIIRS raw data, including calibration and geolocation, within 20 minutes from the time the raw data are available. This requirement is a strong reminder that VIIRS is an operational instrument.

For the Imagery EDR products, the challenges posed by the SRD time requirement are minimal. The geolocation and calibration algorithms used to produce Explicit Imagery are not computationally intensive in nature. NCC Imagery requires the use of pre-generated lookup tables that are simple and straightforward to apply, as has been demonstrated by the operational OLS product. Manual cloud ARPs are generated in real time by analysts. The sea ice ARPs do not involve any kind of iteration or inversion of physically-based models. We optimized our scheme of choosing parameters in the sliding search window. As a result of this improvement, the requirement to retrieve ice products on a global, operational basis in a 20 minute time frame places no constraints on our algorithms.

### 3.7.2 Programming and Procedural Considerations

VIIRS Phase II efforts are largely software-focused, and the methodology for this development work is based on sound and proven principles, as discussed in the VIIRS Algorithm Software Development Plan [Y6635]. The present maturity of the VIIRS software is detailed in the VIIRS Algorithm Software Maturity Assessment document [Y6661]. The maturity and remaining Phase II tasks for the algorithms themselves is summarized in the VIIRS Algorithm/Data Processing Technical Report [Y7040].

Except for manual cloud analysis, all procedures are automatic, to perform in the operational environment. The Imagery EDR products are produced in an integrated software system within the VIIRS Ground Segment of the IDPS. The software is composed of a set of independent testable units. These include the Imagery Unit, which produces the Explicit Imagery and the NCC Imagery, and the Ice Quality, Ice Concentration Units, which produce the Sea Ice ARPs. The software designs relevant to these units are summarized in the VIIRS Context Level Software Architecture [Y2469], Build SDR Module Level Software Architecture [Y2479], Snow Ice Module Level Software Architecture [Y2477], Imagery Unit Level Detailed Design [Y3273], Operational Design Document for the VIIRS Sea Ice Quality IP and ST IP [D42821], Operational Design Document for the VIIRS Sea Ice Concentration IP [D42820]. These designs will be tested at the system level as described in the most recent versions of the VIIRS Software Integration and Test Plan [Y3236], Algorithm Verification and Validation Plan [Y3237], and System Verification and Validation Plan [Y3270]. A summary of the ultimate strategy for operational application of the system of VIIRS algorithms is provided in the VIIRS Operations Concept document [Y2468]. The VIIRS

Interface Control Document (ICD [Y2470]) provides more detail on the specifics of ancillary data requirements for VIIRS EDR products.

### 3.7.3 Configuration of Retrievals

The Imagery algorithms require the availability of input data from a variety of sources, including VIIRS SDRs, VIIRS IPs, and a number of LUTs. A detailed list of these sources can be found in the Build SDR Module Level Software Architecture [Y2479], Snow Ice Module Level Software Architecture [Y2477], Imagery Unit Level Detailed Design [Y3273], Operational Algorithm Description Document for the VIIRS Sea Ice Quality IP and ST IP [D42821], Operational Algorithm Description Document for the VIIRS Sea Ice Concentration IP [D42820]. The NPOESS/VIIRS processing configuration is designed to satisfy these expectations [Y2469].

### 3.7.4 Quality Assessment and Diagnostics

Quality flags will be attached to each Imagery EDR product. A description of the quality flags can be found in the detailed design documents.

### 3.7.5 Exception Handling

The software is designed to handle a wide variety of processing problems, including bad and missing data and fatal errors. In the event that processing problems prevent the production of useful EDR data, error flag information will be written to the output EDR file as metadata.

## 3.8 ALGORITHM VALIDATION

Validation of the Imagery EDR and the Imagery Application-Related Products will be conducted as part of the VIIRS System Verification and Validation Plan [Y3270].

Verification of calibration and geolocation will be conducted for the VIIRS SDRs. TOA radiance, TOA reflectance, and EBBT in the Imagery EDR will be verified by inspection, by comparison with the equivalent fields in the VIIRS SDR. Degrading characteristics of the imagery (e.g. striping) will be checked by manual inspection. If necessary, either pre-calibration or post-calibration corrections may be applied to minimize these characteristics.

Verification that bow tie deletion has not caused a gap in coverage will be made by manual inspection of imagery obtained from the same region for different orbits. All surface features present in nadir-viewing imagery should also be present when the same region is observed at edge of scan.

Verification of NCC Imagery will be by inspection. A trained analyst viewing the terminator imagery will be able to observe whether or not a near constant contrast is preserved across the terminator.

Verification of manual cloud analysis products will be made by a comparison of the products obtained from a number of qualified analysts. The variation in the cloud cover and cloud type

results obtained by the different analysts will provide a quantitative error estimate. If warranted, independent lidar measurements can be made to provide a VIIRS-independent source of “truth”.

Initialization and validation of the sea ice algorithms will be coordinated with the National Ice Center, with the purpose of assuring that the VIIRS data products can be incorporated into their strategic product.

Radiative transfer models will be applied to large solar zenith angle data to optimize the models for polar conditions. MODIS data taken at solar zenith angles greater than 70 degrees will be studied to assist in determining the reflectance band weighting function. The limiting factor is believed to be the reliability of atmospheric correction at larger solar zenith angles. Plane parallel radiative transfer algorithms are inaccurate for angles greater than 70-75 degrees. Development of improved radiative transfer models at larger angles will allow us to relax this constraint. To solve the Radiative Transfer Equation appropriately one would have to take into account the spherical shell atmosphere geometry (Thomas and Stamnes, 1998). It is expected that “truth” can be established from *in situ* data obtained from MODIS validation campaigns.

The pre-launch plan includes sensitivity studies, analysis of simulated VIIRS data, and verification using MODIS data. Observations from AVIRIS, MAS, MODIS, GLI, and NPP/VIIRS will be used in the pre-launch phase to study the error characteristics and optimum techniques for the algorithm. It is expected that MODIS validation data will be of great value. The NPP/VIIRS will be critical in adjusting and verifying the values of the parameters in our LUTs. This process will be essential in making the sea ice algorithms operational prior to the NPOESS mission. We recommend an NPP/VIIRS validation campaign that includes *in situ* field measurements, ER-2 underflights (AVIRIS and MAS), and low level aircraft measurements at spatial resolutions as fine as 10 meters (e.g. RC-10 camera data). NPP/VIIRS data can be re-processed many times with various combinations of band weight functions and search window parameters, and resulting ice concentration and edge location can be compared to “truth” established from the auxiliary data. In this way, optimum band weight functions and search window parameters can be selected.

Our plan is designed to interface smoothly with post-launch validation activity. The availability of NPP/VIIRS data prior to the NPOESS mission will be of enormous benefit. We would propose to conduct an NPP/VIIRS validation campaign similar to the MODIS validation activity, and use it as a model for the post-launch NPOESS/VIIRS validation campaign. In this sense, post-launch validation will already have been simulated by the pre-launch validation activity. Following launch, we would substitute real VIIRS data for the pre-launch simulated data. Cross-validation with NPOESS/MIS provide a valuable extra capability.

## 4.0 ASSUMPTIONS AND LIMITATIONS

### 4.1 ASSUMPTIONS

The following assumptions apply to the algorithms described in this document:

- The reflectivities and emissivities for materials classifications used in the VIIRS simulations represent the real world.
- An effective cloud mask over snow and ice surfaces will be available from the VIIRS Cloud Mask IP [Y2412].
- Directional surface reflectance will be derived from TOA radiance as a Surface Reflectance IP, with errors as specified in the VIIRS System Specification [SS154640-001].
- A Surface Temperature IP will be provided, with errors as specified in the VIIRS System Specification [SS154640-001].

### 4.2 LIMITATIONS

The following limitations apply to the algorithms described in this document:

- The accuracy of cloud analysis in the manually generated cloud products of the Imagery EDR are limited to cloud features which can be detected by the VIIRS horizontal spatial resolution. The VIIRS design may not detect all sub-pixel clouds.
- The accuracy of manual analyses generated from simulated VIIRS imagery is limited by the analysts ability to create cloud, no cloud analyses with the Cloud Ground Truth Analysis (CGTA) software. Cloud edges represent the greatest challenge. However, experienced image interpreters agree within about 1-2 percent in total cloud, no cloud analyses of complex scenes.
- The capability to recommend TBD values for “obscured/not cloudy if the LOS extinction optical thickness is = 0.03 (TBD)” is limited by the standard profiles and atmospheric conditions available within MODTRAN 4.0. The software does not support small, incremental changes in aerosol LOS conditions, e.g., say stratospheric aerosol optical depths in the range of 0.010 to 0.050 at 0.005 increments.

Limitations applying specifically to the automated sea ice retrieval are:

- Clear conditions only. The definition of "clear" will be developed in coordination with the development of the VIIRS Cloud Mask IP [Y2412]. It will depend upon the capability of the cloud mask over snow and ice surfaces and upon the capability of radiative transfer modeling through thin clouds.

## 5.0 REFERENCES

- Ackerman, S. A., K. Strabala, P. Menzel, R. Frey, C. Moeller, L. Gumley, B. Baum, C. Schaaf, and G. Riggs (1997). Discriminating Clear-Sky From Cloud With MODIS Algorithm Theoretical Basis Document (MOD35). Version 3.2
- Allen, R. C., P. A. Durkee, and C. H. Wash (1990). Snow/cloud discrimination with multispectral satellite measurements. *J. Appl. Met.*, 29, 994-1004.
- Arbeiter, R., 2008: Operational Algorithm Description Document for the VIIRS Ground Track Mercator (GTM) Imagery, EDR Software, D42815, Raytheon Company, pp 41.
- Bohren, C.F., and B.R. Barkstrom (1974). Theory of the optical properties of snow. *J. Geophys. Res.*, 79, 4527-4535.
- Bolsenga, S.J. (1983). Spectral reflectances of snow and fresh-water ice from 340 through 1100 nm. *J. Glaciology*, 29(102), 296-305.
- Crane, R.G. and M.R. Anderson (1984). Satellite discrimination of snow/cloud surfaces. *Intl. J. Remote Sens.*, 5(1), 213-223.
- Dozier, J. (1984). Snow reflectance from Landsat-4 Thematic Mapper. *IEEE Trans. Geosci. Remote Sens.*, 22(3), 323-328.
- d'Entremont, R. P., Thomason, L. W. and J. T. Bunting, 1987: "Color composite image, processing for multispectral meteorological satellite data, *Proceedings of SPIE - The International Society for Optical Engineering*, pp. 96-106, Cambridge, MA.
- Dozier, J. (1989). Spectral signature of alpine snow cover from the Landsat Thematic Mapper. *Remote Sens. Environ.*, 28, 9-22.
- Grenfell, T.C., and G.A. Maykutt (1977). The optical properties of ice and snow in the Arctic Basin. *J. Glaciology*, 18(80), 445-463.
- Grenfell, T.C., and D.K. Perovich (1984). Spectral albedos of sea ice and incident solar irradiance in the southern Beaufort Sea. *J. Geophys. Res.*, 89(C3), 3573-3580.
- Grenfell, T.C., D.K. Perovich, and J.A. Ogren (1981). Spectral albedos of an alpine snowpack. *Cold Regions Sci. Technol.*, 4, 121-127.
- Hutchison, K. D and A. P. Cracknell, 2006: VIIRS – A New Operational Cloud Imager, CRC Press, Taylor and Francis Group, ISBN-100-415-32129-8, pp 230.
- Hutchison, K. D., VIIRS Risk Reduction Plan for Manually-Generated Cloud Products, Raytheon Information and Technical Systems, Version 1.0, Revision 0.1, May, 1999.



- Hutchison, K. D., VIIRS Imagery Flowdown Results , EDR: Manually-Generated Cloud Products from Imagery, October, 1998.
- Hutchison, K., and P. Janota, "Cloud Models Enhancement Project Phase 1 Report," The Analytic Sciences Corporation (TASC), Technical Report TR-5773-1, August, 1989.
- Hutchison, K., Peterson, R., and P. Janota, "Cloud Models Enhancement Project Phase 2 Report," The Analytic Sciences Corporation (TASC) Technical Report TR-5773-2, August, 1990.
- Hutchison, K. D., and J. K. Locke (1997). Snow identification through cirrus cloudy atmospheres using AVHRR daytime imagery," *Geophysical Research Letters*, 24, 1791-1794
- Hutchison, K. D., B. J. Etherton, and P. C. Topping (1997). Validation of automated cloud top phase algorithms: distinguishing between cirrus clouds and snow in a-priori analyses of AVHRR imagery. *Optical Engineering*, 36, 1727-1737
- IORD-I. Integrated Operational Requirements Document – NPOESS.
- Liou, K-N. (1980). *An Introduction to Atmospheric Radiation*. Academic Press.
- Mannen, J. T. (1996). *Cost and Operational Benefits Requirements Analysis Report (COBRA)*, NPOESS Integrated Program Office, June 12, 1996.
- Massom, R., and J.C. Comiso (1994). The classification of Arctic sea ice types and the determination of surface temperature using AVHRR data. *J. Geophys. Res.*, 99(C3), 5201-5218.
- Planet, W.G. (ed.), (1988). *Data extraction and calibration of TIROS-N/NOAA radiometers*. NOAA Technical Memorandum NESS 107 – Rev. 1, Oct. 1988. 130 pp.
- Scorer, R. S. (1990). *Satellite as Microscope*. Ellis Horwood Limited.
- Thomas, G., and K. Stamnes (1998). *Radiative transfer in the atmosphere and ocean*. Textbook, Cambridge Atmospheric and Space Sciences Series.
- Valovcin, F. R. (1978). *Spectral radiance of snow and clouds in the near infrared spectral region*, AFGL-TR-78-0289, Air Force Geophysics Laboratory, Hanscom AFB, MA.
- Warren, S.G. (1982). Optical properties of snow. *Rev. Geophys. Space Phys.*, 20(1), 67-89.
- Warren, S.G., and W.J. Wiscombe (1980). A model for the spectral albedo of snow.II. Snow containing atmospheric aerosols, *J. Atmos. Sci.*, 37(12), 2734-2745.
- Westinghouse Electric Corp. (1993). *Technical Operating Report for Block 5D-3 Operational Linescan System (OLS) OLS 17-21*.

Wiscombe, W.J., and S.G. Warren (1980). A model for the spectral albedo of snow,1,pure snow. J. Atmos. Sci., 37(12), 2712-2733.